Crystallization of $Zr_2Pd_xCu_{(1-x)}$ and $Zr_2Ni_xCu_{(1-x)}$ metallic glass

by

Min Xu

A dissertation submitted to the graduate faculty

in partial fulfillment of the requirements for the degree of

DOCTOR OF PHILOSOPHY

Major: Materials Science and Engineering

Program of Study Committee:
Matthew J. Kramer, Co-major Professor
Daniel J. Sordelet, Co-major Professor
Steve W. Martin
Alan I. Goldman
Xueyu Song

Iowa State University

Ames, Iowa

2008

DEDICATION

To my husband Zhen Yu and my son Gavin Yu------

Your love is amazing.

To my mother Chengquan Xu and father Chenggui Lu------

I am much indebted to you.

In memory of my grandmother Yujiao Gu and grandfather Delin Lu------

You are always in my heart.

I love you!

TABLE OF CONTENTS

ABSTRACT

One interesting aspect of metallic glasses is the numerous instances of the deviation of the phase selection from the amorphous state to thermodynamically stable phases during the crystallization process. Their devitrification pathways allow us to study the relationship between the original amorphous structure and their crystalline counter parts. Among the various factors of phase selections, size and electronic effects have been most extensively studied. Elucidating the phase selection process of a glassy alloy will be helpful to fill in the puzzle of the changes from disordered to ordered structures. In this thesis, Two model $Zr_2Pd_xCu_{(1-x)}$ and $Zr_2Ni_xCu_{(1-x)}$ (x = 0, 0.25, 0.5, 0.75 and 1) glassy systems were investigated since: (1) All of the samples can be made into a homogenous metallic glass; (2) The atomic radii differ from Pd to Cu is by 11%, while Ni has nearly the identical atomic size compare to Cu. Moreover, Pd and Ni differ by only one valence electron from Cu. Thus, these systems are ideal to test the idea of the effects of electronic structure and size factors; (3) The small number of components in these pseudo binary systems readily lend themselves to theoretical modeling.

Using high temperature X-ray diffraction (HTXRD) and thermal analysis, topological, size, electronic, bond and chemical distribution factors on crystallization selections in $Zr_2Pd_xCu_{(1-x)}$ and $Zr_2Ni_xCu_{(1-x)}$ metallic glass have been explored. All $Zr_2Pd_xCu_{(1-x)}$ compositions share the same *C11b* phase with different pathways of meta-stable, icosahedral quasicrystalline phase (*i*-phase), and *C16* phase formations. The quasicrystal phase formation is topologically related to the increasing icosahedral short range order (SRO) with Pd content

in $Zr_2Pd_xCu_{(1-x)}$ system. Meta-stable *C16* phase is competitive with *C11b* phase at x = 0.5, which is dominated by electronic structure rather than size effects. Cu-rich and Ni-rich compositions in $Zr_2Ni_xCu_{(1-x)}$ trend to divitrify to *C11b* or *C16* phases respectively. In the proposed pseudo binary phase diagram, the domain of *C16*, *C11b* and co-existence phases are mainly related with the topology in the amorphous structure and formation enthalpies of crystalline phases.

CHAPTER 1. GENERAL INTRODUCTION

Introduction

Understanding the phase selection process during the crystallization of metallic glass is critical for gaining a better grasp on both the thermodynamics and kinetics aspect of phase transformations in the metallurgical field. There are various driving forces which control the directions of devitrification pathways in metallic glass. The question then arises: what's the relationship between the amorphous structure and the crystallization pathways?

In order to understand the above question, numerous attempts have been made to correlate the factors, which control the devitrification, to short-range-order, atomic size or electronic structure of the elements, thermodynamics, *etc.*, Several competing ideas about the amorphous structure and crystallization process are listed below:

One of the famous hypothesis proposed by F. C. Frank [1] about 55 years ago, that there is a very common grouping in the liquid: one atom at the center of each face of a regular dodecahedron. This configuration has five-fold axes, which are abhorrent to crystal symmetry since this kind of configuration cannot be continuously extended in three dimensions. It should be note that Frank's hypothesis was based on one-component materials (all the spheres are identical), whereas no pure metal has yet been quenched in the glassy state. Later, Kelton [2] first directly demonstrated Frank's hypothesis by experiment, showing that a growing icosahedral short-range order with decreasing temperature in deeply

undercooled $Ti_{39.5}Zr_{39.5}Ni_{21}$ liquids by synchrotron x-ray structural studies. Because metallic glasses are rapidly quenched from melt liquid, one can expect some atomic configurations kept in the structure of metallic glass from liquid, and understand the structure in the metallic glass based on Frank's hypothesis and Kelton and his collaborators' work.

Inoue [3] proposed three empirical rules for discovering "good" systems for metallic glass formation: (1) multicomponent systems consisting of more than three elements; (2) significant difference in atomic sizes with the size ratios above about 12% among the three main constituent elements; and (3) negative heats of mixing among the three main constituent elements. Although there are many examples of multiple component systems which readily form metallic glass, there are a number of binary alloys [4, 5] which have been found to be reasonable glass formers. Collected from the published reports on glass formation of 66 binary systems, Egami and Waseda (1984) [6] used an atomic elasticity theory to show that the minimum solute concentration C_{min}, which is necessary to obtain binary amorphous alloys by rapid quenching from the melt, is inversely related to the atomic volume mismatch. This result indicates that the atomic size ratio is the most important factor in the determination of value of C_{min}.

Miracle [7, 8] investigated the topology on the formation of the glass. The ratio, R, of the solute atom radius to the solvent atom radius is the only topological parameter considered. After analysis of a large number of binary and complex metallic glasses, the first compelling atomic structural model, dense packing of atomic clusters, was presented based on efficient atom packing in the first coordination shell of solute-centered clusters. It shows that solutes have specific and predictable sizes relative to the solvent atoms (specific critical radius ratios R*) in metallic glass. It predicts the number of solute atoms in the first coordination shell of a

typical solvent atom. It also predicts that the local structure of metallic glasses is efficiently packed in systems where the solutes occur at fixed radius ratios R*, in which, alloy composition is not important in the comparison.

Hume-Rothery [9] derived a series of rules, based mainly on the investigation of Cu and Ag alloys, indicating the factors which favor the formation of a specific structure in a certain composition range. The most important rule concerns the preferential formation of specific structures in a certain range of electrons-per-atom ratio e/a: number of all valence electrons in the alloy relative to the atomic number.

The relative importance of size and electronic factors in determining the structural trends for a limited chemistry, AB_2 phases, was also investigated by Ohata [10] using a tight binding d bond model. Structures formations were interpreted within a two-step process. In the first step, the volumes of the different structure types are adjusted to guarantee the same repulsive energy. In the second step, the bond energies are compared at these prepared volumes in order to see which structure is most stable. A predicted structure map was proposed. Compared with the experimental structure, good qualitative agreement with the experimental AB_2 structure map is found only if both size and electronic factors are taken into account within the tight bonding model.

The above previous work about glass forming and phase selection theories are very helpful for guiding the metallic glass design and crystallization investigation. But all of these ideas have shortcomings. An important one is that Frank's hypothesis, Egami's atomic elasticity theory and Miracle's dense cluster-packing model all describe pure topological factor and atoms has been treated simply as hard spheres, whereas all metallic glass should counted chemical factors in. For example, Zr_2Cu will devitrify to *C16* phase if only

efficiency packing is considered, but from observation of devitrification process, *C11b* phase forms as the primary phase from the amorphous structure. Thus, topological factor is not sufficient to explain all the devitrification process. Inoue's three empirical rules are helpful in searching for new metallic glass, but more and more binary alloys are found to be fine glass formers. Hume-Rothery concluded that the structure of an alloy depends on the size of the component atoms, as well as the valence electron concentration, and electrochemical difference, while the alloy systems limited to sp-valence elements such as Al, Zn, Si, Ge and Sn. Also, although Ohata's theoretical structure maps included both size and electronic factors in, but it is only for transition metal AB_2 family. In conclusion, both packing and electronic factors are very important on glass forming and phase selection process from the above competing ideas, which will be given later in the literature review section in more details.

The various possibilities of the phase selections in metallic glasses are affected by both thermodynamic and kinetic aspects. We need to explore the various factors, such as topology and chemistry, on devitrification to answer the question of the relationship between the amorphous structure and the crystallization pathways. Designing suitable systematic metallic glasses is very important to test multiple factors during structural changes from disorder to order in the crystallization of metallic glasses, including primary phase selection, meta-stable phase formation, thermodynamics stable phase transformation, *etc.* In our present work, we designed two series of metallic glasses forming alloys: $Zr_2Pd_xCu_{(1-x)}$ and $Zr_2Ni_xCu_{(1-x)}$, (x = 0, 0.25, 0.5 , 0.75 and 1), as two systematic models to perform crystallization investigations. Through studying how the crystallization pathways will be affected by the additive elements Pd or Ni, it allows us to test the multiple ideas, such as

topological, size, electronic factors, *etc.*, during the crystallization process for the following reasons:

(1) The phase diagrams [11] of Zr-Cu, Zr-Pd and Zr-Ni binary systems are very similar around Zr is 66.7at.% (congruently melt). Since all $Zr_{66.7}Cu_{33.3}$, $Zr_{66.7}Pd_{33.3}$ and $Zr_{66.7}Ni_{33.3}$ are reasonable glass formers, the composition of $Zr_2Pd_xCu_{(1-x)}$ and $Zr_2Ni_xCu_{(1-x)}$ become of particular interest, because the starting amorphous alloy has the same composition as the final AB_2 equilibrium phases.

(2) Although it is easier to form metallic glass in systems within many different elemental components and very different metallic radii [12], many-component systems do not easily lend to theoretical modeling. The small number of components makes $Zr_2Pd_xCu_{(1-x)}$ and $Zr_2Ni_xCu_{(1-x)}$ metallic glass easier to carry out the theoretic simulations.

(3) Noble metals are very sensitive for *i*-phase formation in Zr-based metallic glass. $Zr_2Pd_xCu_{1-x}$ system is an ideal system to reveal the relationship between the room temperature SRO and the primary crystallization phase formation with increasing Pd.

(4) According to Hume-Rothery [9] rule: mutual solubility of the elements is very restricted when the atomic radii differ by more than 15%. In $Zr_2Pd_xCu_{(1-x)}$ and $Zr_2Ni_xCu_{(1-x)}$ metallic glasses, considering atomic size Zr 1.58Å, Cu1.27 Å, Pd1.41 Å, Ni 1.28 Å [6], and electron configuration: Zr $4d^25s^2$, Cu $3d^{10}4s^1$, Pd $4d^{10}$, Ni $3d^84s^2$, Pd and Ni can substitute each other with Cu and form solid solution. Thus, $Zr_2Pd_xCu_{(1-x)}$, $Zr_2Ni_xCu_{(1-x)}$ system are good to study: (a). both the electronic factor and size factor during the crystallization process; (b). how will the continuous content changes of additive elements Pd or Ni affect the phase selection.

Literature review

Formation and stability of Metallic glass

Metallic glasses have also been called glassy alloys or amorphous alloys. The first metallic glass was reported in 1960 by Duwez *et al* [13]. To make metallic glass, the cooling occurs rapidly enough that the nucleation of liquid alloys can be completely suppressed. There is no-long-range order but only short-range-order in the structure of a glass. A glass transition like that observed in conventional glass-forming melts has beeen detected in many rapid quenched metallic glasses. The glass transition temperature, T_g, is a kinetic parameter, which depends on the melt cooling rate. It defines a pseudo second order phase transition in which a supercooled melt yields glass structure on cooling process. Below the glass transition temperature, Tg, amorphous solids are in a glassy state. In inorganic glasses, with increased temperature, more and more joining bonds are broken by thermal fluctuations so that broken bonds begin to form clusters. Above T_g, these clusters become larger to facilitate the flow of material and make the structure re-arrangement possible.

In constructing models of the atomic structure of metallic glass, it can be assumed that the structure, in which the atoms are closely packed, will have the lowest total energy and yield the highest density. Among numerous investigation of the geometry and topology of metallic glass, there are mainly three important metallic glass models: (1) Mirocrystallite models [14]: those models propose that metallic glass actually consist of innumerable small regions with a crystalline short range order embedded in a matrix of randomly interconnected atoms; (2) Dense random packing of hard spheres [15]: it could be described as an assembly

of tetrahedrons distorted in various ways and combined with small voids, which are bounded by triangular faces. The dense random packing is topologically equivalent to a random network in which vertexes are connected to one another by four bonds each; (3) polyhedral models [16]: those models derive explicitly from the observation that a tetrahedral configuration is denser than any crystalline one for a cluster of a few atoms. Frank showed that the tetrahedral packing is favored for as many as 13 atoms [1]. He also pointed out that among three possible 13-atom cluster configurations; the icosahedral assembly is energetically preferred over face center cubic (fcc) or hexagonal close packing (hcp) structures.

Turnbull [17] predicted that the reduced glass transition temperature, $T_{rg} = T_g/T_l$ (the ratio of glass transition temperature T_g to the liquidus temperature T_l of alloy, can be used as a criterion for determining the glass-forming ability (GFA) [18]. According to Turnbull's criterion, a liquid with $T_g/T_l = 2/3$ becomes very sluggish in its crystallization within conventional cooling rates for casting. Up to now, the Turnbull criterion for the suppression of crystallization in undercooled melts remains most popular for predicting the GFA [19]. However, the reduced glass transition temperature also has some limits. First, although it is good for predict binary systems, it might not reliable for multiple component systems, since T_g and T_l differ significantly [20] in multiple component systems; Secondly, T_{rg} theory arises from the requirement that viscosity must be large at the temperatures between T_l and T_g, thus, it might not hold for some systems since the temperature variation of viscosity is different from system to system.

Apart from T_{rg}, another extensively used parameter for GFA is ΔT_x ($=T_x-T_g$), which is equal to the difference between the onset temperature of the first crystallization temperature

(T_x) and the glass transition temperature (T_g). However, Lu *et al.* [20] reported that GFA shows very weak dependence on ΔT_x in many metallic glass systems. Although both ΔT_x and the ratio T_g /T_l are used as indicators of the GFA for metallic glasses, they did show contrasting trends on GFA in many alloy systems [21, 22].

A refined parameter taking T_x, T_g and T_l into account was therefore proposed recently by Lu and Liu [20]. They provided a new concept to understand the nature of GFA based on the analysis of the characteristic features of time-temperature-transformation (TTT) curves [23]. It was found that the glass-forming ability for noncrystalline materials was related mainly to two factors, i.e., $1/(T_g+T_l)$ and T_x, and could be predicated by a unified parameter γ defined as $\gamma = \frac{T_x}{T_g + T_x}$. They also combined numerous literatures for a wide variety of systems and then compared the results of γ parameter to others' experimental observations. To determine the γ values, constant heating rate is required. Thus, it is worthwhile to notice that γ is dependent to heating rates.

As state above, Inoue [3] postulated that the alloys with the stabilized supercooled liquid state have three features in common, i.e. multi-component systems, significant atomic size ratios above 12%, and negative heats of mixing. One shortcoming of the multi-component system is that they do not lead to easier modeling. However, more and more binary or ternary systems [24, 25] are found to be moderate glass former. Zr-based glasses with a transition or noble metal element as the second component are the most typical example of pure binary metallic glass. Zr-Cu and Zr-Ni are probably the most widely studied among these alloys [26]. Both systems have the advantage that they can be made amorphous by melt spinning over a relatively wide range of composition: over a composition range of

30–70 at.% Cu in Zr–Cu system [27], and two composition ranges 33-42 an 60-76 at. % Zr in Zr–Ni system [28]. These binary systems are good model systems for theoretic investigation.

As mentioned before, Egami [6] investigated the correlation between the atomic size ratio of the constituent elements and the glass formability for both metal-metal and metal-metalloid systems. A new rule was presented: when an element B is alloyed into an element A, the minimum solute concentration to form glass, C_{min}, is small if the size ratio between the two elements is for from unity, while C_{min} is large if the size ratio is close to unity. The relationship between C_{min} and the volume mismatch is:

$$C_{min} = \frac{0.1}{\left|(\frac{R_B}{R_A}) - 1\right|}$$

Where, R_A and R_B are radii of host atom A and solute atom B, respectively. It is pointed out that the size factor plays a dominant role in determining the composition limit for glass formation and there is essentially no difference between the metal-metal and metal-metalloid system as far as the mechanism of glass formation is concerned. As mentioned in the general introduction part, the drawback is that only topological factor was included in this rule.

Metallic glasses can lower their free energy by crystallization during subsequent heating, since they are meta-stable. The dynamic crystallization temperature, T_x, provides a useful and quick means to compare the relative thermal stabilities of different glasses. T_x values depend not only on the heating rate but also on many other factors such as the thermal history of the glass, method of preparation, and amount of trapped gas. For most metallic glass, T_x is between 0.4 and $0.6T_m$ [29, 30].

Numerous attempts [31] have been made to correlate the relative thermal stabilities of different glasses to crystallographic or electronic factors. Nagel *et al.* [32] treated the glass as a near free electron solid and argued that the glassy phase should be most stable at the compositions where the Fermi level is at minimum in the density of the state (DOS). Naka *et al.* [33] reported that when Fe is partially substituted by various transition metals in iron-metalloid glasses, T_x is in proportion with the electron/atom ratio (*e/a*). Inoue *et al.* [34] have shown that, in (Fe, Co, Ni)-M-B glasses, where M is transition metal, T_x increases with the difference in electro-negativity between (Fe, Co, Ni) and M. For all of the above ideas about the stability of metallic glass: glassy phase stabilized at the minimum of Fermi level is commonly accepted. While T_x increases with *e/a* is just unique in certain system. For example, the T_x increases a little (within 2%), but the *e/a* values decreases 33% from Zr_2Cu to Zr_2Ni. The relationship between the difference of the electro-negativity values and T_x fits the data in $Zr_2Pd_xCu_{(1-x)}$ and $Zr_2Ni_xCu_{(1-x)}$ system very well: the electro-negativity values of Zr, Ni, Pd and Cu are 1.33, 1.91, 2.20 and 1.90 accordingly; in those two systems, T_x does increase with the difference of the electro-negativity values between (Zr, Cu) and TM (TM = Pd. Ni).

Crystallization of Zr-based metallic glass

General introduction of crystallization in metallic glass

Time-Temperature-Transformation (TTT diagram) can show schematically the relationship between the temperature and the time when crystalline structures form from an under-cooled melt from the kinetics aspect. The overall shape of TTT diagram is a "C" shape.

This shape is the result of the competition between the increasing driving force for crystallization and the slowing down of kinetics (effective diffusivity) of atom movement. Most measurements of transformation kinetics are made well below the nose of the diagram. In TTT diagram, if the glass is heated slowly from room temperature, crystallization begins at the temperature T_x, which is increases with the heating rate. If the glass is heated to a temperature ($T_g < T < T_x$), and held isothermally for a time, it will also crystallize. The longer the glass spends at the higher temperature, the easier to crystallize. Although, glassy state will appear quite stable and unchanging under T_g, it is actually kinetically stable. From thermodynamic viewpoint, all glassy state is meta-stable state and prone to crystallize.

The relationship between local structure and primary devitrification process

The primary crystalline phase has structural correlation with the local structure in metallic glass. In 1950, Turnbull [35] demonstrated that a metallic liquid could be cooled far below its equilibrium melting temperatures without crystallization. The undercooling is due to the energy barrier to form nuclei in the liquid. However, for metal systems, it was thought that this barrier was small. To explain this surprising result, Frank [1] hypothesized that the local structures of undercooled metallic liquids are actually quite different from those of crystal phases, containing a significant degree of icosahedral order that is incompatible with the extended periodicity of the crystal. Such structure differences must create a great barrier to the formation of crystal phases.

Based on Franks' hypothesis, vigorous interest has led to describing the linkage between the short-range order (SRO) and the formation of *i*-phase. To confirm Frank's

hypothesis, icosahedral short range order (ISRO) in the liquid must be coupled with the nucleation barrier for crystallization.

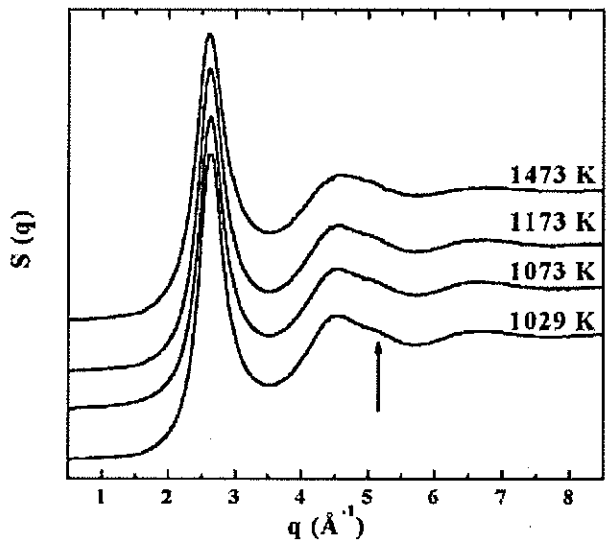

Figure 1. $S(q)$ for the $Ti_{39.5}Zr_{39.5}Ni_{21}$ liquid as a function of temperature. An increase in the intensity of the shoulder on the second peak (indicated by the arrow) is observed as the temperature is lowered below the liquidus temperature (1083 K).

Kelton *et al.* [2] determined the x-ray structure factors extracted from the scattering data for the $Ti_{39.5}Zr_{39.5}Ni_{21}$ liquid (Figure 1-2). They showed that this increasing ISRO is responsible for the nucleation of a metastable Ti-Zr-Ni icosahedral quasicrystal phase (*i* phase) from the undercooled liquid instead of the stable polytetrahedral C14 Laves phase. Since the driving free energy for nucleation is larger for the C14 phase, the preferred nucleation of the *i* phase signals a smaller nucleation barrier, indicating that the short range order of the liquid is more similar to that of the *i* phase than to the tetrahedral structure of the C14 phase. One interesting aspect of the data is the enhancement of a shoulder on the high-q side of the second peak in $S(q)$ with increasing undercooling. In the same temperature range,

nucleation of the icosahedral quasicrystalline phase (*i*-phase) becomes favorable. This shoulder is consistent with local icosahedral order [36]. The relative locations of the first two peaks in $S(q)$, $q_2/q_1 = 1.72$, and the location of the shoulder on the second peak over the first peak, $q_{shoulder}/q_1 = 1.97$, are in good agreement with those expected for a perfect icosahedron [36].

Miracle [7, 8] presented the first compelling atomic structural model, which based on the dense packing of atomic clusters (Figure 1-1).

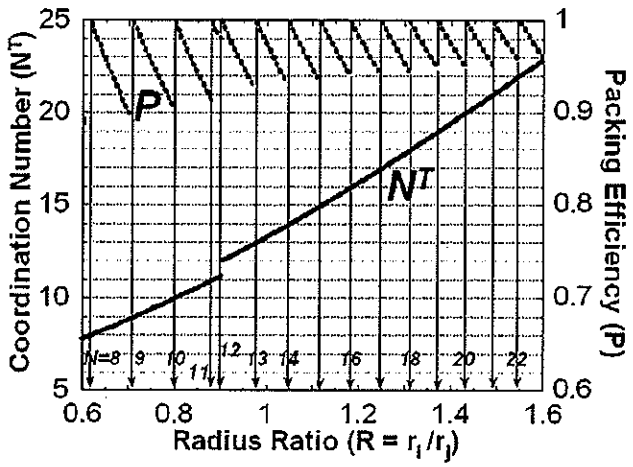

Figure 2. The theoretical coordination number N^T and packing efficiency P as functions of radius ratio R

In Miracle's structure model, the influence of efficient atomic packing on the constitution of metallic glass has been investigated. The theoretical coordination number N^T and packing efficiency P can be deduced as functions of radius ratio R for three-dimensional clusters of spheres, in which, $R = \frac{r_j}{r_i}$, r represents atomic radius, and subscripts i and j indicate the solute and solvent atoms, respectively. A discontinuity occurs at R=0.902, which

related to a coordination number of 12, or icosahedra solute-centered cluster in the metallic glass.

Quasicrystalline phase formation in the Zr-based metallic glass

Quasicrystals are known to exhibit many special properties [37, 38], such as high hardness, high corrosion resistance, low coefficient of friction, low adhesion, interesting electrical, thermal transport properties, *etc*. Recently, many Zr-based alloy systems [39, 40] have been found to form *i*-phase upon crystallization process. Murty, Ping and Hono [41] suggested that the composition of the quasicrystals is close to 70 at. % Zr in $Zr_{65}Cu_{27.5}Al_{7.5}$ alloy by 3-D atomic probe (3DAP).

I-phase formation appears to depend strongly on the minor element additions. The addition elements can be roughly divided into three types: the effect of oxygen, the effect of noble metals and the effect of other element.

(1) The effect of oxygen:

Koester's first report [42] of *i*-phase formation during crystallization of Zr-Cu-Ni-Al alloy with high oxygen content has stimulated the considerable research interest in Zr-based alloys. Eckert *et al.* [43] first demonstrated that the quasicrystallization is significantly influenced by the amount of oxygen in the $(Zr_{0.65}Al_{0.075}Cu_{0.175}Ni_{0.10})_{100-x}O_x$ metallic glasses. Later, several investigators [44, 45] indicated that oxygen stabilizes the *i*-phase in Zr based alloys. Murty reported the first direct evidence for the oxygen stabilization of *i*-phase in $Zr_{65-x}Cu_{27.5}Al_{7.5}O_x$ (x=0.43 and 0.82) alloys using 3DAP. Saida [46] reported that a quasicrystalline phase in the Zr-based alloys is precipitated under the existence of oxygen impurity above 1700 ppm mass% and the precipitation of the icosahedral phase strongly

depends on the cooling rate and oxygen content in the sample preparation. Murty have recently reported [47] that the *i*-phase is indeed stabilized by the presence of oxygen in Zr–Cu–Al amorphous alloy beyond a critical concentration of 0.4 at.%. Sordelet [48] also studied oxygen-stabilized glass formation in Zr-Pt melt-spun ribbons. It was pointed out that there is critical oxygen content of 1053 ppm for forming fully amorphous at a specific quench rate. When the oxygen is low, the ribbons are fully crystallized. At higher oxygen, the system forms mixed amorphous and quasi-crystalline structures. Adding more oxygen into the system as high as 4737 ppm, it was found that the ribbons consist of quasicrystalline and crystalline phases in an amorphous matrix.

However, since the control of oxygen content is difficult, the reproducibility of the these experiments is poor [49].

(2) The effect of noble metals:

In contrast, the reproducibility of *i*-phase precipitation in NM-containing (noble metal, NM=Pd, Pt, Au or Ag) Zr-based metallic alloys is good [50]. There are also numerous reports about *i*-phase precipitation in NM-containing Zr-based metallic alloys [50]. Therefore, it has been concluded that the addition of noble metals to the Zr-based alloys is important for the formation of a reproducible *i*-phase. For these reasons, the formation of the *i*-phase and the crystallization pathways in the NM-containing Zr-based alloys has attracted great attention.

In the Zr-Pd-Cu metallic glass, Saksl [51] reported that when the $Zr_{70}Cu_{29}Pd_1$ glassy alloy was annealing up to 850 K, the formation of icosahedral quasicrystalline phase followed by crystallization of tetragonal $CuZr_2$ has been observed. While, the binary $Zr_{70}Cu_{30}$ alloy only shows a single glassy to crystalline $CuZr_2$ phase transformation. From figure 1-3,

the *in situ* high-temperature XRD (with a wavelength of 0.05904 nm) patterns indicate that only substituting 1% Cu by Pd can change the crystallization pathway of $Zr_{70}Cu_{30}$ amorphous alloy.

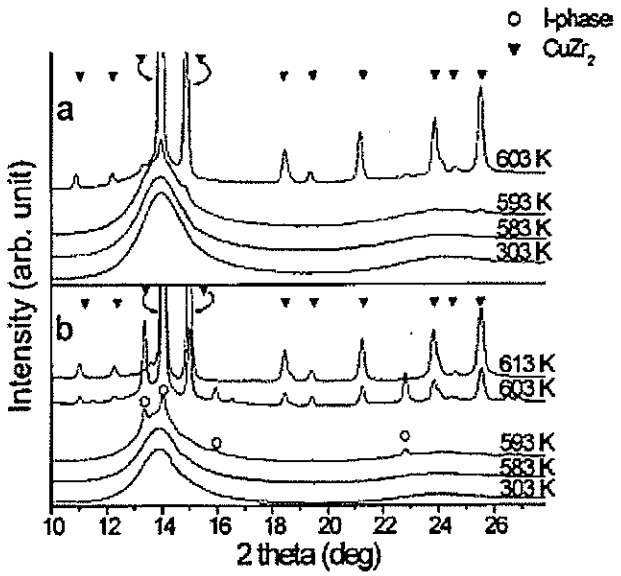

Figure 3. *In situ* high-temperature XRD patterns of (a) $Zr_{70}Cu_{30}$ and (b) $Zr_{70}Cu_{29}Pd_1$ ribbon samples

(3) The effect of other elements

The addition of other elements can also cause the formation of the *i*-phase. Xing *et al.* [52] and Li [49] both reported nanoquasicrystallization in the Zr–Ni–Cu–Al amorphous alloy containing Ti. Saida [53, 54] studied icosahedral quasicrystalline phase formation in Zr-Al-Ni-Cu glassy alloys by addition of Nb, Ta and V elements. Ouyang[55] recently reported devitrification of Zr-Ni-Al-Cu-Ti (Nb,Ta) glassy alloys by x-ray diffraction, TEM, and differential scanning calorimetry. He pointed out that icosahedral phase was found to coexist with crystalline structures in alloys contain 5 at.% Ta.

Metastable and stable crystalline phase formation in the Zr-based metallic glass

Trying to explain the nature of the meta stable and stable phase formation during the crystallization process in metallic glass, besides Hume-Rothery's earlier work [9] combined the size and electron factor together, Dong *at al.* [56] have developed a constant e/a criteria for bulk metallic glass-related phases, including quasicrystals and crystalline counterparts. The authors reported that quasicrystals and their approximants share similar electron concentrations.

As briefly mentioned above, Ohata and Pettifor [10] discussed the different roles played by atomic size and electronic factors in stabilizing the transition metal Laves phases AB_2 against the two competing phases: *C11b* and *C16*. In the first step, the volume of the different structures is adjusted, based on the following equation (Figure 1-4 (a)):

$$\frac{\Delta V}{V} = \frac{3}{10}\frac{\Delta\alpha_{AB} + R^5\Delta\alpha_{AA} + R^{-5}\Delta\alpha_{BB}}{\alpha_{AB} + R^5\alpha_{AA} + R^{-5}\alpha_{BB}}$$

In which, R is the relative size factor which is defined by $R = \frac{r_A}{r_B}$, α is the structure coefficients. The lef-hand panel of figure 1-4 shows that For R = 1, BCC-based lattice *C11b* ($MoSi_2$) is more closely packed than either the Laves phases or *C16* ($CuAl_2$); For R > 1.31, Laves phase assume a more compact lattice than BCC; *C16* becomes more compact as R < 0.84.

In the second step, an experimental AB_2 structure map (Figure 1-4 (b)) is found if size and electronic factors are both included, which is shown as the right-hand panel in figure 1-4. In the structure map, the closed circle is *C14* phases, the open circle is *C15* phase, the open square is *C36* phase, the cross symbol is *C11b* phase, and the open diamond is *C16* phase.

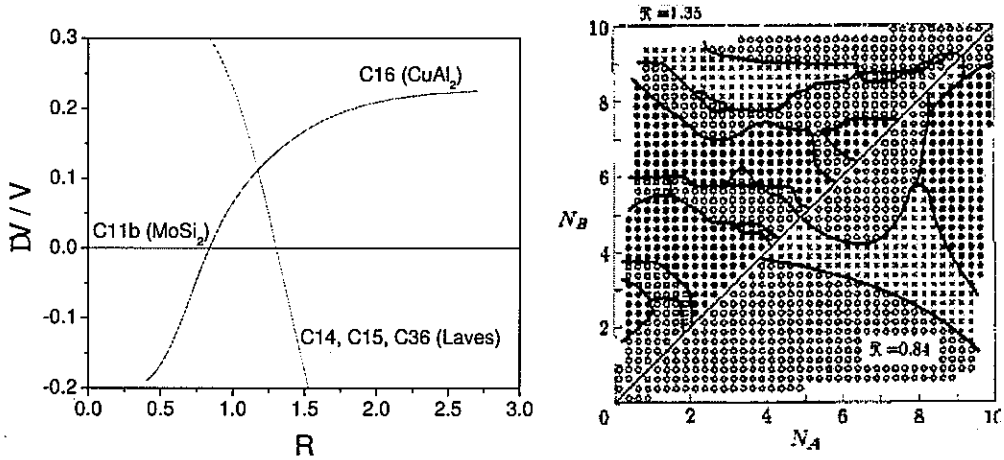

(a) (b)

Figure 4. (a) The fractional change in prepared volume ΔV/V with respect to the *C11b* ($MoSi_2$) lattice versus the relative size factor R; (b) The theoretical structure maps for R=1.35 and R=0.84

There are numerous reports about the meta stable and stable phase formation during the crystallization process in Zr-based metallic glass [51, 57].Using high temperature X-ray diffraction (HTXRD), Kramer [58] studied the devitriffication of $Zr_{70}Pd_{30}$ and $Zr_{70}Pd_{20}Cu_{10}$ metallic glasses (Figure 1-5). Crystal structure of the meta-stable phase and stable phase were obtained by Rietveld fitting the XRD patterns.

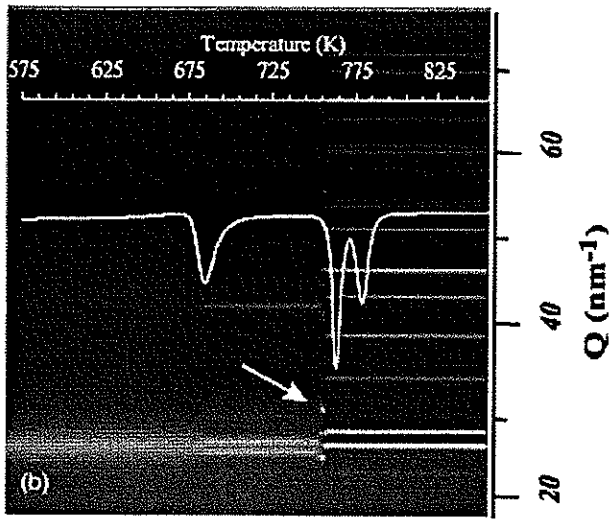

Figure 5. Image plate data for $Zr_{70}Pd_{20}Cu_{10}$ at a heating rate of 40 K/min using HEXRD. The white lines are an overlay of the DSC curves.

From the study, both alloys have similar as-quenched structures and initially devitrify to form a meta-stable quasicrystalline phase. The HTXRD data for the $Zr_{70}Pd_{30}$ alloy shows the coexistence of the quasicrystalline and the *I4/mmm* crystalline structure over a range of 25 K. Conversely, the $Zr_{70}Pd_{20}Cu_{10}$ alloy shows an additional transformation of the quasicrystalline phase to a meta-stable Zr_2(Pd/Cu) intermetallic *I4/mcm* structure (also *C16*), which polymorphically transforms to the *C11b* phase over a very narrow temperature range.

Brauer *et al.* report [59] that cubic phase (space group O_h^7) formed in the crystallization of amorphous Zr_2Ni. But according to Ohata's theoretical structure maps [10], the radius ratio $R = \frac{r_{Ni}}{r_{Zr}} = 0.81$; valence electrons of outer shell N_{Zr}=2, N_{Ni}=8, it indicates that *C16* phase should be the equilibrium phase for Zr_2Ni metallic glass, if both size and electronic factors are considered. Considering that slightly higher Oxygen contents (1 at.%) cause cubic phase formed in Zr-Cu-Ni-Al metallic glass [60]. The reported cubic equilibrium

phase in Zr_2Ni metallic glass may be affected by oxygen content since the oxygen content was not mentioned in the literature.

Experimental methods

Arc melting: We use arc melting to melt the high purity meal elements and obtain homogenous alloy ingots. Arc furnaces consist of five basic components: a chamber with refractory vertical cylindrical sidewall, a removable electrode with support arms, a power transformer, water-cooled system, and evacuation/gas system. Electric power is supplied from a three phase multi-voltage transformer. The arc is produced by striking current from a charged electrode to the metal. The electrodes are connected by heavy flexible cables to the transformer, which is located as close to the furnace as possible to avoid excessive power loss. The metal acts as an electrode, and is melted by striking an arc between a charged electrode and the metal.

Melt spinning: We use melt spinning to make metallic glass ribbons. Melt spinning is the preferred method of cooling of liquids. A copper wheel is rotated internally in a high purity Helium atmosphere. The ingot, which is made by arc melting, is melted in the graphite crucible by heating coil, and a thin stream of liquid is forced onto the rapidly rotating copper wheel by a Helium blast, causing rapid solidification. The cooling rates achievable by melt-spinning are on the order of 10^4 ~10^7 K/s. However, the melt spinner is only able to produce small thin ribbon shaped specimens. This limits melt spinning to mainly production of research specimens for alloys with high critical cooling rate.

Differential scanning calorimetry (DSC): DSC is a technique we use to study what happens to metallic glass when they're heated. Both the sample and reference are maintained at nearly the same temperature throughout the experiment. We use it to study the thermal transitions, such as subtle glass transitions and phase transformations. This technique is associated with the later introduced X-ray diffraction and synchrotron radiation, which provide detail structural information during the thermal transitions. The basic principle underlying this technique is that, when the sample undergoes a physical transformation such as phase transitions, more (or less) heat will need to flow to it than the reference to maintain both at the same temperature.

Differential thermal analysis (DTA): We use DTA to determine the melting temperature of two designed system alloys. A DTA apparatus consist of a sample holder comprising thermocouples, sample containers and a ceramic or metallic block, a furnace, a temperature programmer, and a recording system. The key feature is the existence of two thermocouples connected to a voltmeter. One thermocouple is placed in an inert material such as Al_2O_3, while the other is placed in a sample of the material under study. In DTA, the metallic glass under study and an inert reference are heated (or cooled) under identical conditions.

Annealing: We use torch to seal the quarts tubes, which contain the target alloys in wrapped Tantalum foil, then anneal them in a temperature controlled furnace. Annealing is carried out in a high purity Argon atmosphere to avoid oxidation. We use this technique to get the high temperature equilibrium phase for future X-ray diffraction structural analysis. Annealing is a very common heat treatment in metallurgy and material science. It is a process that produces conditions by heating and maintaining a suitable temperature, and then cooling.

Annealing occurs by the diffusion of atoms within a solid material, so that the material progresses towards its equilibrium state.

Transmission electron microscope (TEM) and Energy dispersive spectroscopy (EDS): We use TEM to observe the grain growth process in the metallic glass, with the specimens prepared by DSC, which are quenched rapidly in DSC cells at different points on the phase transformation curve. The alloy ribbons are ion beam milled thin enough for the beam to penetrate. TEM is a microscopy technique, in which, a beam of electrons is transmitted through an ultra thin specimen, interacting with the specimen. After magnified and focused by an objective lens, an image is formed. The high resolution TEM (HRTEM) technique allows the direct observation of alloy structure at atomic scale. We use EDS to determine the grain compositions of different phases during the crystallization process. EDS is an analytical technique for the elemental analysis. Its fundamental characterization principle is based on that each element of the periodic table has unique atomic structure, and the x-rays, which are characteristic of an element's atomic structure, be uniquely distinguished from each other.

X-ray diffraction (XRD), Synchrotron radiation and Rietveld refinement: We extensively use x-ray scattering techniques and Rietveld refinement to study both amorphous and crystalline structures during the whole crystallization process. X-ray scattering techniques are based on observing the scattered intensity of an x-ray beam hitting a sample as a function of scattered angle. Conventional x-ray diffractometers consist of an x-ray generator, a goniometer, sample holder, and an x-ray detector. X-ray tubes generate x-rays by bombarding a metal target with high-energy (10 - 100 keV) electrons, which knock out core electrons. An electron in an outer shell fills the hole in the inner shell and emits an x-ray

photon. We use a common target Cu, which have strong Kα x-ray emission at 1.5418 Å. X-rays can also be generated by accelerating charged particles in a synchrotron ring, which are used for a wide range of analytical techniques. These sources produce a continuous spectrum of x-rays and require a crystal monochromator to select a single wavelength. Some properties of the Synchrotron radiation are: (1) High intensity, which is many orders of magnitude more than with X-rays produced in conventional X-ray tubes; (2) High brilliance, which exceeds other natural and artificial light sources by many orders of magnitude; (3) High collimation with small angular divergence of the beam; (4) Widely tunable in energy/wavelength by monochromatization; (5) High level of polarization.

Most our synchrotron experiments are performed at the Advanced Photon Source (APS) in Argonne National Laboratory (ANL), which is a national synchrotron x-ray research facility funded by the Office of Basic Energy Sciences, U.S. Department of Energy. The APS provides high energy and the brightest x-ray beams in the west hemisphere. The extremely high photon flux of HEXRD allows rapid data collection with controlled temperature programs, which make real time *in situ* observation of crystallization studies possible. The high energy of the X-ray provides short wavelength and such *in situ* studies provide detailed structural information about the crystallization material throughout the transformation. Moreover, it is very convenient for rapidly changing and controlling the state of the system under study, which is better than those of conventional techniques [39]

Our synchrotron radiation experiments (also named high energy x-ray diffraction "HEXRD" or high temperature x-ray diffraction "HTXRD" in this thesis) performed at both room temperature environment and in temperature controlled furnace. The instruments are presented below.

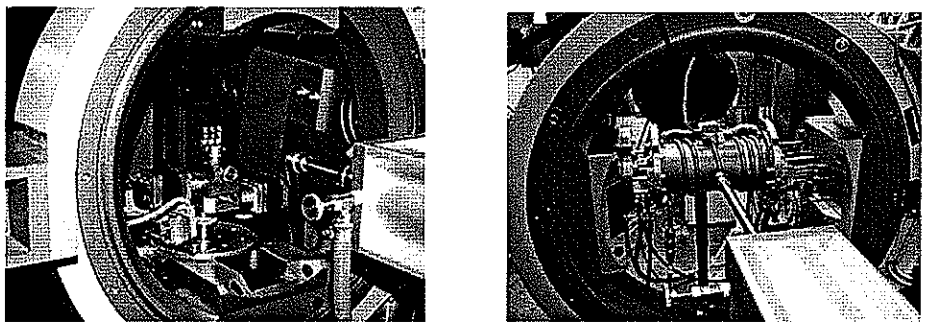

(a) (b)

Figure 6. Synchrotron radiation experimental instruments performed (a) at room temperature; (b) at temperature controlled furnace.

To characterize the crystallographic structure, we need to mention Bragg's Law first. Bragg's Law explains the diffraction of x-rays or neutrons of crystal surfaces at certain angles. The equation refers to the simple equation $n\lambda = 2d\sin\theta$, which was derived by the English physicists Sir W.H. Bragg and his son Sir W.L. Bragg [61]. The variable d is the distance between atomic layers in a crystal, and the variable lambda λ is the wavelength of the incident X-ray beam, n is an integer. We use Rietveld refinement [62] to characterize the x-ray diffraction patterns with peaks in intensity at certain positions. The Rietveld method uses a least squares approach to refine a theoretical line profile until it matches the measured profile. The height, shape and position of these peaks can be used to determine materials structure. Using Rietveld analysis, we can get quantitative overview of all parameters based on structures, such as lattice, atomic positions and phase fractions. There are lots of Rieveld software available, such as GSAS (General Structure Analysis System), Rietica, Hugo Rietveld, *etc.* We use the GSAS software package with the EXPGUI interface to perform Rietveld analysis. GSAS has been created by Allen C. Larson and Robert B. Von Dreele at Los Alamos National Laboratory. It is a comprehensive system for the refinement of

structural models for both x-ray and neutron diffraction data. We must start with approximate values for all parameters, then, we allow the software to optimize a small subset of the parameters before any progress can be made. Slowly, additional parameters are selected to be refined, until all parameters in the model (if the data support that) are refined.

Ab initio calculation: The Latin term *ab initio* means "from the beginning". In science, "*ab initio*" or "first principles" relies on basic and established laws of nature without additional assumptions. *Ab initio* calculation is a molecular dynamics simulation package. We use Vienna *Ab initio* Simulation Package (VASP) to theoretically evaluate the phase stability. VASP is a package for performing *ab initio* quantum-mechanical molecular dynamics (MD) using pseudopotentials and a plane wave basis set. The approach implemented in VASP is based on a finite-temperature local-density approximation, with the free energy as variational quantity, and an exact evaluation of the instantaneous electronic ground state at each MD-step. Electronic structure calculations are employed to get the total energies of the competing crystalline structures. All calculations are performed within the density functional theory formalism.

Thesis organization

The thesis is divided into six chapters. The first chapter is the general introduction, including the thesis organization, literature review and motivation.

The second chapter focuses on the study of *i*-phase formation during the devitrification of the $Zr_2Pd_xCu_{(1-x)}$ metallic glass. In this chapter, the short range order (SRO)

and the thermal characteristics of the $Zr_2Pd_xCu_{(1-x)}$ metallic glass will be described and discussed. The influence of Pd on formation of amorphous and quasicrystal phases will be summarized and discussed.

The third chapter will mainly discuss the meta-stable *C16* phase formation in the $Zr_2Pd_xCu_{(1-x)}$ metallic glass. In this chapter, the experimental observation of devitrification pathways in $Zr_2Pd_xCu_{(1-x)}$ metallic glass will be described. The electronic structure of the *C11b* and *C16* phases at five compositions will be calculated. Finally, the relationship between the theoretical and experimental studies of devitrification pathways in the $Zr_2Pd_xCu_{(1-x)}$ system will be presented.

The fourth chapter details the high temperature stability of *C11b* phase in $Zr_2Pd_xCu_{(1-x)}$ metallic glass. This chapter focuses particularly on the role of Pd on changing the bonding of the *C11b* lattice. The changes in the crystalline lattice as a function of temperature and composition were measured using *in situ* high energy X-ray diffraction (HTXRD) observation. The coefficients of thermal expansion are determined and these results are interpreted in light of and *ab initio* calculations.

The fifth chapter discusses the crystallization pathways of $Zr_2Ni_xCu_{(1-x)}$ metallic glass by HEXRD, thermal analysis and transmission electron microscopy (TEM). Both meta-stable and stable phases in the crystallization pathways will be described and discussed. A schematic phase diagram for the $Zr_2Ni_xCu_{(1-x)}$ system will be proposed.

Chapter six is a general conclusion which summarizes the effects of additive elements Pd and Ni on the crystallization pathways in the $Zr_2Pd_xCu_{(1-x)}$ and $Zr_2Ni_xCu_{(1-x)}$ metallic glass.

Reference

[1] F. C. Frank, Proc. Roy. Soc. (London) 215A, 43-6 (1952).

[2] K. F. Kelton, G. W. Lee, A. K. Gangopadhyay, et al., Physical Review Letters 90, 195504/1 (2003).

[3] A. Inoue, T. Zhang, and T. Masumoto, Journal of Non-Crystalline Solids 156-158, 598-602 (1993).

[4] M. Laridjani and J. F. Sadoc, Journal of Non-Crystalline Solids 106, 42-6 (1988).

[5] J. Z. Jiang, K. Saksl, J. Saida, A. Inoue, H. Franz, K. Messel, and C. Lathe, Applied Physics Letters 80, 781-783 (2002).

[6] T. Egami and Y. Waseda, Journal of Non-Crystalline Solids 64, 113-34 (1984).

[7] D. B. Miracle, W. S. Sanders, and O. N. Senkov, Philosophical Magazine 83, 2409-2428 (2003).

[8] D. B. Miracle, Nature Materials 3, 697-702 (2004).

[9] W. Hume-rothery, Philosophical Magazine (1798-1977) 13, 196-7 (1932).

[10] Y. Ohta and D. G. Pettifor, Journal of Physics: Condensed Matter 2, 8189-94 (1990).

[11] T. B. Massalski, Binary Alloy Phase Diagrams, 1987

[12] A. Inoue, Acta Materialia 48, 279-306 (2000).

[13] W. Klement, Jr., R. H. Willens, and P. Duwez, Nature (London, United Kingdom) 187, 869-70 (1960).

[14] J. D. Bernal, Nature (London, United Kingdom) 183, 141-7 (1959)

[15] C. N. J. Wagner, Advances in X-Ray Analysis 12, 50-71 (1969)

[16] R. Yamamoto and M. Doyama, Journal of Physics F: Metal Physics 9, 617-27 (1979)

[17] D. Turnbull, Contemp. Phys. 10 437-488 (1969)

[18] D. Turnbull and J. C. Fisher, Journal of Chemical Physics 17, 71-3 (1949).

[19]W. L. Johnson, MRS Bulletin 24, 42-55 (1999).

[20] Z. P. Lu and C. T. Liu, Acta Materialia 50, 3501-3512 (2002).

[21] T. A. Waniuk, J. Schroers, and W. L. Johnson, Applied Physics Letters 78, 1213-1215 (2001).

[22] A. Inoue, W. Zhang, T. Zhang, and K. Kurosaka, Acta Materialia 49, 2645-2652 (2001).

[23] Z. P. Lu and C. T. Liu, Physical Review Letters 91, 115505/1-115505/4 (2003).

[24] M. Laridjani and J. F. Sadoc, Journal of Non-Crystalline Solids 106, 42-6 (1988).

[25] J. Z. Jiang, K. Saksl, J. Saida, A. Inoue, H. Franz, K. Messel, and C. Lathe, Applied Physics Letters 80, 781-783 (2002).

[26] Z. Altounian, G. Tu, and J. O. Strom-Olsen, Journal of Applied Physics 54, 3111-16 (1983).

[27] B. S. Murty, D. H. Ping, and K. Hono, Applied Physics Letters 77, 1102-1104 (2000).

[28] Y. D. Dong, G. Gregan, and M. G. Scott, Journal of Non-Crystalline Solids 43, 403-15 (1981).

[29] A. Calka, M. Madhava, D. E. Polk, B. C. Giessen, H. Matyja, and J. Vander Sande, Scripta Metallurgica 11, 65-70 (1977).

[30] W. L. Johnson, S. J. Poon, J. Durand, and P. Duwez, Physical Review B: Solid State 18, 206-17 (1978).

[31] H. S. Chen, Applied Physics Letters 29, 12-14 (1976).

[32] S. R. Nagel and J. Tauc, Physical Review Letters 35, 380-3 (1975).

[33] M. Naka, S. Tomizawa, T. Masumoto, and T. Watanabe, Rapidly Quenched Met., Int. Conf., 2nd, 273-9 (1976).

[34] A. Inoue, K. Kobayashi, and T. Masumoto, Proc. - Conf. Met. Glasses: Sci. Technol. 2, 217-22 (1981).

[35] D. Turnbull, Journal of Applied Physics 21, 1022-7 (1950).

[36] S. Sachdev and D. R. Nelson, Physical Review Letters 53, 1947-50 (1984).

[37] F. S. Pierce, S. J. Poon, and Q. Guo, Science 261, 737 (1993).

[38] C. Janot, Phys. Rev. B 53, 181 (1996).

[39] B. S. Murty, D. H. Ping, K. Hono, and A. Inoue, Scripta Materialia 43, 103-107 (2000).

[40] M. Matsushita, J. Saida, C. Li, and A. Inoue, J. Mater. Res. 15, 1280 (2000).

[41] B. S. Murty, D. H. Ping, K. Hono, and A. Inoue, Applied Physics Letters 76, 55-57 (2000).

[42] U. Koester, J. Meinhardt, S. Roos, et al., Applied Physics Letters 69, 179 (1996).

[43] J. Eckert, N. Mattern, M. Zinkevitch, and M. Seidel, Mater. Trans., JIM 39, 623 (1998).

[44] U. Koster, A. Rudiger, and J. Meinhardt, in Proceedings of the 6th International Conference on Quasicrystals, ed. S. Takeuchi and T. Fuziwara, p. 317, World Scientific, Singapore (1998).

[45] D. Zander, R. Janleeing, A. Rudiger, and U. Koster, Mater. Sci. Forum. 307, 25 (1999).

[46] J. Saida, M. Matsushita, C. Li, and A. Inoue, Applied Physics Letters 76, 3558-3560 (2000).

[47] B. S. Murty, D. H. Ping, K. Hono, and A. Inoue, Acta Materialia 48, 3985-3996 (2000).

[48] D. J. Sordelet, X. Y. Yang, E. A. Rozhkova, M. F. Besser, and M. J. Kramer, Applied Physics Letters **83,** 69-71 (2003).

[49] C. Li and A. Inoue, Journal of Alloys and Compounds 325, 230 (2001).

[50] A. Inoue, T. Zhang, M. W. Chen, T. Sakurai, J. Saida, and M. Matsushita, Applied Physics Letters 76, 967-969 (2000).

[51] K. Saksl, H. Franz, P. Jovari, et al., Applied Physics Letters 83, 3924 (2003).

[52] L. Q. Xing, J. Eckert, W. Loser, and L. Schultz, Applied Physics Letters 74, 664-666 (1999).

[53] J. Saida and A. Inoue, Journal of Physics: Condensed Matter 13, L73 (2001).

[54] J. Saida and A. Inoue, Journal of Non-Crystalline Solids 312-314, 502 (2002).

[55] L. J. Ouyang, D. V. Louzguine, H. M. Kimura, et al., Materials Research Bulletin 39, 1347 (2004).

[56] C. Dong, A. Perrot, J. M. Dubois, and E. Belin, Materials Science Forum 150-151, 403-16 (1994).

[57] J. Saida, M. Matsushita, and A. Inoue, Journal of Applied Physics 88, 6081-6083 (2000).

[58] M. J. Kramer, M. F. Besser, N. Yang, *et al.*, Journal of Non-Crystalline Solids 317, 62 (2003).

[59] S. Brauer, J. O. Strom-Olsen, M. Sutton, *et al*, Physical Review B, 45, 7704 (1992).

[60] U. Koster, D. Zander, and R. Janlewing, Materials Science Forum 386, 89 (2002)

[61] W. L. Bragg, Z. Anorg. Chem. 90, 153-68 (1915)

[62] H. M. Rietveld, Journal of Applied Crystallography 2, 65-71 (1969)

CHAPTER 2. INFLUENCE OF PD ON FORMATION OF AMORPHOUS AND QUASICRYSTAL PHASES IN RAPIDLY QUENCHED $ZR_2CU_{(1-X)}PD_X$

A paper published in Philosophical Magazine

MIN XU[1,2], Y YE[1,2], J. MORRIS[3], D. J. SORDELET[1,2], M.J. KRAMER[1,2,*]

Abstract

The role of Pd in the transformation from an amorphous state to a metastable icosahedral quasicrystalline phase in $Zr_2Cu_{(1-x)}Pd_x$ (x = 0 to 1) metallic glasses was investigated using high-energy synchrotron X-rays and differential scanning calorimetry. The total scattering functions show an increasing development of the high-Q side of the second diffuse scattering peak at 5.09 $Å^{-1}$ with increasing Pd content. The reduced radial distribution functions reveals that the bonding distance of the Zr-(Pd/Cu) pairs increases from 2.76 Å to

---

Reprinted with permission of Philosophical Magazine 86, 389-395 (2006)

[1]Department of Materials Science and Engineering, Iowa State University, Ames, IA 50011, USA

[2]Materials and Engineering physics Program, Ames Laboratory(USDOE) Ames, IA 50011, USA

[3]Metals and Ceramics Division, Oak Ridge National Laboratory, Oak Ridge, TN 37831-6115, USA

*Corresponding author: email: mjkramer@ameslab.gov; phone: 515-294-0276

2.82 Å when x increases from 0.00 to 1.00, while the distance for the Zr-Zr pairs remains almost constant at 3.10Å. Thermal analysis and X-ray diffraction together show that an amorphous-to-quasicrystal phase transition is not observed in the Zr_2Cu alloy, but partial or total substitution of Cu by Pd in $Zr_2Cu_{(1-x)}Pd_x$ alloys does lead to quasicrystal formation.

Keywords: Zr-based alloys; Amorphous; Icosahedral quasicrystal; Short-range order; Thermal analysis

Introduction

Koester's first report of icosahedral quasicrystalline (*i*-phase) formation during crystallization of a Zr-Cu-Ni-Al amorphous alloy [1] has stimulated considerable research interest in metastable phases in Zr-based alloys. Eckert *et al.* [2] first demonstrated that crystallization to the *i*-phase is influenced significantly by the amount of oxygen in a $Zr_{65}Al_{7.5}Cu_{17.5}Ni_{10}$ metallic glass. Murty[3] and Saida[4] reported that *i*-phase formation appears to depend strongly on the minor element additions of Pd, Pt, Au, V, Nb and Ta to comparable Zr-Cu-Ni-Al systems. In addition, *i*-phase formation in Zr-Pd-Cu metallic glasses has been extensively reported in recent years [5~9], but no systematic study has been published to explain the effect of the Pd:Cu ratio on the *i*-phase formation process. It is uncertain what the linkage is between the short-range order (SRO) in an as-quenched glass and the formation of a quasicrystalline phase [10, 11] in these particular systems, particularly because most investigations have mainly focused on Zr-Pd binary systems [12, 13] or the

ternary Zr-Pd-Cu metallic glass [6, 14]. In the current study, a systematic investigation was performed to examine the relationship between SRO and *i*-phase formation of Zr-Pd-Cu metallic glasses. The as-quenched amorphous structure of amorphous $Zr_2Cu_{(1-x)}Pd_x$ (x = 0.00, 0.25, 0.50, 0.75 and 1.00) alloys were compared, in conjunction with thermal analysis, to determine what effect of substituting Pd for Cu has on formation of a quasicrystalline phase during crystallization of these alloys.

Experimental

Five alloys of $Zr_2Cu_{(1-x)}Pd_x$ (x = 0.00, 0.25, 0.50, 0.75 and 1.00) were prepared by arc melting mixtures of pure Zr (99.95 mass%), Pd (99.97 mass%) and Cu (99.99 mass%) metals in an ultra-high purity Ar atmosphere. The alloys were melt spun at a wheel speed of 25m/s and a constant over pressure of 1.6×10^4 Pa in an ultra-high purity He atmosphere. The O content of the as-quenched ribbon samples was analyzed by inert gas fusion to be less then 250 ppm mass.

High-energy X-ray diffraction (HEXRD) (130keV, ? = 0.09537 Å) at the Advanced Photon Source, Argonne National Laboratory, was used to investigate the changes in the total scattering function (S(Q)) of amorphous as-spun and partially devitrified annealed alloys. Thermal characteristics of these alloys were studied using a Perkin-Elmer differential scanning calorimeter (DSC) under N_2 in a continuous heating mode of 0.67K/s. Laboratory Cu-Ka X-ray diffraction (XRD) was performed with a Philips Model 1783 Diffractometer to determine the structure of initial metastable devitrification phases.

Results and discussion

Structure of as quenched $Zr_2Cu_{(1-x)}Pd_x$ alloys

The corrections of the raw intensity HEXRD data to obtain the total scattering function, *S(Q)* [5, 14], involve the subtraction of the instrument background, correction for absorption, self-absorption, multiple scattering, polarization, Compton scattering, Laue diffuse scattering, and finally normalization to the *S(Q)*. The *S(Q)* data for the as-quenched samples are shown in Fig. 1.

With increasing Pd content, the most prominent change in the S(Q) data is the enhancement of the shoulder at 5.09$Å^{-1}$ on the high-Q side of the second diffuse peak, which systematically increases in magnitude from 1.04 to 1.10 with increasing Pd:Cu ratio. The relative locations of the first two peaks in *S(Q)*, Q_2/Q_1 = 1.71 and $Q_{shoulder}/Q_1$ = 1.97, where $Q_{shoulder}$ is the location of the shoulder on the second peak, are in good agreement with the values reported by Kelton *et al.*[10], Q_2/Q_1 = 1.72 and $Q_{shoulder}/Q_1$ =1.97, which they proposed as an indication of local icosahedral order. Our *S(Q)* data appear to suggest increasing icosahedral SRO (ISRO) in the as-quenched alloys with increasing Pd.

The reduced radial distribution functions, G(r), for these five as-quenched melt spun $Zr_2Cu_{(1-x)}Pd_x$ alloys, Fig. 2, were obtained by Fourier transforming the *S(Q)* results. The radial distances for the atomic shells are about 3.00Å, 5.38 Å, 7.71 Å and 10.28 Å, which correspond to the first four nearest-neighbor distance in $Zr_2Cu_{(1-x)}Pd_x$. The first diffuse

scattering peaks in the G(r) data exhibit a dramatic change of the first shell with substitution of Pd for Cu. All the alloys show a split in the first shell, indicating two distinctly different groupings of pair-pair lengths. However, in the first shell an increasing intensity of the left side relative to the right side with increasing Pd content indicates that substitution of Cu by Pd has a profound influence on the SRO. The shorter bond distances increase with Pd from 2.76 Å to 2.82 Å, while the radial distance of the right side peaks remain almost at the same position at 3.10Å ($0 = x = 1$). The differences in the values of the radial distances of the five samples are reasonably in good agreement with contributions from Cu/Pd-Cu/Pd to Zr-(Pd/Cu) or Zr-Zr pairs. For Zr-Pd-Cu system, Zr-Zr and Zr-(Pd/Cu) pairs dominate the scattering, while Pd/Cu-Pd/Cu pairs only make a small contribution [12]. The intensity increase in the left-side of the first peak with increasing Pd relative to the right side may be due to increasing Zr-Pd pairs, consistent with the stronger affinity of Pd for Zr compared to Cu. The shift of the left side peak towards bnger radial distances with increasing Pd content is consistent with the slightly larger bonding radius of Pd (1.28Å) compared to Cu (1.17Å).

The apparent increase in the ISRO in the as quenched $Zr_2Cu_{(1-x)}Pd_x$ alloys supports the observation of the quasicrystal formation in $Zr_2Cu_{(1-x)}Pd_x$ alloys when $x > 0$. However, earlier reports of only a small addition of Pd (~ 1 at. %) giving rise to the formation of the *i*-phase during devitrification [4] indicates that Pd may be an even more potent minor alloying addition than our scattering data would suggest.

Thermal characteristics study on as quenched $Zr_2Cu_{(1-x)}Pd_x$ alloys

The DSC results for $Zr_2Cu_{(1-x)}Pd_x$ alloys are shown in Fig. 3, and the tabulated values for the glass transition temperature (T_g), onset temperatures for crystallization (T_x) and exothermic heat (? H) of the first crystallization peak are presented in Table 1.

Consistent with the structural changes discussed above, substituting Pd for Cu strongly affects the devitrification behavior. The DSC results from the amorphous binary Zr_2Cu alloy show only one exothermic peak, resulting when the high-temperature, stable $MoSi_2$-type tetragonal C11b structure (Space group: *I4/mmm*) forms directly from the glass (see below). By substituting Pd for Cu, the alloys crystallize in multiple stages. The temperature of the primary crystallization to the *i*-phase increases from 661 to 733 K with increasing Pd (Table 2-1). The subsequent devitrification involves two closely spaced exothermic events, whose details vary with temperature. The exothermic heats in the formation of *i*-phase of $Zr_2Cu_{(1-x)}Pd_x$ system have a maximum value at $x = 0.50$; moreover, a distinct glass transition temperature is not observed at $x = 0.75$ and 1.00.

In order to understand the nature of the first stage of crystallization, isothermal DSC runs were performed to more closely examine the evolving structure during initial devitrification. All five alloys were heated in the DSC at 0.67 K/s to 20K below the first crystallization onset temperature, annealed for 500 seconds and then rapidly cooled. The isothermal DSC data show that the onset time of the transformation for the primary metastable phase was delayed by approximately 103 s when Pd was varied from $x = 0.25$ to 1.00. This might suggest that Pd enhances the stability of the amorphous phase relative to the *i*-phase. The evolving structures of the samples from the isothermal runs were subsequently studied by XRD. As seen in Fig. 4, the XRD spectra demonstrate that all the

alloys, except Zr_2Cu, yielded a quasicrystalline phase as the first devitrification product, while the diffraction pattern of Zr_2Cu was indexed as the $MoSi_2$-type tetragonal C11b phase. Thus, the substitution of Pd for Cu clearly altered the devitrification pathways of the amorphous alloys. The first crystallization peak observed in DSC of $Zr_2Cu_{(1-x)}Pd_x$ (x = 0.25, 0.50, 0.75 and 1.00) alloys can be attributed to the precipitation of *i*-phase from the amorphous phase. This agrees reasonably well with our current HEXRD *S(Q)* data for the $Zr_2Cu_{(1-x)}Pd_x$ alloys as well as previous reports from time-resolved HEXRD [7, 14].

Conclusion

Using HEXRD, the effect of Pd on altering the SRO of $Zr_2Cu_{(1-x)}Pd_x$ (x = 0.00, 0.25, 0.50, 0.75 and 1.00) alloys was demonstrated. The *S(Q)* data show a systematic increase in the high Q-side shoulder of the second diffuse scattering peak around 5.09Å, which is consistent with increasing ISRO. The radial distance corresponding to Cu/Pd – Cu/Pd and Zr-(Pd/Cu) pairs and the number of these pairs increases with increasing Pd content. XRD analysis illustrates that the *i*-phase is the first devitrification product for ternary alloys (i.e., x > 0). Thermal analysis with DSC reveals distinctly different devitrification pathways among the $Zr_2Cu_{(1-x)}Pd_x$ alloys with increasing Pd/Cu ratio. Addition of Pd tends to delay the onset time for and temperature of the transformation from amorphous to *i*-phase, indicating increased stabilization of the amorphous structure. It remains unclear, however, why the substitution of Pd for Cu is such a potent modifier of the structure and devitrification pathway in this system.

Acknowledgements

This research has been sponsored by the Division of Materials Sciences and Engineering, Office of Basic Energy Sciences, U.S. Department of Energy under contract DE-AC05-00OR-22725 with UT-Battelle and contract W-7405-ENG-82 with Iowa State University. The Midwest Universities Collaborative Access Team (MUCAT) sector at the APS is supported by the US Department of Energy, Office of Science, Basic Energy Sciences, through the Ames Laboratory. Use of the Advanced Photon Source was supported by the US Department of Energy, Office of Science, Basic Energy Sciences, under Contract No. W-31-109-Eng-38.

References

[1] Koester, U., Meinhardt, J., Roos, S., and Liebertz, H., Applied Physics Letters **69**, 179 (1996).

[2] Eckert, J., Mattern, N., Zinkevitch, M., and Seidel, M., Mater. Trans., JIM **39**, 623 (1998).

[3] Murty, B. S., Ping, D. H., Hono, K., and Inoue, A., Scripta Materialia **43**, 103 (2000).

[4] Saida, J., Matsushita, M., Li, C., and Inoue, A., Philosophical Magazine Letters **80**, 737 (2000).

[5] Kramer, M. J., Besser, M. F., Yang, N., Rozhkova, E., Sordelet, D. J., Zhang, Y., and Lee, P. L., Journal of Non-Crystalline Solids **317**, 62 (2003).

[6] Saksl, K., Franz, H., Jovari, P., Klementiev, K., Welter, E., Ehnes, A., Saida, J., Inoue, A., and Jiang, J. Z., Applied Physics Letters **83**, 3924 (2003).

[7] Sordelet, D. J., Rozhkova, E., Besser, M. F., and Kramer, M. J., Applied Physics Letters **80**, 4735 (2002).

[8] Murty, B. S., Ping, D. H., and Hono, K., Applied Physics Letters **77**, 1102 (2000).

[9] Jiang, J. Z., Saksl, K., Saida, J., Inoue, A., Franz, H., Messel, K., and Lathe, C., Applied Physics Letters **80**, 781 (2002).

[10] Kelton, K. F., Lee, G. W., Gangopadhyay, A. K., Hyers, R. W., Rathz, T. J., Rogers, J. R., Robinson, M. B., and Robinson, D. S., Physical Review Letters **90**, 195504/1 (2003).

[11] Lee, G. W., Gangopadhyay, A. K., Kelton, K. F., Hyers, R. W., Rathz, T. J., Rogers, J. R., and Robinson, D. S., Physical Review Letters **93**, 037802/1 (2004).

[12] Al-Hajry, A., Al-Assiri, M., and Cowlam, N., Journal of Physics and Chemistry of Solids **59**, 1499 (1998).

[13] Takagi, T., Ohkubo, T., Hirotsu, Y., Murty, B. S., Hono, K., and Shindo, D., Applied Physics Letters **79**, 485 (2001).

[14] Kramer, M. J., Besser, M. F., Rozhkova, E., and Sordelet, D. J., Intermetallics **12**, 1119 (2004).

Table 1. Results of the thermal analysis of the $Zr_2Cu_{(1-x)}Pd_x$ alloys

x	Tg (K)	T_{x1} (K)	ΔH (J/g)
0.00	606	669	98.75
0.25	626	661	19.15
0.50	647	678	21.72
0.75	-	699	21.04
1.00	-	734	18.76

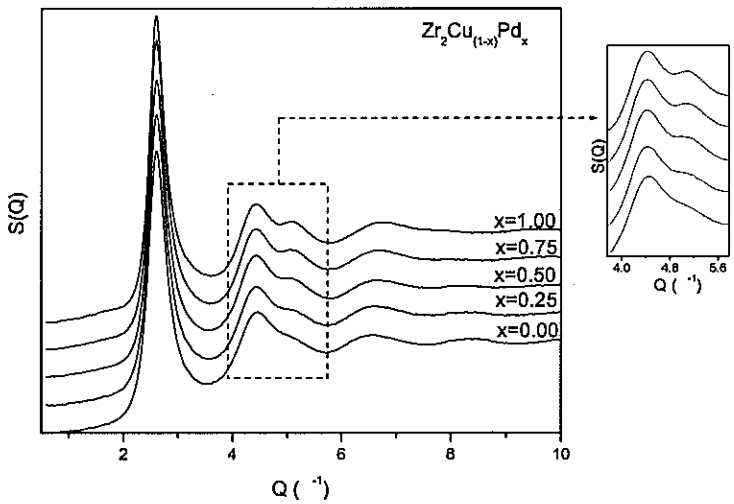

Fig 1. The structure factors S(Q) of the as quenched melt spun $Zr_2Cu_{(1-x)}$ Pd_x alloys

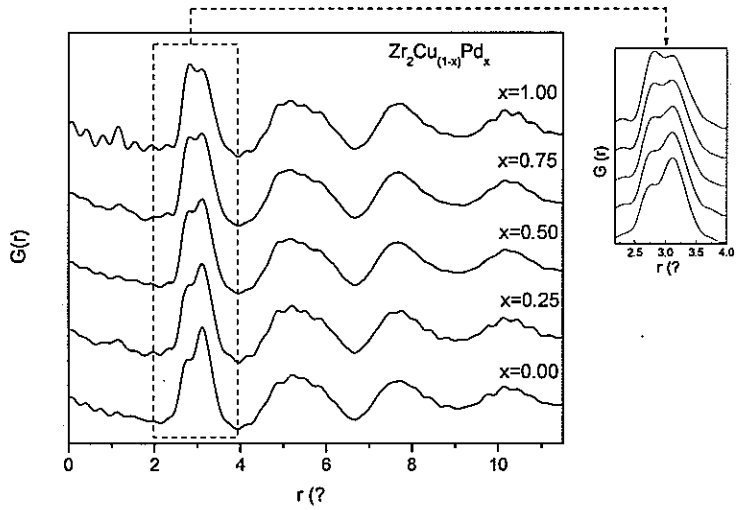

Fig. 2. The reduced radial distribution functions *G(r)* of the as quenched melt spun $Zr_2Cu_{(1-x)}Pd_x$ alloys

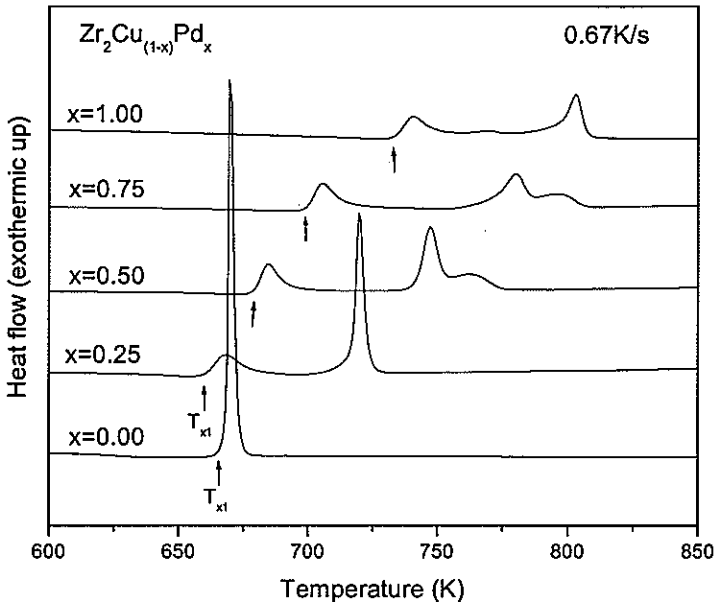

Fig. 3. Differential scanning calorimetric thermograms of the $Zr_2Cu_{(1-x)}$ Pd_x alloys

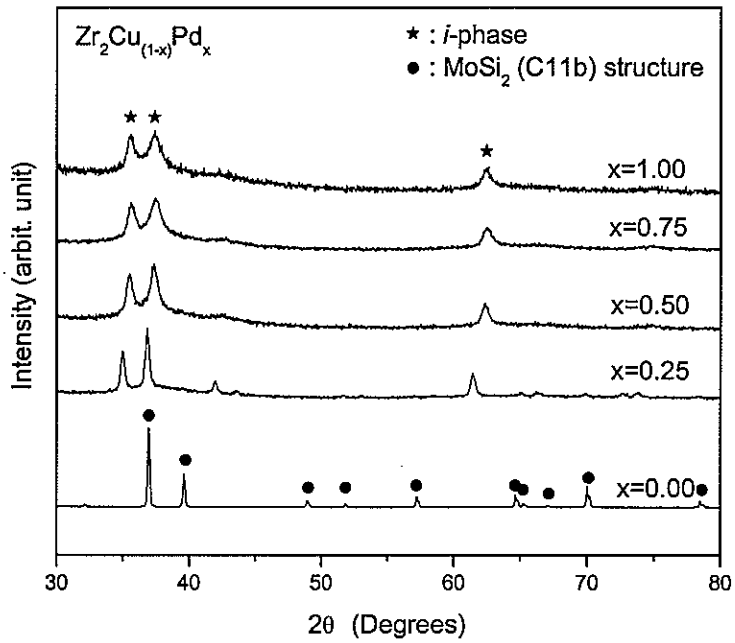

Fig. 4. X-ray diffraction patterns of the $Zr_2Cu_{(1-x)}$ Pd_x alloys annealed for 500 seconds at the temperatures about 20K before the primary phase transition

CHAPTER 3. THEORETICAL AND EXPERIMENTAL STUDIES OF DEVITRIFICATION PATHWAYS IN THE $ZR_2CU_{1-X}PD_X$ METALLIC GLASS SYSTEM

A paper published in Acta Materialia **55,** 5901-5909 (2007)

J. R. Morris [1,2], Min. Xu[3,4], Y. Y. Ye[4,5], D. J. Sordelet[3,4], and M. J. Kramer[3,4]

Abstract

Using a model amorphous alloy series, $Zr_2Cu_{1-x}Pd_x$ (x = 0, 0.25, 0.5, 0.75 and 1), we demonstrate that *ab initio* calculations can be used to help predict likely metastable phase formation during devitrification by comparing these with time-resolved X-ray scattering studies. All compositions share the same equilibrium $C11_b$ phase, yet they follow different devitrification pathways. Only x = 0.5 leads to a metastable *C16* phase formation. This

---

Reprinted with permission of Acta Materialia **55,** 5901-5909 (2007)

[1] Metals and Ceramics Division, Oak Ridge National Laboratory, Oak Ridge, TN 37831-6115, USA;

[2]Department of Materials Science and Engineering, University of Tennessee, Knoxville, TN 37996-2200

[3]Department of Materials Science and Engineering, Iowa State University, Ames, IA 50011, USA

[4]Materials and Engineering Physics Program, Ames Laboratory (USDOE) Ames, IA 50011, USA

[5]Center of Analysis and Testing, Wuhan University, Wuhan, 430072, Hubei, China

*Corresponding author: email: mjkramer@ameslab.gov; phone: 515-294-0276

corresponds precisely to calculations showing that for this composition, the *C16* phase is closest in energy to the stable $C11_b$ phase. The competition is shown to be dominated by electronic structure rather than size effects, with the favored composition for the *C16* phase forming a pseudo-gap at the Fermi energy. All Pd-containing compounds devitrify first into a quasicrystalline phase that has a composition near 75 at.-% Zr. $Zr_2Cu_{1-x}Pd_x$ compounds based on the $NiTi_2$ O_h^5 structure, which has been previously suggested to be related to the quasicrystal phase, are higher in energy relative to the *C16* and $C11_b$ structures for all compositions, and the calculations show no increase in stability with Pd concentration.

Introduction

Metallic glasses have received increased attention in the last few years as experimental work has produced alloys with significantly decreased critical cooling rates, allowing for bulk production of amorphous metallic alloys [1]. However, the fundamental understanding of such materials is still lacking. Much of the alloy work being performed is based on a few common strategies [2]. In particular, an emphasis is placed on including many different elemental components, with very different metallic radii [3]. However, many-component systems do not easily lend themselves to theoretical modeling, particularly for material-specific predictions on the effect of particular alloy additions. The difficulty of detailed experiments examining local atomic order, as well as the statistical nature of describing the local structure of materials, makes it difficult to directly test theoretical results.

Scientifically, the devitrification process of these materials is a problem of crystal nucleation and growth during heating of the glass. As such, the relevant thermodynamic properties include the driving force for nucleation, the interfacial free energy and interfacial mobility. In the case where the crystallization couples to a compositional change, solute flow is also critical for both nucleation and growth processes [4]. In the BMG materials, often the devitrification process occurs not directly to the stable phase, but first to a metastable phase. The preferential nucleation of a metastable phase can be due to the requirement of solute flow, or to a lower nucleation barrier for a metastable crystal phase as can also occur in quenched liquids [5], [6]. In some cases, multiple metastable phases appear before the stable structure forms.

To study the effect of composition on devitrification pathways, we have chosen the $Zr_2Cu_{1-x}Pd_x$ system. These alloys are reasonable glass formers, and these and similar alloys have been studied extensively experimentally [7-12]. The small number of components makes these alloys easier to study theoretically. These alloys share the same equilibrium high temperature $C11_b$ crystal phase (Fig. 1a), and for this composition range this phase can nucleate and grow without partitioning. Amorphous Zr_2Cu, when heated, undergoes devitrification directly to this crystal structure. However, small amounts (~1 atomic %) of Pd cause the system to first transform to a metastable, quasicrystalline structure (referred to here as the *i*-phase) [13]. Moreover, similar compositions devitrify into the metastable *C16* structure (Fig. 1b) [12], which is the stable phase for the related compound Zr_2Ni. The formation of the quasicrystalline phase has been attributed to a lower interfacial free energy, due to the presence of icosahedral clusters "frozen in" during the quench from the liquid [8,

9]. While this is plausible, there is little direct evidence; furthermore, it does not explain why Zr_2Cu does not form the *i*-phase, though it forms with small additions of Pd.

These results are tantalizing since no reports to date have unequivocally shown any relationship between the experimentally detected metastable phases formation and theoretical predictions. Further, little is known about the thermodynamic properties of the metastable phases. Understanding this competition is a fundamental problem in BMG research: the stability of the amorphous phase may be determined not just by its competition with the stable phase, but also with the metastable crystal structures. In this paper, we present experimental and theoretical results on a series of alloys, $Zr_2Cu_{1-x}Pd_x$ (x = 0, 0.25, 0.5, 0.75 and 1), in order to clarify the trends in the observed devitrification pathway for these materials [14]. The compositions have been particularly chosen to match the compositions of the stable crystalline phases [15] and with supercell first-principles calculations of the competing crystal structures [16-18]. The *i*-phase has been reported to have a composition closer to $Zr_{75}Pd_{25}$ [9]. In order to devitrify from the amorphous Zr_2Pd compound into the *i*-phase, there are three possibilities. First (and most likely), it can nucleate and grow only when the diffusion rates are sufficient for a change in composition to occur. Secondly, it may nucleate and grow with the composition of the glass, rather than with the preferred composition; however, the compositional determination was performed on a devitrified sample, contradicting this. Finally, it may nucleate and grow only where *local* concentrations are different (higher in Zr); however, the growth will be limited into regions with lower Zr content (which will be the bulk of the matrix). In any case, the preferential composition change for the *i*-phase should retard its nucleation and growth from the amorphous matrix.

There is a third crystalline phase that may compete as well: the $NiTi_2$ "big cube" type structure (O_h^5) shown in Fig. 2. This phase is FCC-based, with 24 atoms per primitive unit cell, and with local structural similarities to icosahedra. These local structures and chemical similarity with Zr_2Cu have led to suggestions that this may be a crystalline approximant to the observed *i*-phase [19, 20]. However, these clusters lack icosahedral symmetry, due to their composition, and therefore we feel that they are unlikely to be related to motifs present in the fully symmetrical *i*-phase. Never the less, this structure could in principle be a metastable phase for the $Zr_2Cu_{1-x}Pd_x$ compounds, and therefore this structure will be included in our analysis below.

In this work, we examine the devitrification process and phase competition through the use of time-resolved x-ray diffraction, and *ab initio* calculations. By comparing the experimental and theoretical calculations, we find that the observation of the *C16* metastable phase during devitrification occurs only when this phase competes closely with the stable $C11_b$ phase. This occurs only at the $Zr_2(Cu_{0.5}Pd_{0.5})$ composition. The O_h^5 phase is higher in energy (relative to the $C11_b$ and *C16* phases) and shows no evidence of stabilization by additions of Pd. The paper will be organized as follows: In section 2, the experimental and theoretical methods will be introduced. Section 3 will discuss the time-resolved x-ray diffraction and present the computational results, including a comparison of the lattice parameters for the observed metastable and stable phases. Finally, in Section 4, we will discuss the implications of our results.

Methods

Experimental

The devitrification pathways of these alloys during heating were studied using a combination of differential scanning calorimetry (DSC) and high-energy X-ray diffraction (HEXRD). HEXRD studies were performed at the Advanced Photon Source (APS) at Argonne National Laboratory using an energy of 99.55 keV, which corresponds to a wavelengths (λ) of 0.0124(7) nm. The diffraction data were obtained at the 6ID-D beamline at APS in collaboration with the Midwest Universities Collaborative Access Team (MUCAT). Silicon double-crystal monochromators were employed to select the wavelength. All samples were sealed in thin-walled silica capillaries using Ar. The HEXRD was obtained in a time-resolved manner using a MAR CCD in an off-beam-axis mode where only a 60 degree arc of the Debye cones intersect the CCD. This geometry was a compromise between obtaining a high reciprocal space data set every 20 s yet maintained a sufficiently high signal to noise ratio to resolve subtle details of the phase transition at a modest heating rate of 10 K/min. The sample distance to the detector was calibrated using NIST Si (640C) standard. The melting temperatures T_m of these alloys were obtained by a DTA at a heating rate of 10K/min. Room temperature lattice parameter determinations for the *C11b* structures were done on sample quenched from 700°C after annealing for 96 hrs. The XRD powder patterns were obtained using Cu_{ka} and fitted using Rietveld analysis.

Electronic Structure Calculations

To theoretically evaluate the effect of alloying on the phase stability, we used electronic structure calculations to examine the total energies of the competing crystalline structures. Our simulations were carried out using the Vienna *Ab initio* Simulation Package (VASP) [16-18]. The density functional calculations are performed using a plane-wave pseudopotential representation, with ultra-soft pseudopotentials[16] for all species and with a plane-wave energy cutoff of 300 eV. The *k*-point sampling was chosen to converge all of the total energies to an accuracy of 2 meV/atom. The *k*-point grid used for structural relaxation was 12x12x12, chosen according to the Monkhorst-Pack scheme [21], and symmetry reduced to the irreducible Brillouin zone. For the electronic density of states, a 20x20x20 grid was used. For each configuration, the total force on each ion is calculated using the Hellmann-Feynman theorem; the ionic positions were then relaxed to an accuracy of 0.01 eV/Å. In addition, all periodic unit cells were relaxed to minimize the total energy. The relaxation of both internal degrees of freedom and lattice parameters were performed together, as these are often coupled, to find the local minimum in energy.

Results

Devitrification Pathways

The diffraction data, presented in 2D form (Fig. 3), was taken at 10 K/min, the identical rate as the thermal analysis which is shown as a light line overlaid on the diffraction

data. The amorphous Zr_2Cu phase devitrifies directly to the $C11_b$ structure, while small amounts (x=0.25) of Pd causes the system to first transform to the metastable *i*-phase. Increasing Pd to x = 0.5 leads to the formation of a metastable *C16* prior to the $C11_b$ phase. Yet for higher Pd contents, the *C16* phase is no longer observed, but we observe a wide temperature range of coexistence of the *i*-phase and the $C11_b$ phase. The HEXRD also indicate that the reflections for the *i*-phase broaden with increases in x. These results indicate that at low Pd concentrations, the nuclei of the *i*-phase are probably separated and their diffusion fields do not overlap during growth [22]. At higher concentrations, the overlap of their diffusion fields results in the stabilization of a nanostructure. The Pd is apparently necessary to help stabilize the *i*-phase. The transition from the *i*-phase to the $C11_b$ for x = 0.25, 0.75 and 1.00 show a continuity between the (221001) and the (103) reflections of the *i*-phase and $C11_b$ phase respectively. It is only for x = 0.5 that a sharp transition between the *i*-phase and the meta-stable *C16* is observed. Single phased *C16* rapidly gives way to $C11_b$ over only 15 degrees.

Theoretical calculations

The goal of these calculations is to examine the stability of the three crystal structures shown in Figs. 1 and 2, as a function of composition. In the simplest case, the energies of all three structures would vary linearly with composition. More generally, for a given crystal structure, we may write

$$x(Zr_2Pd)+(1-x)(Zr_2Cu)+\Delta H_{mix} = Zr_2Pd_xCu_{1-x} \qquad (1)$$

where ΔH_{mix} is the heat of mixing. If the reverse reaction is favored (ΔH>0) then the Cu and Pd can (in principle) diffuse and phase separate into regions of Zr_2Cu and Zr_2Pd.

In all cases, the lowest energy structure was found to be the $C11_b$ phase, consistent with experiments. For this phase, the enthalpy of mixing from the elemental components was found to be -40 kJ/mol for Zr_2Cu and -140 kJ/mol for Zr_2Pd. If the energies for the mixtures are linear in the composition (ΔH_{mix}=0), then the enthalpies of formation are given by

$$\Delta H = -40 \text{ kJ/mol} - x(100 \text{ kJ/mol}) \quad (2)$$

where the $x = 0$ value is the energy/formula unit for the Zr_2Cu phase, and the x = 1 value is for the Zr_2Pd phase. The strong decrease in energy with increasing Pd content is consistent with the experimentally observed, nearly linear rise in melting temperature from 1296K to 1384K with x increasing from 0 to 1. These values are in reasonable agreement with experimental values of -17 kJ/mol for Zr_2Cu [23], and -126 kJ/mol for Zr_2Pd [24, 25].

We show the calculated heats of formation, lattice parameters, and bulk modulus for Zr_2Cu and Zr_2Pd in Table 1, for all three crystal structures. The lattice parameters and the heats of formation for the ternary phases are presented in Table 2. For the stable $C11_b$ phase, we compare with room temperature experimental values [26]. As can be seen, for this phase, the calculated lattice parameters are within 1% of the experimental values, as is the c/a ratio. The variable Zr atomic position ($4e$) is also in good agreement with experimental values. We also show the calculated heats of formation, relative to the elemental phases. For all three crystal structures, this is positive, demonstrating the general tendency of these systems to mix, consistent with the "deep eutectic" that occurs in this system [27], and the fact that the stable phase is a line compound.

In Fig. 4, we show the enthalpies of mixing as a function of composition. In the bottom part of the figure, the trend given in Eq. 2 has been subtracted. In the figure, a convex envelope represents the stable phases ($\Delta H > 0$ in Eq. 1). We show results not only for the stable $C11_b$ and metastable $C16$ structures, but also for the O_h^5 crystal structure shown in Fig. 2. For the stable $C11_b$ structure, all calculations are close to the energy predicted by Eq. 2, indicating that Cu and Pd are nearly ideally mixing even at $T=0$. At $x=0.5$, we have considered two different orderings of Cu and Pd. The energy for one ordered structure (corresponding to alternating layers of Cu and Pd) is slightly lower than the trend, while a second (shown in Fig. 1a) is slightly higher (shown as an open symbol in Fig. 4). The energy difference between these orderings is quite small, less than 10 meV/formula unit (~1 kJ/mol). Thus, we expect that the Cu and Pd atoms will in fact form a disordered sublattice at ambient temperatures. Even at low temperatures, they will not phase separate; energetically, they would prefer to form an ordered superstructure. Above the ordering temperature, the entropy of mixing will further stabilize the ternary phase, particularly at the composition $x=0.5$. For $x=0.25$ and $x=0.75$, we have considered only one ordering; thus, our results should be taken to be upper bounds to the energies. Again, the energies are close to the trend of Eq. 2, indicating a low order-disorder temperature for the Cu-Pd sublattice. This easy disordering also suggests that the size difference between Pd and Cu (about 7%) does not play a role in the thermodynamics of these materials.

A stronger trend is shown for energetics of the metastable $C16$ structure. The energies range from about 200 meV/formula unit higher than the $C11_b$ phase down to a minimum of 60 meV/formula unit at $x=0.5$. Thus, the calculations show that the $C16$ phase has a minimum in energy precisely at the composition where this phase appears as a

devitrification product. This minimum again indicates that the Cu and Pd will not phase separate: alloying to $x=0.5$ both lowers the total energy as well as maximizes the entropy of mixing. Again, we have considered two different possible Cu/Pd orderings for $x=0.5$: the one shown in Fig. 1b has the lowest energy, while an alternate one (with lines of pure Cu or pure Pd atoms, maximizing the separation of the Cu and Pd atoms) is higher in energy (also open symbol in Fig. 3). The energy gap between these two structures is larger than for the $C11_b$ structure, indicating a higher order-disorder transition. Again, however, the energy is not very large, and the system is likely disordered at the glass transformation temperature. The stronger ordering tendency of the *C16* system relative to that of $C11_b$ is understood by recognizing that the Cu/Pd atoms in the latter structure contain only Zr near neighbors; thus, the Cu-Pd interactions only occur through second-nearest (or higher) neighbors.

To examine why the metastable *C16* phase has an energy minimum at the composition $Zr_2Cu_{0.5}Pd_{0.5}$, Fig. 5 shows the electronic density of states (DOS) for this composition as well as the binaries Zr_2Cu and Zr_2Pd. We see that for the ternary compound, the Fermi level is at a broad minimum in the DOS, unlike the binaries. The binaries have weak minima, above the Fermi level for Zr_2Pd and below it for Zr_2Cu. The ternary is optimal, as it forms a pseudogap at the Fermi level, filling the bonding states while not occupying the anti-bonding states. Thus, the origin of the energetic minimum of the metastable state (and the corresponding maximum in the glass transition temperature) is primarily due to electronic structure effects.

For all compositions, the enthalpy of mixing of the O_h^5 structure is negative, but with a much lower magnitude than the *C16* phase (by <25 kJ/mol). The enthalpy difference between the $NiTi_2$ and the $C11_b$ phases is *greater* with increasing Pd content. Thus, the

observation that small amounts of Pd added to Zr_2Cu promote the formation of the quasicrystalline *i*-phase is in strong contrast to the calculations for the O_h^5 structure, and we conclude that the O_h^5 structure is probably *not* closely related to the *i*-phase. We also note that the "icosahedral" structures in O_h^5 are irregular and formed by a Ni atom surrounded by 9 Ti atoms and 3 Ni atoms. While the geometry of this cluster is similar to an icosahedron, the local icosahedral symmetry is broken by topological and compositional effects. This makes it unlikely that the O_h^5 structure is an approximant phase for *any* quasicrystalline system. We also note that Murty *et al.* [9] have analyzed the composition of the Zr-Pd quasicrystalline phase using atom-probe tomography, and find a composition closer to $Zr_{75}Pd_{25}$. Preliminary spectroscopy for $x=0.5$ support an enrichment of Zr in the *i*-phase over the bulk composition.

Discussion

For all of the $Zr_2Cu_xPd_{1-x}$ compounds, the $C11_b$ ($MoSi_2$) crystal structure is the thermodynamically stable phase. As in previous work [8-10], [28] no icosahedral phase occurs for Zr_2Cu, which devitrifies directly into the stable phase. In contrast, all Pd-containing compounds devitrify first into an *i*-phase. This demonstrates that even when the composition is identical to the stable structure, the Zr-rich *i*-phase prefers to nucleate.

For the $x=0.5$ composition (equal amounts of Cu and Pd), the *i*-phase transforms to the metastable *C16* phase (Al_2Cu-type structure) on heating, before transforming to the stable

phase. This is shown using the time-resolved diffraction data, and supported by the calorimetry work. The calculations show that the composition at $x=0.5$ maximizes the competition between the ground state structure and the nearby metastable phase. This is the first demonstration that the devitrification paths may be understood from theoretical considerations of the competing crystalline structures. For the alloys studied, this competition is determined by electronic structure effects in the metastable phase, dominating atomic size effects, chemical phase separation, or other factors. The apparent epitaxy between the *i*-phase and the $C11_b$, as evidenced by the continuity between the (221001) and the (103) reflections of the *i*-phase and $C11_b$ phase, would argue for a lower barrier of formation of the $C11_b$ relative to the *C16* for all compositions where the *i*-phase exists. We speculate that there is a low interfacial free energy between the *C16* phase and glass, relative to that between the stable $C11_b$ structure and the glass, leading to its preferential nucleation.

A remaining challenge is to understand the quasicrystalline *i*-phase, and the factors that affect its formation. As the *i*-phase occurs only for Pd-containing compositions, not the pure Zr_2Cu phase, the expectation is that related metastable phases will compete more closely with increasing Pd-content. In the absence of precise knowledge of local structures, it is difficult to understand the strong effect of Pd on the formation of this phase. If the O_h^5 phase, as shown in Fig. 2, is an approximant structure to the *i*-phase we would expect that the difference between the binding energy of this phase and the metastable phase would decrease with increasing Pd content. Instead, our calculations demonstrate the opposite effect: this phase increases in energy relative to the stable $C11_b$ phase as the Pd-content increases. We note again that although the O_h^5 phase contains motifs that geometrically are close to

icosahedra, the local chemical structure in these clusters break the symmetry of these clusters, strongly suggesting that the O_h^5 phase cannot be an approximant structure for an icosahedral phase. Furthermore, the composition of the *i*-phase appears to be significantly richer in Zr than would be expected for a phase approximated by the O_h^5 structure [8-10].

Presumably, the nucleation of a crystalline phase from the amorphous state follows similar tendencies of crystal nucleation from the melt: the balance of interfacial free energy and driving force may favor the nucleation into a metastable phase that has a lower interfacial free energy. Two simple arguments are suggested by the observation of *i*-phase nucleation with Pd additions. First, the *i*-phase is likely to be strongly stabilized by small amounts of Pd, so that the driving force for nucleation is large. Second, the local structure of the amorphous state may be sensitive to the Pd content, with small amounts of Pd increasing local structural similarity toward the quasicrystalline phase, thereby reducing the interfacial free energy [8-10].

The present studies suggest something more complex, however. The simple nucleation arguments above ignore the role of chemical diffusion, which can dramatically alter both the energetics and the dynamics of crystal nucleation and growth from the amorphous phase. Certainly, it is expected that crystalline structures close in composition to the amorphous phase would tend to be preferred devitrification products. For all compounds studied here, the glass may transform directly into either the stable $C11_b$ or metastable *C16* structure without a change in composition. In contrast, the *i*-phase has a higher Zr content, so the devitrification into the *i*-phase occurs either with a change of composition during the process of nucleation and growth, or only occurs in Zr-rich regions in the glass. Previous

work on a related alloy, BAM-11, suggest that the dynamics involve the coupled change in structure and composition [4]. Once formed, the Zr-rich *i*-phase must leave behind a Zr-poor amorphous matrix. In order to form either the stable $C11_b$ phase or the metastable *C16* phase (both line compounds), again chemical diffusion must occur.

In summary, the $Zr_2Cu_xPd_{1-x}$ amorphous compounds share the same equilibrium high temperature $C11_b$ crystal phase; however, their devitrification pathways are compositionally dependent. Small amounts of Pd cause the system to first transform to a metastable *i*-phase first. *Ab initio* calculations show that the *C16* phase has a minimum in energy precisely at $x=0.5$ where this phase appears as a metastable devitrification product observed in the HEXRD. This minimum in enthalpy at this composition indicates that the Cu and Pd will not phase separate. Alloying to $x=0.5$ both lowers the total energy as well as maximizes the entropy of mixing. This is the first demonstration that the devitrification paths may be understood from theoretical considerations of the competing crystalline structures. For the alloys studied, this competition is dominated by electronic structure rather than size effects: the difference in radii between Cu and Pd is less than 7 %. For the *C16* phase, only the ternary $x=0.5$ is optimal, as it forms a pseudogap at the Fermi level, filling the bonding states while not occupying the anti-bonding states.

A remaining challenge is to understand the atomic structure of the *i*-phase, and the factors that affect its formation. We have demonstrated that this phase is not closely related to the O_h^5 structure. Future work will entail developing a better understanding of local structure based on similar chemistries in the Ti-Zr-Ni system [29].

Acknowledgements

The research at Oak Ridge National Laboratory and Ames Laboratory has been sponsored by the Division of Materials Sciences and Engineering, Office of Basic Energy Sciences, U.S. Department of Energy under contract DE-AC05-00OR-22725 with UT-Battelle, LLC and contract under Contract No. DE-AC02-07CH11358 with Iowa State University, respectively.

The Midwest Universities Collaborative Access Team (MUCAT) sector at the APS is supported by the US Department of Energy, Office of Science, Basic Energy Sciences, through the Ames Laboratory.

References

[1] Chen HS. Thermodynamic Considerations on Formation and Stability of Metallic Glasses. Acta Metallurgica 1974;22:1505.

[2] Chaudhari P, Giessen BC, Turnbull D. Metallic Glasses. Scientific American 1980;242:98.

[3] Inoue A. Stabilization of metallic supercooled liquid and bulk amorphous alloys. Acta Materialia 2000;48:279.

[4] Wang XL, Almer J, Liu CT, Wang YD, Zhao JK, Stoica AD, Haeffner DR, Wang WH. In situ synchrotron study of phase transformation behaviors in bulk metallic glass by simultaneous diffraction and small angle scattering. Physical Review Letters 2003;91.

[5] Herlach DM. Metastable materials solidified from undercooled melts. Journal of Physics-Condensed Matter 2001;13:7737.

[6] Greer AL, Walker IT. Primary crystallization in (Fe, Ni)-based metallic glasses. Journal of Non-Crystalline Solids 2003;317:78.

[7] Murty BS, Ping DH, Hono K. Nanoquasicrystallization of binary Zr-Pd metallic glasses. Applied Physics Letters 2000;77:1102.

[8] Murty BS, Ping DH, Hono K, Inoue A. Icosahedral phase formation by the primary crystallization of a Zr-Cu-Pd metallic glass. Scripta Materialia 2000;43:103.

[9] Murty BS, Ping DH, Ohnuma M, Hono K. Nanoquasicrystalline phase formation in binary Zr-Pd and Zr-Pt alloys. Acta Materialia 2001;49:3453.

[10] Murty BS, Hono K. On the criteria for the formation of nanoquasicrystalline phase. Applied Physics Letters 2004;84:1674.

[11] Sordelet DJ, Rozhkova E, Besser MF, Kramer MJ. Synthesis route-dependent formation of quasicrystals in Zr70Pd30 and Zr70Pd20Cu10 amorphous alloys. Applied Physics Letters 2002;80:4735.

[12] Kramer MJ, Besser MF, Yang N, Rozhkova E, Sordelet DJ, Zhang Y, Lee PL. Devitrification studies of Zr-Pd and Zr-Pd-Cu metallic glasses. Journal of Non-Crystalline Solids 2003;317:62.

[13] Saksl K, Franz H, Jovari P, Klementiev K, Welter E, Ehnes A, Saida J, Inoue A, Jiang JZ. Evidence of icosahedral short-range order in Zr70Cu30 and Zr70Cu29Pd1 metallic glasses. Applied Physics Letters 2003;83:3924.

[14] Xu M, Ye Y, Morris JR, Sordelet DJ, Kramer MJ. Influence of Pd on formation of amorphous and quasicrystal phases in rapidly quenched Zr2Cu(1-x)Pdx. Philosophical Magazine 2006;86:389.

[15] Jiang JZ, Rasmussen AR, Jensen CH, Lin Y, Hansen PL. Change of quasilattice constant during amorphous-to-quasicrystalline phase transformation in Zr65Al7.5Ni10Cu7.5Ag10 metallic glass. Applied Physics Letters 2002;80:2090.

[16] Kresse G, Furthmuller J. Efficiency of ab-initio total energy calculations for metals and semiconductors using a plane-wave basis set. Computational Materials Science 1996;6:15.

[17] Kresse G, Furthmü ller J. Efficient iterative schemes for ab initio total-energy calculations using a plane-wave basis set. Phys. Rev. B 1996;54:11169.

[18] Kresse G, Hafner J. Ab initio molecular dynamics for liquid metals. Phys. Rev. B 1993;47:558.

[19] Aslanov LA, Markov VT. A Crystal-Chemical Model of Atomic Interactions .6. Intermetallic Phase Structures. Acta Crystallographica Section A 1992;48:281.

[20] Li CF, Wang LM, Inoue A. Precipitation of icosahedral quasicrystalline and crystalline approximant phases in Zr-Cu-(Co, Rh or Ir) metallic glasses. Journal of Non-Crystalline Solids 2002;306:175.

[21] Monkhorst HJ, Pack JD. Special Points for Brillouin-Zone Integrations. Physical Review B 1976;13:5188.

[22] Kelton KF. Nucleation in glasses and liquids and nanostructure formation. Physics and Chemistry of Glasses 2004;45:64.

[23] Ansara I, Pasturel A, Buschow KHJ. Enthalpy Effects in Amorphous-Alloys and Intermetallic Compounds in the System Zr-Cu. Physica Status Solidi a-Applied Research 1982;69:447.

[24] Stolen S, Matsui T. Thermodynamic Analysis of the Palladium-Zirconium System. Journal of Nuclear Materials 1992;186:242.

[25] Stolen S, Matsui T, Naito K. Mass-Spectrometric Vaporization Study on Palladium Zirconium Alloys. Journal of Nuclear Materials 1990;173:48.

[26] Villars P, Calvert LD. Pearson's Handbook of Crystallographic Data for Intermetallic Phases. Materials Park, Ohio: ASM International, 1997.

[27] Wang WH, Lewandowski JJ, Greer AL. Understanding the glass-forming ability of Cu50Zr50 alloys in terms of a metastable eutectic. Journal of Materials Research 2005;20:2307.

[28] Murty BS, Hono K. Nanoquasicrystallization of Zr-based metallic glasses. Materials Science and Engineering a-Structural Materials Properties Microstructure and Processing 2001;312:253.

[29] Hennig RG, Kelton KF, Carlsson AE, Henley CL. Structure of the icosahedral Ti-Zr-Ni quasicrystal. Physical Review B 2003;67.

[30] Nevitt MV, Downey JW. Family of Intermediate Phases Having Si2mo-Type Structure. Transactions of the Metallurgical Society of Aime 1962;224:195.

[31] Maeland AJ, Lukacevic E, Rush JJ, Santoro A. Neutron Powder Diffraction and Inelastic-Scattering Study of the Structures of Zr2Pd,Zr2Pd1.70 and Zr2Pd1.96. Journal of the Less-Common Metals 1987;129:77.

Table 1. Structural parameters, calculated heats of formation, and bulk moduli for the $MoSi_2$ ($C11_b$), Al_2Cu ($C16$) and $NiTi_2$ (O_h^5) type-structures, for Zr_2Cu and Zr_2Pd. The value of z is an internal degree of freedom for the structure. For previous experimental work, see also Ref. [26].

		Zr_2Cu	Zr_2Pd
$MoSi_2$ structure (C_{11b})			
a_0 (Å)	Theory	3.240	3.343
	Experiment	3.2204[30] 3.220(5)(present work)	3.3086[31] 3.303(2) (present work)
c/a	Theory	3.476	3.256
	Experiment	3.473[30] 3.47(6) (present work)	3.292[31] 3.30(0) (present work)
z	Theory	0.347	0.343
	Experiment	0.3460[30] 0.34493 (present work)	0.343[31] 0.34192 (present work)
Heat of formation (kJ/mol)	Theory	-40.2	-140.7
	Experiment	-17.3 [23]	-126 [24, 25]
Bulk modulus (MPa)		1.101	1.062
Al_2Cu structure (C16)			
a_0 (Å)		6.632	6.758
c/a		0.80	0.80
z		0.1576	0.1571
Heat of formation (kJ/mol)		-32.	-133.
Bulk modulus (MPa)		1.065	1.225
$NiTi_2$ structure (O_h^5)			
a_0 (Å)		12.371	12.643
Heat of formation (kJ/mol)		-13.9	-111.3
Bulk modulus (MPa)		1.153	1.057

Table 2. Structural parameters and calculated heats of formation for the $MoSi_2$ ($C11_b$), Al_2Cu ($C16$) and $NiTi_2$ (O_h^5) type-structures, for the ternary compounds $Zr_2Cu_xPd_{1-x}$. The value of z is an internal degree of freedom for the $C11_b$ structure, and x is an internal degree of freedom for the $C16$ structure. Error bars in the lattice constants are on the order of 0.01 Å; those of the heat of formation are on the order of 2 kJ/mol.

		$Zr_2Cu_{0.75}Pd_{0.25}$ ($x=0.25$)	$Zr_2Cu_{0.5}Pd_{0.5}$ ($x=0.5$)	$Zr_2Cu_{0.75}Pd_{0.25}$ ($x=0.75$)
$MoSi_2$ structure (C_{11b})				
a_0 (Å)	Theory	3.24	3.28	3.30
	Experiment	3.2235	3.2364	3.2621
c/a	Theory	3.48	3.45	3.37
	Experiment	3.49	3.48	3.42
z	Theory	0.345	0.344	0.343
	Experiment	0.3473	0.3457	0.3445
Heat of formation (kJ/mol)	Theory	-65	-91	-115
Al_2Cu structure (C16)				
a_0 (Å)	Theory	6.66	6.67	6.72
	Experiment		6.6811	
c/a	Theory	0.80	0.80	0.80
	Experiment		0.79	
x	Theory	0.160	0.161	0.159
	Experiment		0.1560	
Heat of formation (kJ/mol)		-60	-84. (separated) -88. (mixed)	-110
$NiTi_2$ structure (O_h^5)				
a_0 (Å)		Not calculated	12.643	Not calculated
Heat of formation (kJ/mol)			-66	

*Experimental data from HEXRD at 720 K.

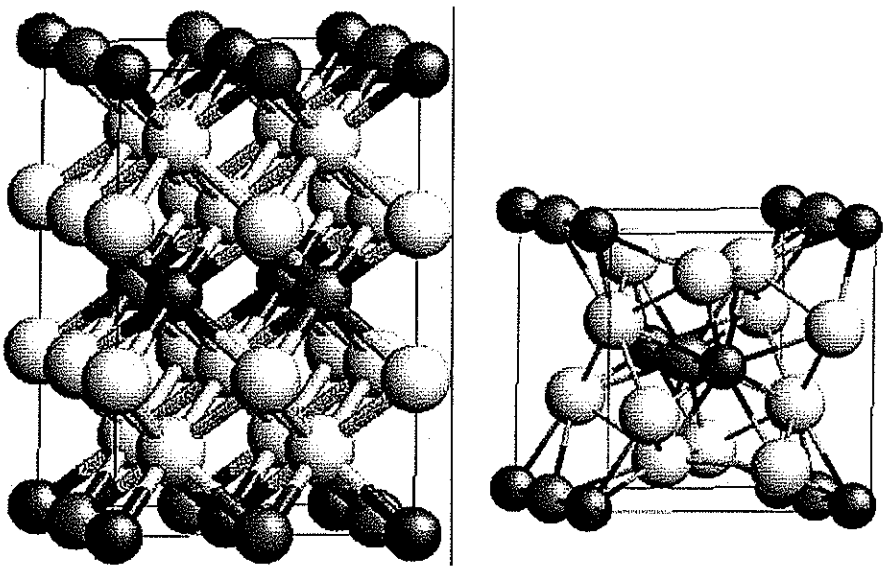

Figure 1. Possible structures for the $Zr_2Cu_xPd_{1-x}$ system. White atoms are Zr, and darker atoms are either Cu or Pd. For the $Zr_2Cu_{0.5}Pd_{0.5}$ composition, one possible ordering is shown. (a) The *C11$_b$* ($MoSi_2$) structure (observed ground state for $Zr_2Cu_xPd_{1-x}$). (b) The *C16* (Al_2Cu) structure (metastable devitrification product).

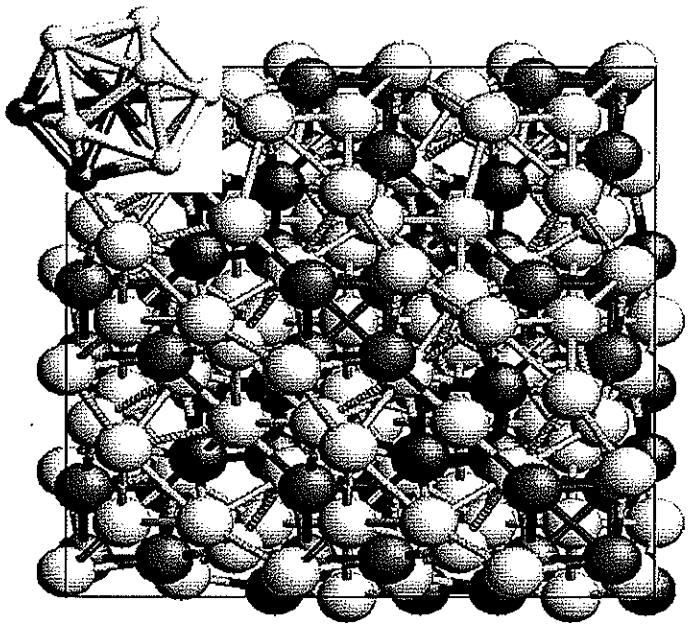

Figure 2. The $NiTi_2$ structure (O_h^5) "big cube" structure. Atom shading is same as for Fig. 1. Inset shows local "icosahedral" cluster occurring in the crystal structure, as well as the chemical variation that breaks icosahedral symmetry in the cluster.

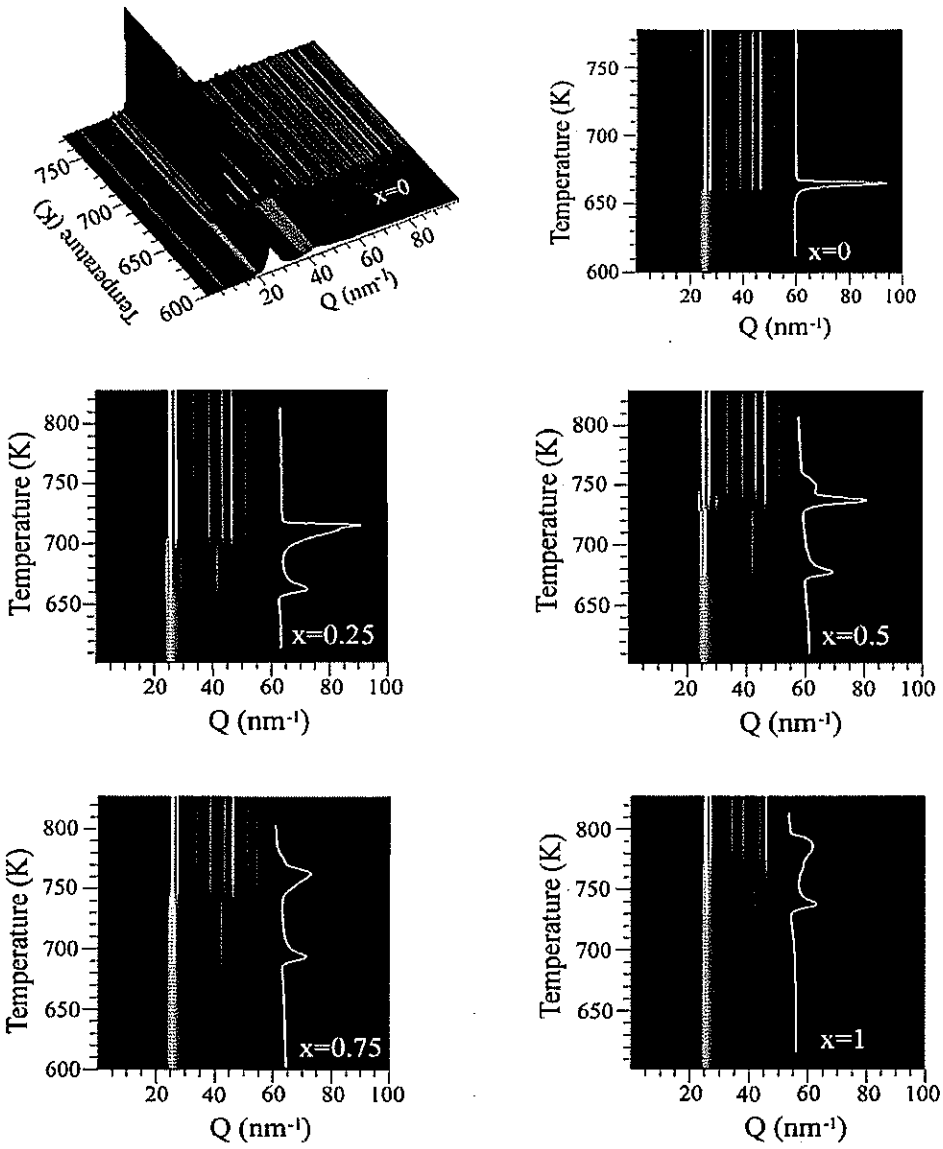

Figure 3. Top left, a 3D representation of the time-resolved XRD of the devitrification of the Zr_2Cu amorphous alloy. The next five images are a 2D representation of the XRD (bright regions indicate stronger scattering intensity) of the 5 alloys. The light line is an overlay of the DSC data obtained at the same heating rate.

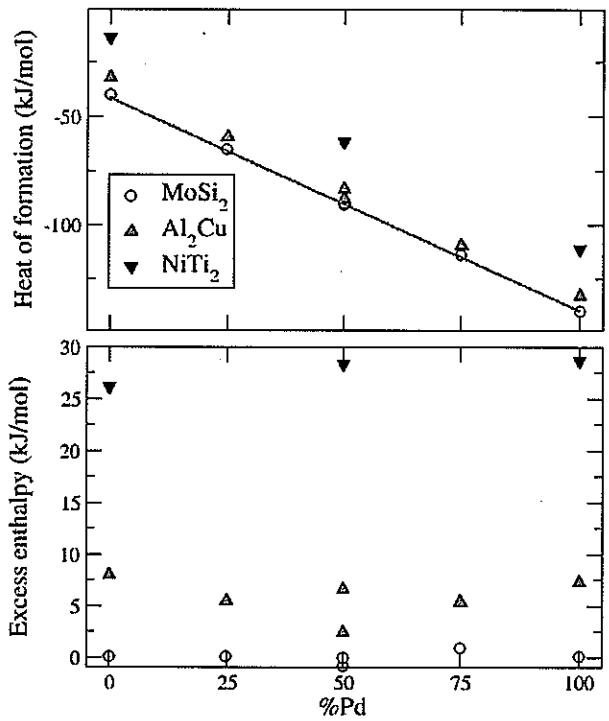

Figure 4. (Top) Enthalpies of formation of all structures, as a function of Pd content. The straight line indicates a linear interpolation between the results for the $C11_b$ ground state structure for Zr_2Cu and Zr_2Pd, as given in Eq. 2. (Bottom) The linear relation given in Eq. 2 has been subtracted out, indicating the excess enthalpies. Positive numbers indicate less strong binding than the linear trend shown in the top.

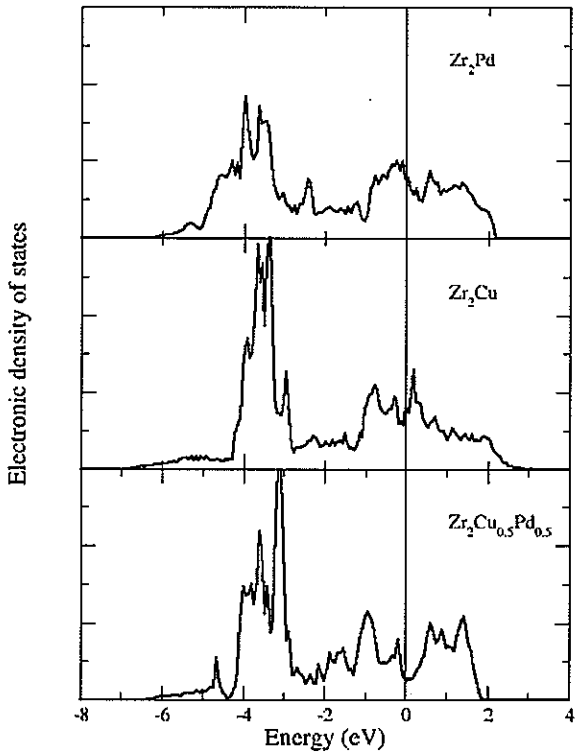

Figure 5. Electronic density of states for the metastable *C16* (Al_2Cu) structure, for Zr_2Pd, Zr_2Cu, and $Zr_2Cu_{0.5}Pd_{0.5}$. The energy is adjusted so that the Fermi level is at E_F=0.

CHAPTER 4. *IN SITU* OBSERVATION OF THERMAL EXPANSION OF TETRAGONAL C11B PHASE IN $ZR_2CU_{(1-X)}PD_X$ ALLOYS

A Paper to be submitted to intermetallics

Min Xu[1,2], Y. Y. Ye[2,4], J. R. Morris[3,5], D. J. Sordelet[1,2], M. J. Kramer[1,2,*]

Abstract

The *C11b* phase crystalline structure (structure type $MoSi_2$, space group *I4/mmm*) in the $Zr_2Cu_{(1-x)}Pd_x$ (x=0, 0.25, 0.5, 0.75 and 1) alloys was examined *in situ* using high temperature X-rays diffraction (HTXRD) and Rietveld refinement of the data obtained at a constant heating rate. While the cell volume increases with increasing Pd as expected by the larger atomic radii, the coefficients of thermal expansion (CTE) do not follow a uniform trend. The bonding in the basal plane is more elastically rigid than along the *c*-axis for all compositions. The CTE is more anisotropic for Zr_2Pd than for Zr_2Cu, which is consistent

[1] Department of Materials Science and Engineering, Iowa State University, Ames, IA 50011, USA

[2]Materials and Engineering physics Program, Ames Laboratory(USDOE) Ames, IA 50011, USA

[3]Meatals and Ceramics Division, Oak Ridge National Laboratory, Oak Ridge, TN 37831-6115, USA

[4]Center of Analysis and Testing, Wuhan University, Wuhan, 430072, Hubei, China

[5]Department of Materials Science and Engineering, The University of Tennessee, Knoxville, TN 37996-2200

*Corresponding author: email: mjkramer@ameslab.gov; phone: 515-294-0276

with the first-principles calculations that illustrate the rigidity of *c*-axis relatively to *a*-axis to be the less for Zr_2Pd. The CTE of the *a*-axis for Zr_2Pd is in fact negative over the temperature range measured.

Keywords: **B.** anisotropy, crystal chemistry of intermetallics, electronic structure of metals and alloys, thermal stability; **F.** X-ray diffraction

Introduction

In the pseudo-binary Zr(Pd,Cu) metallic glass system, AB_2 phases have been found as both metastable phases and high temperature stable phases. Saksl et al. [1] observed that a tetragonal Zr_2Cu crystalline phase formed in the $Zr_{70}Cu_{30}$ and $Zr_{70}Cu_{29}Pd_1$ alloys. Both Saida et al. [2] and Murty et al. [3] reported that an intermetallic Zr_2Pd *C11b* compound formed in the binary $Zr_{70}Pd_{30}$ system at high temperatures. Jiang et al. [4] and Murty et al. [5] studied the phase transformations in binary Zr_2Pd and Zr_2Cu metallic glass and found that a single Zr_2TM (TM=Pd, Cu) *C11b* phase formed at high temperature in both alloys. Kramer at el. [6] reported that additional transformation of a metastable intermetallic structure, *C16* phase, was found in $Zr_{70}Pd_{20}Cu_{10}$ metallic glass; while *C11b* phase is the high temperature stable phase in both alloys. We also reported that [7], although icosahedral phase (*i*-phase), *C16* and *C11b* phases can be formed during the divitrification process of $Zr_2Cu_{(1-x)}Pd_x$ (x = 0~1) glassy alloys depending on temperature and composition, all compositions share the same high temperature *C11b* phase. In our previous work [8], it was found that the devitrification

process of Zr-Cu based glassy alloys is very sensitive to Pd content [1, 7]. Furthermore, it was confirmed that *C11b* phase is the thermodynamically stable phase by using a*b initio* calculations [9, 10].

At a 66.7at.% Zr composition, Zr-Cu and Zr-Pd binary phase diagrams are very similar [11] since both Zr_2TM compounds melt congruently. According to Hume-Rothery rules [12], Pd and Cu can form a solid solution and fully substitute for each other in Zr_2 (Pd, Cu) alloys since Cu:Pd atomic radii differ less than ~15%, even though they have different ground state electronic structures (Cu is $[Ar]3d^{10}4s^1$ and Pd is $[Kr]4d^{10}$) and the *e:a* ratio varies by more than 30%. Moreover, the whole composition range of $Zr_2Cu_{(1-x)}Pd_x$ (x = 0~1) alloys are reasonable glass formers. Ohata and Pettifor [13] studied the various crystal structures for the AB_2 family of transition-metal compounds and proposed a two-step process for their formation. In the first step, the volumes of the different structure types are adjusted to guarantee the same repulsive energy. In the second step, the bond energies are compared in order to see which structure is most stable. When considering only the effect of size; as R decreases under 0.837 ($R = \frac{r_A}{r_B}$), the *C16* is favored over the *C11b* and the Laves phases (*C14*, *C15* and *C36*) due to its higher packing density. However, when both size and electronic factors are considered, Ohata and Pettifor's theoretical structure maps are in accord with the experimentally observed *C11b* structure in the $Zr_2Cu_{(1-x)}Pd_x$ alloys [8] using the radius ratio $R = \frac{r_{TM}}{r_{Zr}} = 0.80 \sim 0.89$ (TM = Cu, Pd, r_{Zr} = 1.58 Å; r_{Pd} = 1.41 Å; r_{Cu} = 1.27 Å [14]). Thus, the high temperature stable *C11b* formation in the Zr(Pd,Cu) system is controlled by both atomic size and electronic factors [8].

While, previously performing *in situ* high temperature X-ray diffraction (HTXRD) devitrifcation studies [7], we noted that the lattice parameter data obtained at temperatures well in excess of the formation of the stable *C11b* phase showed some unusual coefficients thermal expansion (CTE). It is possible that the CTE is affected by the different electronic structure of Cu and Pd and thus does not follow simple rules of mixture. In this paper, we take a closer look at the high temperature behavior of the stable *C11b* phase as a function of Pd:Cu ratio.

Experimental

Five $Zr_2Cu_{(1-x)}Pd_x$ (x=0, 0.25, 0.5, 0.75 and 1) metallic alloys were prepared by arc-melting of the pure metal pieces (zirconium with a purity of 99.95 wt.%, copper with a purity of 99.99 wt.%, and palladium with 99.97 purity wt.%) in argon atmosphere. After three-fold re-melting, the weight losses were less than 0.1 wt.%. The alloys were melt spun at a wheel speed of 25 m/s and a constant pressure of 1.6×10^4 Pa in ultra-high purity Helium atmosphere and a graphite crucible. After checked by x-ray diffraction (XRD) and transmission electron microscopy (TEM), homogeneous amorphous structure is obtained for all five alloys [7]. Starting from rapidly quenched amorphous structures has an advantage that phase segregation, which can occur during conventional casting, can be eliminated assuring homogeneity of the final high temperature phase.

The crystallization temperature T_x was measured using *in situ* HTXRD and differential scanning calorimeter (DSC). HTXRD experiments were conducted at the

MUCAT beam line at the Advanced Photon Source, Argonne National Laboratory. The energy of the X-rays was 100.601 keV (λ=0.123244 Å). Mosaic Silicon double-crystal monochromators were employed to select the wavelength. Two-dimensional diffraction patterns of single-grain samples were obtained using a MAR charge-coupled device (CCD) detector, which at this heating rate used was about 1 scan every 2 K. The distance from the sample to the detector was determined using the Natural Institute of Standards and Technology Si standard 640c. The Debye–Scherrer geometry is employed for collecting diffraction x-rays. Melt spun ribbons were sealed in a thin walled silica capillary (φ=2mm) under Argon atmosphere at approximately 2.7×10^4 Pa pressure. DSC was also carried out using a refrigerated cooling system with Argon gas DSC cell purge to compare the crystallization process with the HTXRD. Melting temperature T_m was measured by a Perkin Elmer differential thermal analyzer (DTA). All of these measurements have the same heating rate at 0.167K/s. Reitveld refinement was performed using the software GSAS (General Structure Analysis System) to obtain the lattice parameters of *C11b* phase.

Oxygen content plays an important role in the crystallization pathways in Zr-based metallic glass [15]. Murty recently reported [5] that the *i*-phase is indeed stabilized by the presence of oxygen in Zr– Cu–Al amorphous alloy beyond a critical concentration of 0.4 at.% O. To avoid the influence of oxygen during the crystallization process, care was taken in keeping the oxygen content in $Zr_2Cu_{(1-x)}Pd_x$ melt spun ribbons as low as possible: using high purity crystal bar Zr, multiple getterings of the arc furnace and the use of graphite as a crucible [7]. The oxygen contents of the $Zr_2Cu_{(1-x)}Pd_x$ (x=0, 0.25, 0.5, 0.75 and 1) as-quenched ribbons are analyzed by inert gas fusion, which are 126ppm, 60ppm, 110ppm, 108ppm, 114ppm (mass) respectively. These oxygen levels in these alloys is far below the

critical oxygen concentration reported by Murty [5], and its effect on the crystallization process of $Zr_2Cu_{(1-x)}Pd_x$ metallic alloys can presumably be ignored.

We carried out the *ab initio* calculation using the Vienna *ab initio* Simulation Package (VASP) [9, 10] to get the thermodynamic stable structure of *C11b* phase in the $Zr_2Cu_{(1-x)}Pd_x$ system and compare the calculated *C11b* structure changes with the experimental results when x increases from 0 to 1. The density functional calculations are performed using a plane-wave pseudo-potential representation, with ultra-soft pseudo-potentials [16] for all species and with a plane-wave energy cutoff of 300 eV. The *k*-point sampling was chosen to converge all of the total energies to an accuracy of 2 meV/atom. The *k*-point grid used for structural relaxation was 12x12x12, chosen according to the Monkhorst-Pack scheme [17], and symmetry reduced to the irreducible Brillouin zone. In order to provide insight to the experimental thermal expansion of *C11b* phase crystalline structure during the constant heating in the $Zr_2Cu_{(1-x)}Pd_x$ system, the elastic constants were calculated by the full-potential linearized augmented plane-wave (FLAPW) method [18] within the local-density-functional approach. The calculation details of the second-order elastic constants of a tetragonal structure have been described by Fu *et al* [19]. Note that all calculations are at $T=0$.

Results and discussion

C11b phase structure with composition: changes of lattice parameters and bond lengths

Ab initio calculations of the *C11b* structure provide insight into the role of the Pd:Cu ratio on cell lattice parameters, cell volume and the changes in bonding. Although these calculations are carried out at 0 K, the trends observed in the calculations and experiments show striking similarities [8].

To analyze the high temperature phase structure, one common approach is to anneal the samples at a target temperature for a certain period of time, following X-ray diffractions and Reitveld refinement. Using this approach, we annealed all five $Zr_2Cu_{(1-x)}Pd_x$ compositions to 973K for 96 hours in high purity Argon environment to obtain the stable *C11b* phases. After quenching, all compositions were scanned at room temperature by high energy x-ray diffraction (HEXRD) and analyzed by Rietveld refined. We found that the Rietveld fitting factors wRp, Rp, and $\chi 2$ are fairly high for all of the compositions, yet there were no peaks that were missed. One explanation for the poor fitting would be disordering in the *C11b* structure during the quench process after the annealing. For example, when we allowed a stacking fault model to be included in the refinement, the values of wRp, Rp, and $\chi 2$ improved from 22.59%, 17.76%, 29.06 to 18.83%, 13.62%, 20.24, accordingly. This results suggest chemical ordering does occur at low temperatures.

Using *in situ* HTXRD, the effect of quenching process can be avoided. Since we started with amorphous alloys, we define T_{xe} as the temperature of the first scan that the intensity of the major diffraction lines of *C11b* phase reaches a constant value. *In situ* HTXRD patterns were obtained at T_{xe}+100k for all five compositions. From the Rietveld refinements, the goodness of fit factors, wRp, Rp and χ^2, indicate an excellent agreement

between the observed and calculated intensities for x = 0, 0.25, 0.5, and 0.75. However, for x = 1, the goodness of fit factors are all higher wRp (11.59%), Rp(7.84%) and χ^2(11.29) than the other four compositions. While the peak positions and peak shapes fit the model *C11b* structure, the poorer goodness of fit for x = 1 is due to poor modeling of the intensities (Figure 1). The difference in calculation intensity can arise from either texturing or from site disorder. Since no family of planes shows uniform increase over the powder average, we assume that the deviation from ideality is due to site disorder. The refinement of the occupation parameters shows that when about 8% of the Zr position is partially occupied by Pd atoms, χ^2 was improved from 11.290 to 8.925. This indicates that there are more intercalation defects or site disordering in the Zr_2Pd alloy than any other compositions. This would suggest that the entropic term may be more of a factor for the Zr_2Pd compound than the others since it has the highest formation enthalpy, yet has the highest defect concentration.

The measured *a*-axis of the *C11b* structure in $Zr_2Cu_{(1-x)}Pd_x$ (x=0, 0.25, 0.5, 0.75 and 1) alloys shows a non-linear increase from 3.2378(3)Å to 3.3115(5) Å (Figure 2 (a)). This is most likely related to size effects because of the larger radii of Pd relative to Cu. While the *c*-axis exhibits a maximum value of 11.312(2) Å at x = 0.5. Using Pd and Cu atomic radii of 1.41 Å and 1.27 Å [14], the measured lattices show strong deviations from the Vegard's law between the lattice constants and the compositions in the solid solution of Zr_2TM (TM=Pd, Cu). Such deviation is not unusual [20, 21], since Vegard's law only accounts for size. The difference in the electron configuration between Pd ($[Kr]4d^{10}$) and Cu ($[Ar]3d^{10}4s^1$) should be a significant contribution on the variation of the *C11b* structure in $Zr_2Cu_{(1-x)}Pd_x$ system. Since the increase of the basal plane's area is more than the decrease along *c*-axis after x > 0.5, the cell volumes increase with increasing Pd content.

Even though *ab initio* calculations are performed at 0 K, they do provide insight into thermodynamic stability [22, 23]. *Ab initio* calculations can be used to theoretically evaluate the effect of alloying on the phase structure, providing a better understanding into the crystal chemistry. From x = 0 to 0.75, the difference between the calculated values and observed values are small. However, the *a*- and *c*-axis lattice parameters for Zr_2Pd shows the greatest differences between observed and calculated values. The calculated a-axis (at 0 K) is 0.0312Å larger than the observed value (at 895 K), while the calculated c-axis is 0.1881Å smaller than the observed value. This is consistent with the Rietveld fitting which suggests some site disorder, which is difficult to examine using *ab initio* methods since calculations are limited to periodic arrangement of atoms and there is a practical limit to the cell size due to computation time. However, what is more important is that the overall trends in the calculated lattice parameters of the $Zr_2Cu_{(1-x)}Pd_x$ alloys as a function of x are quite similar to the experimental value and that the observed behavior is most likely an intrinsic rather than an extrinsic effect such as defects or second phases.

In the representative *C11b* cell (Figure 2 (d)), the three nearest bond lengths in the cell are Zr1-Zr2, TM-Zr1 and TM-Zr2, in which, TM = Pd, Cu:

$$d_{Zr1-Zr2} = \sqrt{0.5a^2 + (0.5-2z)^2 c^2} \quad (1)$$

$$d_{TM-Zr1} = zc \quad (2)$$

$$d_{TM-Zr2} = \sqrt{0.5a^2 + (0.5-z)^2 c^2} \quad (3)$$

To discuss the effects of both size and electronic factors on *C11b* cell in detail, we calculated the total d-bond overlap populations of TM-Zr per nominal unit with increasing x (Figure 2 (c)). The contribution of TM-Zr bond increases with Pd content and the increasing

rate is more rapid in Pd rich compositions. With the more covalent electrons occupying the d-bond, TM-Zr bonding becomes stronger. This is also consisting in our previous work [7] on the first diffuse scattering peaks in the reduced radial distribution functions of the $Zr_2Cu_{(1-x)}Pd_x$ alloys, in which, the affinity of Pd for Zr is deduced to be stronger compared to Cu. It should be note that although Zr-Pd is stronger than Zr-Cu, the bond lengths are not only affected by the bond affinity, but also by atomic size at the same time. The experimental and calculated bond lengths TM-Zr1 shorten at high Pd content, even though the TM atomic size increases. This is not surprising if we consider the trade-off effects from both size and electronic viewpoint. The TM-Zr1 bond length is relatively longer, and at this bond length, size effect is less than the electronic effect. With the rapid increasing bond overlap population of TM-Zr bond at higher Pd content compositions, the TM-Zr1 pair is more attracted and formed shorter bond lengths. From geometric and symmetric considerations, the *c*-axis length is strongly related with the bond length of TM-Zr1. This would also imply stronger Pd-Zr bonding should account for the decrease in the c-axis with increasing x. The TM-Zr2 bond length trend shows almost the same trends as the a-axis. This is because the length scale of TM-Zr2 is much shorter than TM-Zr1, and, at this bond length the atomic size effect is the main controling factor. The experimental and calculated trends of Zr1-Zr2 bond lengths shows a small discrepancy for x=0.5, which most likely arises from the simplifications used in the calculations. In the case of the solid solutions, there are a large number of possible arrangements for the Pd and Cu. We have not attempted a systematic exploration of these, but consider only likely arrangements based on the mixed system, which was described in our previous work [8].

C11b phase structure with temperature: anisotropic thermal expansions

In situ heating diffraction measurement by HTXRD is an ideal method to obtain the details of the high temperature crystal structure changes for $Zr_2Cu_{(1-x)}Pd_x$ alloys, since it can reveal both stable and metastable phase changes. The T_{xe} (Figure 3) for x = 0, 0.25, 0.5, 0.75 and 1 will be the reference temperatures for each of their respective alloy compositions and provide a relative comparison for the CTE measurements. No variation in the intensity of the major lines for $T > T_{xe}$ and all reflections could be indexed indicating that we maintained a thermodynamically steady state relative to the *C11b* phase and that the powder averaging was good throughout the experiments.

Since the lattice parameters are both a function of composition and temperature, comparing the alloys lattice parameters as a function of temperature is not straight-forward. For instance, T_{xe} and the melting temperature (T_m) both increase with increasing Pd:Cu ratio (Figure 3). But the increase T_{xe} is not linear with composition. This indicates that substitution of Pd for Cu has greater effect on T_{xe} in $Zr_2Cu_{(1-x)}Pd_x$ alloys at lower Pd:Cu ratios. On the other hand, T_m also increases from 1264 K to 1358 K over the whole composition range. The observed trend of experimental melting temperatures are in reasonable agreement with that of the calculated heat of formation [8] for $Zr_2Cu_{(1-x)}Pd_x$ system, which are 0.42, 0.68, 0.95, 1.19 and 1.46 eV/formula unit from x = 0 to 1. To better visualize the structural changes as a function of temperature, we normalize the lattice parameters of the *C11b* structures to the crystallization temperature. We define a 'homologous temperature' $T_H=T/T_{xe}$ as a means of comparing the *C11b* phase over a range of temperatures above T_{xe} during constant heating, and a 'homologous lattice parameters' $a_H=a/a_c$, and $c_H=c/c_c$ as a means of normalizing the lattice parameters, in which, a_c and c_c are the lattice parameters of *C11b* phase at T_{xe}.. For

comparison sake, all experimental homologous lattice parameters are compared at the same homologous temperature.

Rietveld refinement was performed for all compositions for at least a 100 K temperature range above T_{xe}. Fitted parameters include the lattice constants, the refinable atomic positions, thermal parameters, peak shape profiles and background. The *C11b*-type structure ($MoSi_2$) has only two atomic sites: Zr should fully occupy the 4(*e*) 0 0 *z* site, while the TM (TM = Pd, Cu) should fully occupy the 2(*a*) 0 0 0 site in the ideal structure. Overall fitting of the data was uniformly very good except with the Zr_2Pd compound, which had wRp's less than 7% and Rp's less than 5%. The poorer fitting of Zr_2Pd indicates some site disorder or vacancies which were discussed above.

It is observed that c_H increases as function of T_H from x = 0 to 1 (Figure 4). The increasing values of c_H reach 0.17%, 0.18%, 0.14%, 0.22% and 0.25% for all the five compositions, which are much more than those of a_H. a_H increases linearly with T_H for x=0 to 0.75 in the *C11b* phase. The increasing values are pretty small, only 0.04%, 0.02%, 0.07%, and 0.05% for those 4 compositions. The increasing homologous lattice parameters can be deduced by the cell thermal expansion with the increasing temperature. But we can obviously observe an exception at x = 1, a_H decreases with T_H gradually, although the decreasing value is only 0.05%. It indicates in Zr_2Pd alloy, *C11b* structure experiences an abnormally change with increasing T_H, comparing to the other 4 compositions. Using *ab initio* calculation, we simulated the thermal expansion process by extending the *C11b* cell volume for both Zr_2Cu and Zr_2Pd alloys. During the relaxation of the lattice parameters as the unit cell expanding, the *c*-axis shows a rapid increasing for both alloys. While for *a*-axis, it remains almost constant for Zr_2Cu and decreases a little for Zr_2Pd, which confirms the irregular *a*-axis lattice

changes in Zr_2Pd alloy. It also indicates the volume expansions of *C11b* cell during constant heating are depended more on *c*-axis than *a*-axis. The ratio of homologous lattice parameter: *c*-axis over *a*-axis (c_H/a_H), is larger than 1, reflecting the thermal expansion anisotropy in *C11b* structure for all 5 compositions in $Zr_2Cu_{(1-x)}Pd_x$ system. This indicates that the *c*-axis expands more readily for all compositions with increasing temperature. In addition, this anisotropy is nearly linear with the homologous temperature. The calculated slopes from the HTXRD experimental observation of c_H/a_H over T_H are 0.0086(4), 0.0118(4), 0.0052(4), 0.0142(1), 0.0233(4) for x = 0 to 1, accordingly. We can see that the largest anisotropy of thermal expansion between the *c* and *a-axis* directions was observed at x = 1 and the two lowest anisotropy of thermal expansion was for x = 0.5 and x = 0.

The coefficient of thermal expansion, CTE, is an important thermodynamic property of crystalline phases. The experimental CTEs can be calculated as:

$$CET(a) = \frac{1}{a_c}(\frac{\partial a}{\partial T_H}) \tag{4}$$

$$CET(c) = \frac{1}{c_c}(\frac{\partial c}{\partial T_H}) \tag{5}$$

$$CET(V) = \frac{1}{V_c}(\frac{\partial V}{\partial T_H}) \tag{6}$$

Where, V_c is the cell volume of *C11b* phase at T_{xe}. The value of a_c, c_c, and V_c are listed in Table 1. The CTEs in the *a*-axis directions are significantly smaller than those of *c*-axis directions with the increasing homologous temperature, indicating the bond strength in the *a*-axis direction is much more rigid than *c*-axis direction for all compositions. A negative CTE was noted in the *a*-axis direction for x = 1, which suggested *C11b* structure of Zr_2Pd alloy has abnormal thermo-elastic properties compared to the other 4 compositions.

To better understand the results of the thermal expansion data, first principles local-density-function calculation [18, 19] of the elastic properties was carried out for the two binary alloy systems Zr_2Cu and Zr_2Pd. We list the calculated second order elastic constants in Table 2. There are three interesting features in the elastic properties of Zr_2Cu and Zr_2Pd alloys: First, the shear anisotropy ratio A, defined as

$$A = \frac{2C_{66}}{(C_{11} - C_{12})} \tag{7}$$

are 0.515 for Zr_2Cu and 0.836 for Zr_2Pd, indicating the anisotropy of Zr_2Pd is large than that of Zr_2Cu, which is coherent with the experimental observation. Second, the calculated second elastic constants $C_{11}+C_{12}$ is larger than C_{33} for both Zr_2Cu and Zr_2Pd. suggesting that the elastic tensile modulus is higher on the (0 0 1) plane than along the [001] direction. In other words, the bonding in the basal plane is stronger than the bonding of *c*-axis direction. This is consistent with the experimental thermal expansion, where both *C11b* structures of Zr_2Cu and Zr_2Pd show lattice expansion anisotropy $c_H/a_H > 1$ during the whole heating process. The values of $\frac{C_{11}+C_{12}}{C_{33}}$ are 0.515 and 0.836 for Zr_2Cu and Zr_2Pd, respectively. The calculated ratio of the elastic tensile modulus of (0 0 1) plane over [0 0 1] direction is also in good agreement with the experimental results showing greater anisotropy of thermal expansion in the Zr_2Pd. Third, the relation of $C_{66} > C_{44}$ for both alloys suggests that the <1 0 0>{0 0 1} shear is easier than the <1 0 0>{0 1 0} shear. That means, for the (0 0 1) layers, the shear of inter-layer bonds is easier than the shear of intra-layer bonds, which also consistent with the anisotropic CTE's measured in this system [19].

Conclusion

With increasing x in $Zr_2Cu_{(1-x)}Pd_x$ alloys, the lattice parameter along the *a-axis* increases, while lattice parameter along the *c*-axis reaches a maximum value of 11.312(2) Å at x = 0.5, and then decreases from x = 0.5 to 1. The increase in the basal plane dimension more than compensates for the decrease in the *c*-axis for x > 0.5, so the overall volume increases with x. The *ab initio* calculations are in agreement to within 1.7% of the experimental values. Although the shortest bond lengths in *C11b* structure shows some deviation between the experimental data and the calculated results, the overall trends are quite similar, except for the Zr1-Zr2 bond length at x = 0.5, which may caused by simplifications in calculated structure. The shortening of the TM-Zr1 bond accounts for the decrease in the *c*-axis with increasing x. The bond overlap population and atomic size form a trade-off effect on bond changes. The thermal expansion of the *C11b* phase was more anisotropic for the higher Pd containing alloys (x = 0.75 and1). Increasing Pd relative to Cu in the *C11b* system increases the crystallization temperature for the *C11b* phase and melting temperature, which is consistent with the calculated heat of formation. The degree of elastic rigidity is larger in the basal plane (0 0 1) than along the *c*-axis, and the anisotropy of thermal expansion along the *a* and *c*-axes are observed for all five alloys. Using elastic constant calculations, more anisotropy of thermal expansion for Zr_2Pd than Zr_2Cu alloys are confirmed.

Acknowledgements

This research has been sponsored by the Division of Materials Sciences and Engineering, Office of Basic Energy Sciences, U.S. Department of Energy under contract DE-AC05-00OR-22725 with UT-Battelle and contract and DE-AC02-07CH11358 with Iowa State University. The Midwest Universities Collaborative Access Team (MUCAT) sector at the APS is supported by the US Department of Energy, Office of Science, Basic Energy Sciences, through the Ames Laboratory. Use of the Advanced Photon Source was supported by the US Department of Energy, Office of Science, Basic Energy Sciences, under Contract No DE-AC02-06CH11357.

References

[1] Saksl K, Franz H, Jovari P, Klementiev K, Welter E, Ehnes A, Saida J, Inoue A, Jiang JZ. Applied Physics Letters 2003;83:3924

[2] Saida J, Matsushita M, Inoue A. Journal of Applied Physics 2000;88:6081

[3] Murty BS, Ping DH, Hono K. Applied Physics Letters 2000;77:1102

[4] Jiang J. Saksl Z, Saida KJ, Inoue A, Franz H, Messel K, Lathe C. Applied Physics Letters 2002;80:781

[5] Murty BS, Ping DH, Hono K, Inoue A. Acta Materialia 2000;48:3985

[6] Kramer MJ, Besser MF, Yang N, Rozhkova E, Sordelet DJ, Zhang Y, Lee PL. Journal of Non-Crystalline Solids 2003;317:62

[7] Xu M, Ye Y, Morris JR, Sordelet DJ, Kramer MJ. Philosophical Magazine 2006;86:389

[8] Morris JR, Xu M, Ye YY, Sordelet DJ, Kramer MJ. Acta Mat 2007:55:5901

[9] Kresse G, Furthmüller J. Phys. Rev. B 1996;54:11169

[10] Kresse G, Hafner J. Phys. Rev. B 1993;47:558

[11] Thaddeus BM. Binary Alloy Phase Diagrams. 1987

[12] Hume-Rothery W. Atomic Theory for Students of Metallurgy. Fifth Ed., The Institute of Metals, London; 1969.

[13] Ohta Y, Pettifor DG. Journal of Physics: Condensed Matter 1990; 2, 8189

[14] Egami T, Waseda Y. Journal of Non-Crystalline Solids 1984;64:113

[15] Eckert J, Mattern N, Zinkevitch M, Seidel M. Materials Transactions, JIM 1998;39:623

[16] Kresse G, Furthmüller J. Computational Materials Science 1996;6:15

[17] Monkhort HJ, Pack JD. Phys. Rev. B 1996;13:5188

[18] Fu CL, Wang X. Philosophical Magazine Letters 2000;80:683

[19] Fu CL, Wang X, Ye YY, Ho KM. Intermetallics 1999;7:179

[20] Nongkynrih PY, Rao ST, Gupta SK, Rao PVR. Journal of Materials Science 1988;23:3243

[21] Kuo YK, Liou BT, Yen SH, Chu HY. Optics Communications 2004;237:363

[22] Hennig RG, Carlsson AE, Kelton KF, and Henley CL, Physical Review B: Condensed Matter and Materials Physics 2005;71:144103/1

[23] Nicholson DMC, Stocks GM, Shelton WA, Wang Y, and Swihart JC, Metallurgical and Materials Transactions A: Physical Metallurgy and Materials Science 1998;29A:1845

Table 1. Experimental CTE(a), CTE(*c*), and CTE (*V*) for *C11b* phase in $Zr_2Cu_{(1-x)}Pd_x$ metallic alloys (x=0, 0.25, 0.5, 0.75 and 1) over the 100K temperature range measured.

x	0	0.25	0.5	0.75	1
a_c (Å)	3.2364(2)	3.2377(2)	3.254(1)	3.277(1)	3.313(2)
c_c (Å)	11.1931(1)	11.2484(1)	11.297(4)	11.192(4)	11.042(8)
V_c (Å^3)	117.24(1)	117.91(1)	119.6(2)	120.2(1)	121.2(3)
CTE (*a*) (ppm/K)	4.3(6)	2.0(1)	6.6(1)	4.5(8)	-4.9(8)
CTE (c) (ppm/K)	17.3(1)	18.2(1)	13.3(8)	22.1(7)	25.0(1)
CTE (*V*) (ppm/K)	26.0(4)	22.2(3)	26.6(2)	31.3(4)	15.0(2)

Table 2. Theoretical second-order elastic constants (Mbar) of *C11b* phase in Zr_2Cu and Zr_2Pd metallic alloys.

	C_{11}	C_{12}	C_{33}	C_{44}	C_{66}	C_{13}
Zr_2Cu	1.979	0.756	1.553	0.273	0.315	1.016
Zr_2Pd	1.921	0.863	1.493	0.265	0.444	0.981

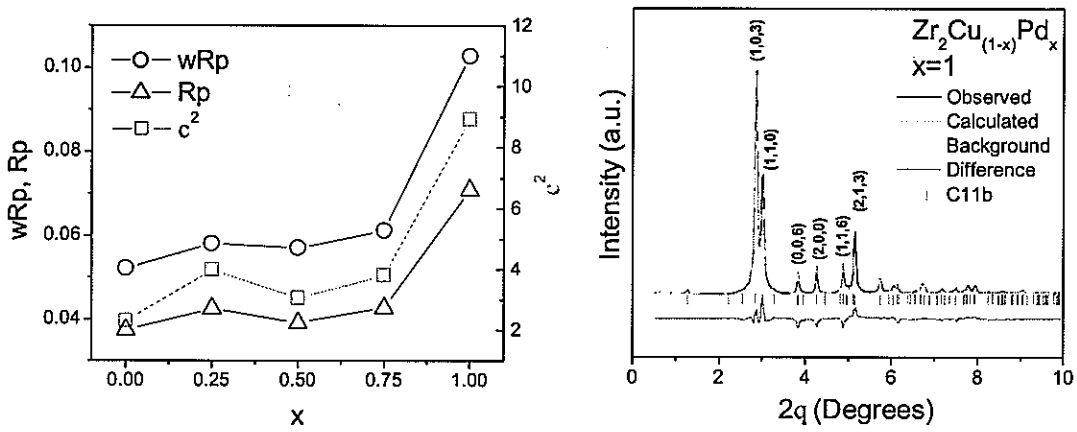

Figure 1. Rietveld refinement profiles of high temperature X-ray diffraction patterns for *C11b* phase in $Zr_2Cu_{(1-x)}Pd_x$ (x=0, 0.25, 0.5, 0.75 and 1) metallic alloys. Experimental, calculated and difference HTXRD patterns for Zr_2Pd at 100K beyond T_{xe}, with *C11b* phase reflections indicated by vertical hash marks.

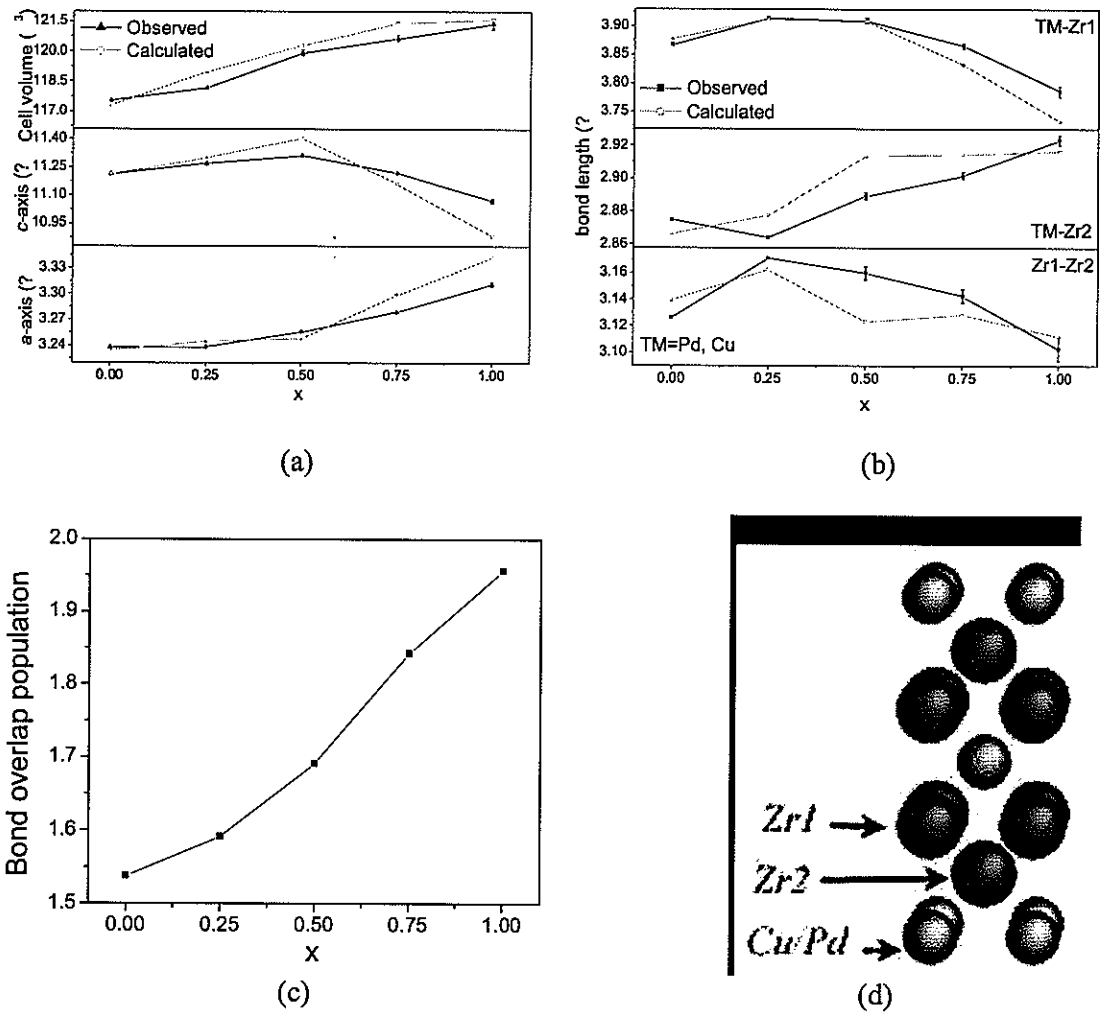

Figure 2. *C11b* structure comparison between experimental results and *ab initio* calculation with increasing x in $Zr_2Cu_{(1-x)}Pd_x$ (x=0, 0.25, 0.5, 0.75 and 1) metallic alloys. (a) lattice parameter *a*, lattice parameter *c*, cell volume; (b) The three types of nearest bonds, Zr1-Zr2, TM-Zr1 and TM-Zr2; (c) d-bond overlap population per nominal unit for transition metal TM (TM = Pd, Cu) and Zr atoms; (d) the representative *C11b* cell, atom Zr1 and Zr2 occupy the (0, 0, *z*) and (0.5, 0.5, 0.5-*z*) positions; TM atom occupies the (0, 0, 0) position.

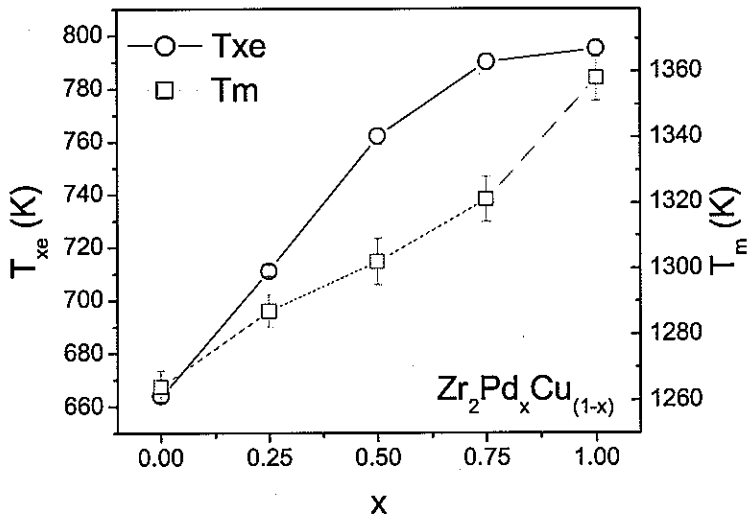

Fig. 3. Crystallization temperatures (T_{xe}) and melting temperature (T_m) of *C11b* phase of $Zr_2Cu_{(1-x)}Pd_x$ (x=0, 0.25, 0.5, 0.75 and 1) metallic alloys obtained by *in situ* HTXRD and DTA.

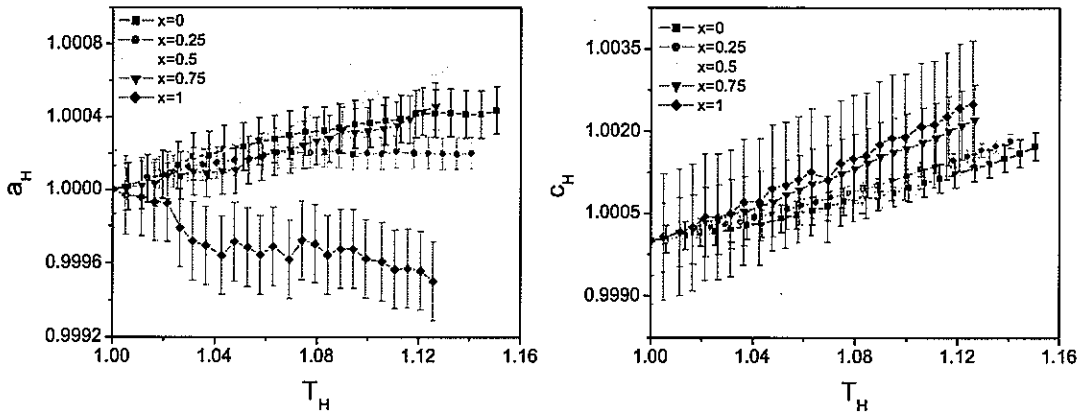

Figure 4. Ratio of homologous lattice parameters of the *C11b* phase, c_H/a_H ($a_H=a/a_c$, $c_H=c/c_c$), as the function of the homologous temperature ($T_H = T/T_{xe}$) during 100K temperature range above T_{xe} in $Zr_2Cu_{(1-x)}Pd_x$ (x=0, 0.25, 0.5, 0.75 and 1) metallic alloys.

CHAPTER 5. PHASE STABILITY AND TRANSFORMATIONS IN THE $ZR_2NI_XCU_{1-X}$ SYSTEM

A paper published in Metallurgical and Materials Transactions A **39A**, 1847-1856 (2008)

M. J. Kramer[1,2], Min. Xu[1,2], Y. Y. Ye[2,3], D. J. Sordelet[2], and J. R. Morris[4,5]

Abstract

Since Ni and Cu differ by only one valence electron, yet have nearly identical atomic sizes (1.27 vs 1.28 Å for Cu and Ni, respectively), the amorphous $Zr_2Ni_xCu_{1-x}$ system is ideal to isolate the effects of electronic structure on short- and medium-range order and their concomitant influence on devitrification pathways. Thermal analysis, time-resolved high energy X-ray diffraction and transmission electron microscopy were used to follow metastable and stable crystalline phase formation during devitrification. Using time-resolved

[1]Department of Materials Science and Engineering, Iowa State University, Ames, IA 50011, USA

[2]Materials and Engineering Physics Program, Ames Laboratory (USDOE) Ames, IA 50011, USA

[3]Center of Analysis and Testing, Wuhan University, Wuhan, 430072, Hubei, China

[4]Materials Science & Technology Division, Oak Ridge National Laboratory, Oak Ridge, TN 37831-6115, USA;

[5]Department of Materials Science and Engineering, University of Tennessee, Knoxville, TN 37996-2200

*Corresponding author: email: mjkramer@ameslab.gov; phone: 515-294-0276

high energy X-ray diffraction, we observed that the first devitrification product in the Zr_2Ni system is the *C16* structure if oxygen is kept sufficiently low, while the Zr_2Cu system forms the *C11b* structure. For x = 0.25, the initial devitrification involves forming co-existing *C11b* and *C16* phases. When Ni is increased to $x \geq 0.50$, the initial devitrification only involves the *C16* structure. These results are in complete accord with electronic structure calculations showing that the enthalpy of formation for the *C11b* phase is favored for x = 0, while enthalpies for *C11b* and *C16* are nearly identical for x = 0.25 and the *C16* phase has the most negative enthalpy for all compositions where x > 0.25.

Introduction

The phase selection process during devitrification of a glassy alloy (i.e., whether stable or metastable crystalline phases initially form), provides insight into the short range order (SRO) of the preceding glassy state. The tendency to devitrify is closely related to the stability of the glass. Studying the devitrification process allows a probe of the origin of the stability: for example, is the stability of the glass (relative to the crystalline compounds) due primarily to packing efficiencies, or to electronic stabilization effects.[1, 2] The range of compositions in Zr-TM (transition metal) alloys that can be made amorphous using rapid solidification methods together with the variability in intermetallic compounds which can form make Zr-based systems ideal for investigations into the structural relationships between the amorphous alloys and their crystalline states.[3, 4, 5] Zr (or mixtures with Ti, Nb and Hf) are alloyed with late transition metals including noble metals (Ni, Cu, Pd, Ag and Pt) to form

a variety of bulk metallic glasses.[6, 7, 8] The stability of the metallic glass is usually enhanced by minor alloying changes and in many cases the increased stability is attributed to increasing icosahedral order in the glassy alloy.[9, 10]

Here we study a model alloy, $Zr_2Ni_xCu_{1-x}$ which isolates the competing aspects between packing efficiencies (i.e., Cu and Ni have very similar Goldschmidt radii of 1.27 vs 1.28 Å, respectively) [11] and that of electronic stabilization effects. Zr_2Cu and Zr_2Ni both melt congruently but have different thermodynamically stable structures, [12] *C11b* and *C16* respectively. Amorphous alloys of Zr_2Cu and Zr_2Ni can be easily made by rapid solidification and have been shown to devitrify in a single step. Scattering studies and X-ray absorption, fine structure spectroscopy (XAFS) have determined that the SRO consists of short Cu-Cu (or Ni-Ni), intermediate Zr-Cu(Ni) and longer Zr-Zr bonds in the first shell. [13, 14] Recent work on the Zr-Cu and Zr-Ni glasses suggests that the former is more icosahedral than the latter, which has polytetrahedral clusters more like the *C16* crystalline phase. [15, 16] The authors attribute the lack of glass transition in the Zr_2Ni due to the similarities in the SRO of the glass and the stable crystalline phase. In this study, we bring together time resolved high energy X-ray diffraction (HEXRD), [17] thermal analysis and *ab initio* calculations to investigate the competition between the two thermodynamically stable phases as the Ni:Cu ratio is varied.

Methods

Experimental

Five alloys of $Zr_2Ni_xCu_{1-x}$ (compositions are expressed in at%, x = 0, 0.25, 0.5, 0.75 and 1) were prepared by arc melting the mixtures of pure Zr (99.95 mass%), Ni (99.99 mass%) and Cu (99.99 mass%) metals in a ultra high-purity argon atmosphere. The alloys were melted several times in order to ensure the compositional homogeneity. Since oxygen content can alter the devitrification pathways, [18] crystal bar Zr having 50 parts per million (ppm) oxygen by mass was used and melt spinning was performed using a graphite crucible to minimize oxygen contamination. [19] Amorphous alloys were obtained by melt spinning with a tangential wheel speed of 25m/s at a constant over pressure of 1.6×10^4 Pa in a ultra high-purity Helium. The melt spun ribbons are approximately 1mm in width and 40μm in thickness. The oxygen content of the as-quenched ribbon samples were analyzed using inert gas fusion and found to be to be less then 250 ppm . The devitrification pathways of these alloys during heating were studied using a combination of differential scanning calorimetry (DSC), differential thermal analysis (DTA), transmission electron microscopy (TEM) and high-energy X-ray diffraction (HEXRD). DSC was performed on these samples using constant heating rates of 0.083, 0.167, 0.333, 0.667 and 1.333 K/s and isothermally with T offsets of 5, 10, 15, 20 and 25 K below T_x. The melting temperatures (T_m) of these alloys were obtained by a DTA at a heating rate of 10 K/min.

Since the initial phases which form during devitrification may not be the thermodynamically stable phase, samples were wrapped in Ta foil, sealed in silica tubes backfilled with Ar and annealed at 0.9 * T_m for 24 hrs then quenched in a water bath. Phase identification, phase fraction and room temperature lattice parameter determinations for these

annealed samples were obtained using Rietveld analysis of XRD patterns obtained using $Cu_{k\alpha}$ radiation. [20]

HEXRD studies were performed at the Advanced Photon Source (APS) at Argonne National Laboratory using an energy of 99.55 keV, which corresponds to a wavelengths (λ) of 0.0124(7) nm. The diffraction data were obtained at the 6ID-D beamline at APS in collaboration with the Midwest Universities Collaborative Access Team (MUCAT). Silicon double-crystal monochromators were employed to select the wavelength. All samples were sealed in thin-walled silica capillaries using Ar. The HEXRD was obtained in a time-resolved manner using a MAR CCD (MAR Reseach, Evanston, IL) in an off-beam-axis mode where only a 60 degree arc of the Debye cones intersect the CCD. This geometry was a compromise between obtaining high reciprocal-space diffraction patterns every 20 s while maintaining a sufficiently high signal-to-noise ratio to resolve subtle details of the phase transitions at a modest heating rate of 10 K/min or using and isothermal hold at 20 K below the crystallization temperature (T_x). The sample to detector distance was calibrated using a NIST Si (640C) standard.

To examine the local atomic structure of the different compositions the HEXRD scans were corrected for absorption, polarization, multiple scattering, and Compton scattering to extract their coherently scattered intensity (Ie(Q)). The total scattering functions, S(Q), were then calculated according to, [21, 22]

$$S(Q) = 1 + \frac{\left[I^e(Q) - \sum_{i=1}^{n} a_i \left| f_i(Q) \right|^2 \right]}{\left| \sum_{i=1}^{n} a_i f_i(Q) \right|^2} \qquad \text{Eq. (1).}$$

where, a_i is the atomic proportion of each element and $f_i(Q)$ is the Q-dependent scattering factor for each element. The reduced pair distribution function (RPDF), $G(r)$, were determined by Fourier transforming the total scattering function:

$$G(r) = 4\pi r[\rho(r) - \rho_0] = \frac{2}{\pi}\int_0^\infty Q[S(Q) - 1]\sin(Qr)dQ \qquad \text{Eq. (2)}$$

where $\rho(r)$ is the atomic density at a distance r from an average atom located at the origin and ρ_o is the average atomic density of the material. The RPDF was utilized for comparing the real-space structure of the different alloy compositions since it does not require independent measurements of the atomic densities of the alloys.

Electronic Structure Calculations

To theoretically evaluate the effect of alloying on the phase stability, we used electronic structure calculations to examine the total energies of the competing crystalline structures. Our simulations were carried out using the Vienna *Ab initio* Simulation Package (VASP). [23, 24, 25] The density functional calculations were performed using a plane-wave pseudopotential representation, with ultra-soft pseudopotentials [25] for all species and with a plane-wave energy cutoff of 240 eV. The *k*-point sampling was chosen to converge all of the total energies to an accuracy of 2 meV/atom. The *k*-point grid used for structural relaxation was 8x8x8, chosen according to the Monkhorst-Pack scheme [26] and symmetry reduced to the irreducible Brillouin zone. For the electronic density of states, a 16x16x16

grid was used. With each configuration, the total force on each ion is calculated using the Hellmann-Feynman theorem; the ionic positions were then relaxed to an accuracy of 0.01 eV/Å. In addition, all periodic unit cells were relaxed to minimize the total energy. The relaxation of both internal degrees of freedom and lattice parameters were performed together, as these are often coupled, to find the local minimum in energy.

Results

The room temperature S(Q) and G(r) results are consistent with previous studies for the binary compounds (Fig. 1). In this study, the $Zr_2Ni_xCu_{1-x}$ series appears to show a systematic trend in the change in the peak positions with x. In the S(Q), there is a very small shift in diffuse scattering peaks to lower Q (< 0.4 %) with increasing Ni. A very small pre-peak (at Q ~ 1.8 Å) is observed in the alloys for x > 0.5. More importantly, the first shell in the G(r) displays distinct shape changes with a bimodal-like distribution that shows increasing separation with increasing Ni concentration. The contribution from the three reduced partial pairs ($G_{Cu,Ni-Cu,Ni}$, $G_{Cu,Ni-Zr}$ and G_{Zr-Zr}) are well separated in this amorphous alloy with the shortest bonds being Cu(Ni)-Cu(Ni) and longest Zr-Zr. [13, 14, 27, 28] The contributions from the Cu(Ni)-Cu(Ni) pairs are small and are nearly identical in average distance of about 2.56 Å. [13, 28] Gaussian fitting of the first shell indicates that the Cu(Ni)-Zr pair separation decreases by 0.06 Å when replacing Ni with Cu while the Zr-Zr pairs separation increases by about the same amount as the Cu(Ni)-Zr pair separation decreases. The shortening of the Cu(Ni)-Zr bonds and a slight increase in the Zr-Zr with increasing Ni is

consistent with Saida et al. [28] results for the $Zr_{70}Cu_{30}$ and $Zr_{70}Ni_{30}$ rapidly quenched alloys they compared. The changes in the average Cu(Ni)-Zr and Zr-Zr pairs are nearly linear in composition which would argue for a complete mixing of the Cu and Ni. The weightings of the three Gaussians varies with the Ni:Cu ratio, indicating that the there may be some change in bond distributions.

The DSC results for constant heating rates 0.083, 0.167, 0.333, 0.667 and 1.333 K/s show only a single exotherm in the vicinity of 640 to 700 K, the temperature regime for devitrification of these alloys. Using the maximum slope method or the peak temperatures, the crystallization temperature varies little with increasing Ni. The alloy with x = 0.25 has the highest onset temperature for all heating rates, but by only a few degrees (Table 1). This is consistent for all heating rates. For x = 0.25 there appears a small exotherm at ~ 750 K while for x = 0.5 the beginning of an exotherm close to the upper temperature limit of our DSC of 873 K was also observed. No hints of a second transition were observed in any other of the samples. These data suggest that for at least these two samples (x = 0.25 and 0.50) a second solid state phase transition occurs distinct from the devitrification.

While the sensitivity of the DTA is too poor to provide any insight into the second exotherms in the DSC, the results indicates that there is a minimum in the T_m (~1200 K) for x = 0.50 compared to Tm of ~1275 and 1295 K for the end members Zr_2Cu and Zr_2Ni respectively. Data on cooling also show two closely related exotherms about 100 K below the T_m for x = 0.50 and only one exotherm for all other compositions. DSC and DTA analysis suggest that there is a two phase region in this pseudo-binary near x = 0.5. Based on the ternary phase diagram, multiple phases are expected in this system [12] with a eutectic forming in this pseudo-binary system. However, DSC and DTA do not provide any direct

information on which phases are forming or the width of the two-phase region. In addition, one is prone to miss metastable phases when performing heat and quench experiments. This is particularly true if the large face centered cubic phase based on the Ni_2Ti-type structure is a transient phase in this ternary system. [29, 30]

Time-resolved HEXRD provides a unique method to observe the full dynamics of the phase selection process.[17, 30] Figure 2 is a montage of 2D representations of the total scattering function (S(Q)) as a function of temperature from 500 to 1000 K using a heating rate of 0.167 K/s. This heating rate and the X-ray data collection frequency provide a temperature resolution of ~4 K. Note that the point of crystallization is sharply demarcated for each of these composition and the temperatures indicated are consistent with the DSC results. The initial devitrification is to a single phase for all alloys except for x = 0.25. In the case of x = 0, only the *C11b* structure forms and is stable up to melting. For x = 0.75 and 1.0, only the *C16* structure forms, but there is a sharpening of the reflections which occurs ~ 800 K, indicating that there may be some disorder relative to the ideal structure or a kinetic limitation to grain growth. For x = 0.5, the initial phase to form is *C16*, but that undergoes a solid state phase transition to *C11b* around 800 K, slightly lower that what was expected from the DSC, but the exact temperature of the second exotherm was difficult to determine since the signal was small and had not returned to the base line before reaching the upper temperature limit of our DSC. So we can assume that the second exotherm in the DSC is due to the *C16* to *C11b* phase transition. Only for the x = 0.25 alloy do we see clear indication of both *C16* and *C11b* forming simultaneously. The two-phase alloy is unstable and it too undergoes a solid state transition to a single phase *C11b* structure. These results are consistent with the DSC measurements.

One question posed by the results presented in Fig. 2 is what is the relative partitioning of Ni:Cu between the *C16* and *C11b* phases and does phase separation occur prior to nucleation? For a given driving force, the nucleation of *C16* appears to be favored over *C11b*, since this compound forms first in x = 0.5 before converting to *C11b*. In the case of x = 0.25, the two structures coexist, but only for a short time before forming *C11b*, indicating that *C16* can nucleate despite the higher driving force for *C11b*. A corollary question would be how does the SRO in the super-cooled liquid impact the energy or kinetics of the phase selection? To help answer these questions, we must examine the details of the phase selection process relative to the thermodynamics of the competing phases.

The HEXRD method has both the time resolution and the sensitivity to probe the initial stages of the devitrification. In each of these alloys, the intensity of the devitrified phase fraction ($I_f(Q)$) can be extracted from the amorphous component by estimating the volume fraction ($F|_t$) of the crystalline component at each temperature or time (t), $F|_t = \sum_{Q_{min}}^{Q_{max}} (I(Q)|_{t_o} - I(Q)|_t)$, where t_o is an initial state when the alloy is assume to be fully amorphous;

$$I_f(Q)|_t = I(Q)|_t - I(Q)|_{t_o} * (1 - F|_t) \qquad \text{Eq. (3)}$$

This technique provides a direct means of determining the volume transformed as a function of time or temperature and an X-ray diffraction pattern with a minimal background more suitable for Rietveld fitting.

Since the temperature resolution was quite coarse for the constant heating rate experiments (Fig. 2), we performed isothermal holds at 628 K, ~20 K below T_x (ΔT_x). The rate of the transition can be controlled by altering ΔT_x since this essentially changes the

driving force for crystallization. Given the high S:N in the synchrotron data, and using Eq. 3, Rietveld analysis of diffraction patterns which represent as little as 2 % of the crystalline fraction can be fit with a high degree of confidence (weighted residuals, wRp, were less than 6%) (Fig. 3). Of primary interest is x = 0.25, which is the only instance where the coexistence of two phases was observed during the initial devitrification.

The results of the isothermal HEXRD show a gradual transition from amorphous to crystalline structures over an interval of approximately 200 s, staring at 300 s after achieving the hold temperature of 628 K (Fig. 4). Extracting the crystalline fraction using Eq. (3), sequential refinements were performed on all $I_f(Q)|t$ up to the point where the alloy was fully devitrified to obtain the changes in ratio of *C16*:*C11b* as a function of the crystallized phase fraction (Fig. 5). Except for the initial transients during the early stages of devitrification, the lattice parameters for the *C16* varied little during the isothermal hold, a-axis = 6.627(3), c-axis = 5.177(6) while the c axis for the *C11b* did under go a 3% contraction in the c-axis (11.679(0) to 11.314(3)) during the initial stages of devitrification while the a-axis was nearly unchanged, 3.291(1). The ratio of *C16*:*C11b* increased slightly from 70 to 80% during the isothermal hold with an uncertainty of 10 % absolute for each phase fraction. The Lorentzian portion of the peak shape profiles for the *C11b* are considerably broader than the *C16*, indicating that the *C11b* grains were smaller and grew slower than the *C16* grains.

To cross check the HEXRD results, we performed isothermal heating in the DSC at 643 K which is a hold temperature of 20 K below T_x followed by quenching the samples after 4 different hold times: 6, 78, 162 and 324 s which represent ~0, 5, 70 and 100 % crystallization (open squares in Fig. 5). Note that the onset for crystallization is occurring quicker and has a slightly sharper transition than the HEXRD results. This is consistent with

a slightly smaller ΔT_x for the DSC results and is consistent with our uncertainty in the absolute temperature calibration between the DSC and the furnace used for the HEXRD experiments which can differ by ~ 5 K. These DSC annealed and quenched samples as well as the as-quenched alloy were then Ar ion milled using a liquid N_2 cooled stage and examined in a FEI Tecnai field emission STEM operated at 200 KeV (Fig. 6). The as-quenched alloy appeared to be homogenously amorphous and no chemical segregation was observed using energy dispersive spectroscopy (EDS). However, when obtaining chemical data in STEM mode, it was noted that partial crystallization could be initiated in the thinner regions if the beam remained in the same position for > 60 s. Samples heated and quenched in the DSC showed a progressively increasing proportion of crystalline phase fraction consistent with the DSC and HEXRD results. The number of grains per area remained nearly constant, but their size increased with annealing time. Initially, *C16* grains were larger, but by the time the sample was fully crystallized, *C11b* and *C16* were nearly the same size. *C11b* and *C16* phases were identified using electron diffraction and EDS. The *C11b* had a lower Ni:Cu ratio than the starting composition and the *C16* lower. In the partially crystallized samples with residual amorphous phase (Figs. 6b and 6c), the Ni:Cu ratio was in between the measured Ni;Cu rations for the crystalline *C11b* and *C16* phases present in the alloy. Phase proportions are difficult to quantify in the TEM, but the ratio of *C16* to *C11b* (80:20) obtained from the Rietveld analysis is consistent with the TEM results. The variations in grain size between the *C11b* and *C16* during the initial stages of the devitrification are also in accord between the TEM and Rietveld analysis since the peak shape profiles obtained for the *C11b* are much broader than the *C16* phase.

The experimental data show a strong competition between the *C11b* and *C16* phases. The initial devitrification clearly favors *C16* for x > 0.25. XRD analysis of the samples annealed to 90% T_m and quenched shows that *C11b* is thermodynamically stable phase for x < 0.5. This would suggest that both enthalpic and entropic terms are important and the phase selection is both temperature and composition dependent. Although the scattering factors for Cu and Ni are too similar in XRD to directly determine their respective partitioning between the two phases using Rietveld analysis, the phase proportions and their lattice parameters do aid in bracketing the partitioning. The change in the lattice parameters as a function of composition for both phases provides insight to the relative strength of the Zr-Cu vs. Zr-Ni bonds. For instance the unit cell volume of *C11b* and *C16* both contract with increasing Ni (Table 2), contrary to the Goldschmidt radii. [11] More specifically, the shortest Zr-(Cu,Ni) bonds in both the *C11b* and *C16* crystal structures decrease with increasing Ni but are not equal. For instance in the x = 0.5 alloy where *C11b* and *C16* coexist, the shortest Zr-(Cu,Ni) bonds in *C11b* are almost 0.01 nm longer than in *C16*.

First principle calculations can provide insight in to the relative stabilities of these two competing phases by comparing their formation enthalpies over the entire composition range for both phases. Information that is not accessible experimentally. The enthalpies are plotted in terms of eV/formula unit (f.u.) so that direct comparison can be made (Fig. 7). The energies of both structures vary linearly with composition. The enthalpy for *C11b* is less than *C16* for only x = 0 while they are nearly equal at x = 0.25. For x > 0.25, the *C16* structure has the most negative enthalpy. For a given crystal structure, we can determine the heat of mixing based on the enthalpies of the two end-members relative to their alloy composition:

$$x \bullet \Delta H[(Zr_2Ni)] + (1-x) \bullet \Delta H[Zr_2Cu] + \Delta H_{mix} = \Delta H[Zr_2(Cu_{1-x}Ni_x)] \quad \text{Eq (4)}$$

where ΔH_{mix} is the Cu-Ni heat of mixing. The ΔH_{mix} is most negative in both systems for x = 0.25, but about 20% more negative for the *C16* structure. The ΔH_{mix} is either positive or very small for x > 0.25 for the *C11b* structure. This would indicate a limited solubility for the Ni in the *C11b* structure for x > 0.25. On the other hand, the ΔH_{mix} is either negative or very small for $0.25 \leq x \leq 0.75$ for the *C16* structure indicating a wider degree of Ni:Cu solubility in this crystal structure. The calculated enthalpies are consistent with the initial devitrification which shows competition between *C11b* and *C16* but a slight preference for the *C16* phase. Of course, these calculations are performed at 0 K, and include no entropy terms; however, the close agreement with experiment indicates that the $T = 0$ contribution to the enthalpy is large, and possibly the dominant contribution to the phase competition between these crystal structures at the devitrification temperature. In addition, we note that the preferentially nucleated phase is determined by a balance of volumetric and interfacial free energies. Assuming that the interfacial free energies are determined by similarities between the atomic structure of the glass and the crystalline phases, a full treatment of nucleation will also require consideration of the SRO of the amorphous alloy relative to the competing phases.

Discussion

The room temperature results of the RPDF in the series in Figure 1 suggest that there is complete mixing of the Cu and Ni in the amorphous alloy. The results of the end-members are in accord with earlier work[13, 14, 28] on similar alloys. In this previous work, it is

established that the average Ni-Zr bond distance is much shorter than that of the Cu-Zr and they are well separated from the average distribution of the Zr-Zr bonds. In the ternary alloys, any phase separation should result in a broadening on the left hand side of the first shell in the PDF. Fitting of Gaussians to the RPDF shows no broadening of the peaks only linear shifting in position with Ni:Cu ratio. The large differences then in the Cu-Zr and Ni-Zr pair distributions in the first shell are in contrast to nearly identical average atomic radii estimated of 1.28 Å for Ni and 1.27 Å for Cu [11] thus ruling out a random hard-sphere packing model for these alloys.

The results on devitrification of the binary end-members of this study are in agreement with the earlier work [3, 4, 31, 32] where Zr_2Cu forms the *C11b* and the Zr_2Ni forms the *C16* crystal structures directly without any other intervening metastable phase. However, Bauer et al., using time-resolved XRD, did report that a face-centered cubic phase with a large unit cell (~12.35 Å) formed first and then converted to the *C16*, body centered tetragonal phase. [30] Most of the work in the ternary amorphous system involved $Zr_{70}(Cu,Ni)_{30}$. [33, 34, 35, 36, 37, 38, 39] This alloy sits in a ternary phase field [12] and therefore the devitrifcation products may not be directly comparable to our study. However, the work by the Wang et al. consistently report on the formation of the 'big cube' phase, a large FCC unit cell which is based on the Ti_2Ni-type structure (O_h^5) which is most likely the same phase reported by Bauer et al. [30] Altounian et al. noted that the a large unit cell FFC phase formed only in the presence of oxygen and other impurities. [29] Minor alloying additions can have profound effect on the phase selection process in Zr-based amorphous alloys. [19, 28, 40, 41] The time-resolved HEXRD in the current study clearly demonstrates

that using high-purity materials and minimizing oxygen contamination precludes the formation of the 'big cube' phase.

By concentrating on the tie-line between Zr_2Cu and Zr_2Ni, we can draw a pseudo-binary projection using the HEXRD and DTA data (Fig. 8). Since Zr_2Cu and Zr_2Ni melt congruently and have different crystal structures, there should be a two phase region separating these two compounds. The DTA data suggests that the eutectic is near x = 0.5. The HEXRD data allows an estimation of the boundaries of the two phase region. The line separating the single phase *C11b* from the two phase region cross x = 0.25 around 770 K. The line separating the two phase region to single phase *C16* crossed x = 0.5 around 810 K. Of all the samples annealed at > 90% T_m and quenched, only x = 0.50 was two phased. The DTA on cooling for x = 0.50 was the only sample which exhibited two exotherms, further indication that the eutectic point is between x = 0.25 and 0.75.

The DSC results indicate very little difference in the thermodynamic stability for these glasses across the range of compositions, regardless of which phase or phases form. The *ab initio* calculations clearly indicate that increasing Ni increases the enthalpy for *C16* over the *C11b* phase. However, the *C11b* phase has a larger region of thermodynamic stability than would be indicated by enthalpy alone. So, why does the *C16* phase preferentially nucleate and grow for x = 0.25 when the *C11b* structure is thermodynamically more stable? The clear separation in the room temperature RPDF argues against phase separation in the as-quenched state, since there appears to be a linear shift in x for the partial pairs. The EDS results of the partially devitrified x = 0.25 samples appears to rule out phase separation of the supercooled liquid. While there does appear to be partitioning of Cu and Ni between *C11b* and *C16*, the residual glass shows no such regions of chemical separation.

A more reasonable explanation for the observation of a metastable *C16* phase for x = 0.25 is that the amorphous state is structurally more similar to the *C16*, as argued by Fukunaga et al. [16] This suggests that the interfacial free energy is lower, which results in a lower barrier to nucleation of the *C16* phase. Thus, when bulk driving forces are similar, nucleation may favor formation of the *C16* over *C11b* phase. This is similar to arguments made for the observation of BCC nucleation in undercooled liquids with a stable FCC phase, such as $Fe_{1-x}Ni_x$. [42] The differences in the growth rates for the competing *C11b* and *C16* are also consistent with this explanation. The schematic phase diagram, Fig. 8, shows that the *C11b* phase has a much lower solubility for Ni than the *C16* phase has for Cu just above the crystallization temperature. When the homogenous glass nucleates, regions around *C11b* will become supersaturated in Ni before the region around the *C16* becomes supersaturated in Cu if their diffusivities are similar. This would explain the faster growth of the *C16* relative to the *C11b* for x = 0.25 during the initial stages of devitrification (Fig. 6).

Conclusions

We have demonstrated that the $Zr_2Ni_xCu_{1-x}$ forms a homogenous metallic glass for all values of x. The pseudo-binary phase diagram constructed using DTA and HEXRD data shows that a eutectic forms between $0.25 \leq x \leq 0.75$. The thermodynamically stable crystalline phase for the Cu-rich end has the *C11b* structure and the *C16* structure for the Ni-rich end. The FCC, 'big-cube' phase was not observed in this study using alloys with oxygen kept below 250 ppm. The *C16* phase is the preferred nucleating phase for $x > 0.25$. However,

the *C11b* is the thermodynamically stable phase for $x \leq 0.25$. First principle calculations show that the *C16* phase has a lower enthalpy of formation for $x > 0.25$ compared to the *C11b* phase. These results suggest that as more Ni is added to the alloy, the amorphous state becomes structurally more similar to the *C16* crystal structure, lowering the interfacial free energy and therefore promoting nucleation of the *C16* over *C11b* phase.

Acknowledgements

This work was supported by the U. S. Department of Energy, Office of Science, Office of Basic Energy Sciences, as follows: efforts at the Ames Laboratory were supported under Contract No. DE-AC02-07CH11358; use of the Advanced Photon Source was supported under Contract No. DE-AC02-06CH11357.

References

[1]. David R. Nelson and Frans Spaepen, in Solid State Physics, Advances in Research and Applications, edited by Henry Ehrenreich, David Turnbull, and Editors (Academic Press, Inc., Boston, 1989), Vol. 42, p. 1-90.

[2]. J. Hafner, *Physical Review B*, 1980, vol. 21 (2), p 406-426.

[3]. Z. Altounian, Guohua Tu, and J. O. Strom-Olsen, *Journal of Applied Physics*, 1983, vol. 54 (6), p 3111-3116.

[4]. Z. Altounian, G. H. Tu, and J. O. Stromolsen, *Journal of Applied Physics*, 1982, vol. 53 (7), p 4755-4760.

[5]. A. A. Turchanin, M. A. Turchanin, and P. G. Agraval, *Metastable, Mechanically Alloyed and Nanocrystalline Materials, Ismanam-2000*, 2001, vol. 360-3, p 481-486.

[6]. X. H. Lin and W. L. Johnson, *Journal of Applied Physics*, 1995, vol. 78 (11), p 6514-6519.

[7]. A. Inoue, *Acta Materialia*, 2000, vol. 48 (1), p 279-306.

[8]. Akinori Inoue, Hajime Yoshida, Shin-ichi Yamaura, Hisamichi Kimura, and Akihisa Inoue, *Materials Science Forum*, 2005, vol. 502 (New Frontiers of Processing and Engineering in Advanced Materials), p 281-286.

[9]. U. Koester, J. Meinhardt, S. Roos, and H. Liebertz, *Applied Physics Letters*, 1996, vol. 69 (2), p 179-181.

[10].A. Inoue, T. Zhang, M. W. Chen, T. Sakurai, J. Saida, and M. Matsushita, *Journal of Materials Research*, 2000, vol. 15 (10), p 2195-2208.

[11].T. Egami and Y. Waseda, *Journal of Non-Crystalline Solids*, 1984, vol. 64 (1-2), p 113-134.

[12].Chih-Hua Liu, Wei-Ren Chiang, Ker-Chang Hsieh, and Y. Austin Chang, *Intermetallics*, 2006, vol. 14 (8-9), p 1011-1013.

[13].M. Laridjani and J. F. Sadoc, *Journal of Non-Crystalline Solids*, 1988, vol. 106 (1-3), p 42-46.

[14].F. Paul and R. Frahm, *Physical Review B: Condensed Matter and Materials Physics*, 1990, vol. 42 (17), p 10945-10949.

[15].T. Fukunaga, K. Itoh, T. Otomo, K. Mori, M. Sugiyama, H. Kato, M. Hasegawa, A. Hirata, Y. Hirotsu, and A. C. Hannon, *Intermetallics*, 2006, vol. 14 (8-9), p 893-897.

[16].T. Fukunaga, D. Touya, K. Itoh, T. Otomo, K. Mori, H. Kato, and M. Hasegawa, *Journal of Metastable and Nanocrystalline Materials*, 2005, vol. 24-25, p 217-220.

[17].M. J. Kramer, L. Margulies, A. I. Goldman, and P. L. Lee, *Journal of Alloys and Compounds*, 2002, vol. 338 (1-2), p 235-241.

[18].U. Koster, A. Rudiger, and J. Meinhardt, Quasicrystals, Proceedings of the International Conference, 6th, Tokyo, May 26-30, 1997, 1998, p 317-320.

[19].Daniel J. Sordelet, Xiaoyun Yang, Elena A. Rozhkova, Matthew F. Besser, and Matthew J. Kramer, *Intermetallics*, 2004, vol. 12 (10-11), p 1211-1217.

[20].A.C. Larson and R.B. Von Dreele, 2004.

[21].Yoshio Waseda, 326 p. (McGraw-Hill International Book Co., New York ; London, 1980).

[22].T. Egami and S. J. L. Billinge, *Pergamon materials series v. 7*,500 pp. (Pergamon, 2003).

[23].G. Kresse and J. Hafner, *Physical Review B: Condensed Matter and Materials Physics*, 1993, vol. 47 (1), p 558-561.

[24].G. Kresse and J. Furthmuller, *Computational Materials Science*, 1996, vol. 6 (1), p 15-50.

[25].G. Kresse and J. Furthmueller, *Physical Review B: Condensed Matter*, 1996, vol. 54 (16), p 11169-11186.

[26].H. J. Monkhorst and J. D. Pack, *Physical Review B*, 1976, vol. 13 (12), p 5188-5192.

[27].A. Lee, G. Etherington, and C. N. J. Wagner, *Journal of Non-Crystalline Solids*, 1984, vol. 61-2 (Jan), p 349-354.

[28].Junji Saida, Masayuki Kasai, Eiichiro Matsubara, and Akihisa Inoue, *Annales de Chimie (Paris, France)*, 2002, vol. 27 (5), p 77-89.

[29].Z. Altounian, E. Batalla, J. O. Strom-Olsen, and J. L. Walter, *Journal of Applied Physics*, 1987, vol. 61 (1), p 149-155.

[30].S. Brauer, J. O. Strom-Olsen, M. Sutton, Y. S. Yang, A. Zaluska, G. B. Stephenson, and U. Koester, *Physical Review B: Condensed Matter and Materials Physics*, 1992, vol. 45 (14), p 7704-7715.

[31].K. H. J. Buschow, *Journal of Applied Physics*, 1981, vol. 52 (5), p 3319-3323.

[32].Z. Altounian, G. H. Tu, J. O. Stromolsen, and W. B. Muir, *Physical Review B*, 1981, vol. 24 (2), p 505-509.

[33].Huan-Rong Wang, Yi-Fu Ye, Jun-Yan Zhang, Xin-Ying Teng, Guang-Hui Min, Zhi-Qiang Shi, and Xue-Lei Tian, *Chinese Physics (Beijing, China)*, 2002, vol. 11 (6), p 592-595.

[34].H. R. Wang, G. H. Min, X. D. Hui, Y. F. Ye, X. Y. Teng, Z. Q. Shi, and J. Y. Zhang, *Journal of Materials Science Letters*, 2002, vol. 21 (21), p 1705-1707.

[35].Huan-Rong Wang, Yu-Fu Deng, Yu-Lai Gao, Xi-Dong Hui, Guang-Hui Min, Yi-Fu Ye, and Ying Chen, *Journal of Alloys and Compounds*, 2003, vol. 350 (1-2), p 174-177.

[36].Huan-Rong Wang, Yu-Lai Gao, Xi-Dong Hui, Guang-Hui Min, Ying Chen, and Yi-Fu Ye, *Journal of Alloys and Compounds*, 2003, vol. 349 (1-2), p 129-133.

[37].Huan-Rong Wang, Yu-Lai Gao, Guang-Hui Min, Xi-Dong Hui, and Yi-Fu Ye, *Physics Letters A*, 2003, vol. 314 (1-2), p 81-87.

[38].Huan-Rong Wang, Yu-Lai Gao, Guang-Hui Min, Yi-Fu Ye, Ying Chen, Zhi-Qiang Shi, and Xin-Ying Teng, *Journal of Alloys and Compounds*, 2003, vol. 349 (1-2), p 140-144.

[39].Huan-Rong Wang, Yu-Lai Gao, Yi-Fu Ye, Guang-Hui Min, Ying Chen, and Xin-Ying Teng, *Journal of Alloys and Compounds*, 2003, vol. 353 (1-2), p 200-206.

[40].Uwe Koster, Daniela Zander, and Rainer Janlewing, *Materials Science Forum*, 2002, vol. 386-388 (Metastable, Mechanically Alloyed and Nanocrystalline Materials), p 89-98.

[41].K. Saksl, H. Franz, P. Jovari, K. Klementiev, E. Welter, A. Ehnes, J. Saida, A. Inoue, and J. Z. Jiang, *Applied Physics Letters*, 2003, vol. 83 (19), p 3924-3926.

[42].A. L. Greer and I. T. Walker, *Journal of Non-Crystalline Solids*, 2003, vol. 317 (1-2), p 78-84.

Table 1. Crystallization temperatures for 5 different heating rates for the 5 samples in $Zr_2Cu_{1-x}Ni_x$. The onset of crystallization is slightly higher for x = 0.25 for all heating rates.

dT/dt(K/s)	0	0.25	0.5	0.75	1
0.083	644	647	643	645	642
0.167	652	655	650	653	651
0.333	661	663	659	660	660
0.667	670	675	669	669	670
1.333	680	685	679	680	682

Table 2. Room temperature lattice parameters and refinable atomic sites for the *C11b* and *C16* crystalline phases $Zr_2Cu_{1-x}Ni_x$ alloys heated to 0.9 T_m and then quenched. The *ab initio* calculations are at 0 K for the same chemistries.

C11b				C16		
x	a-axis	c-axis	z	a-axis	c-axis	x
Calculated						
0	3.233	11.206	0.346	6.632	5.304	0.158
0.25	3.227	11.162	0.345	6.656	5.157	0.157
0.5	3.219	11.068	0.348	6.614	5.166	0.156
0.75	3.232	10.851	0.351	6.562	5.209	0.159
1	3.242	10.671	0.349	6.511	5.226	0.163
Measured						
0	3.212(7)	11.13(8)	0.345(4)			
0.25	3.212(0)	11.14(5)	0.346(3)			
0.5	3.212(7)	11.13(8)	0.345(4)	6.546(0)	5.237(0)	0.163(8)
0.75				6.527(5)	5.238(6)	0.164(4)
1				6.588(0)	5.262(1)	0.166(0)

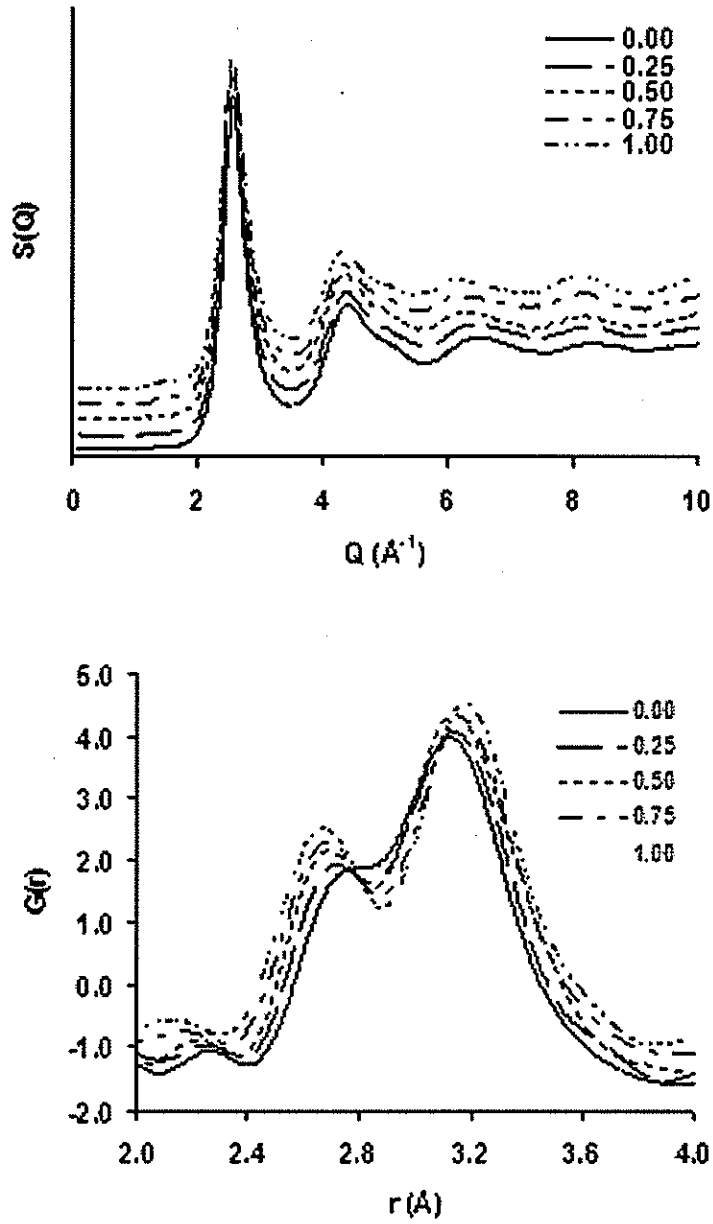

Fig. 1. The as-quenched, room temperatures (a) total scattering function, S(Q) and (b) respective reduced pair distribution function, G(r), for $Zr_2Ni_xCu_{1-x}$

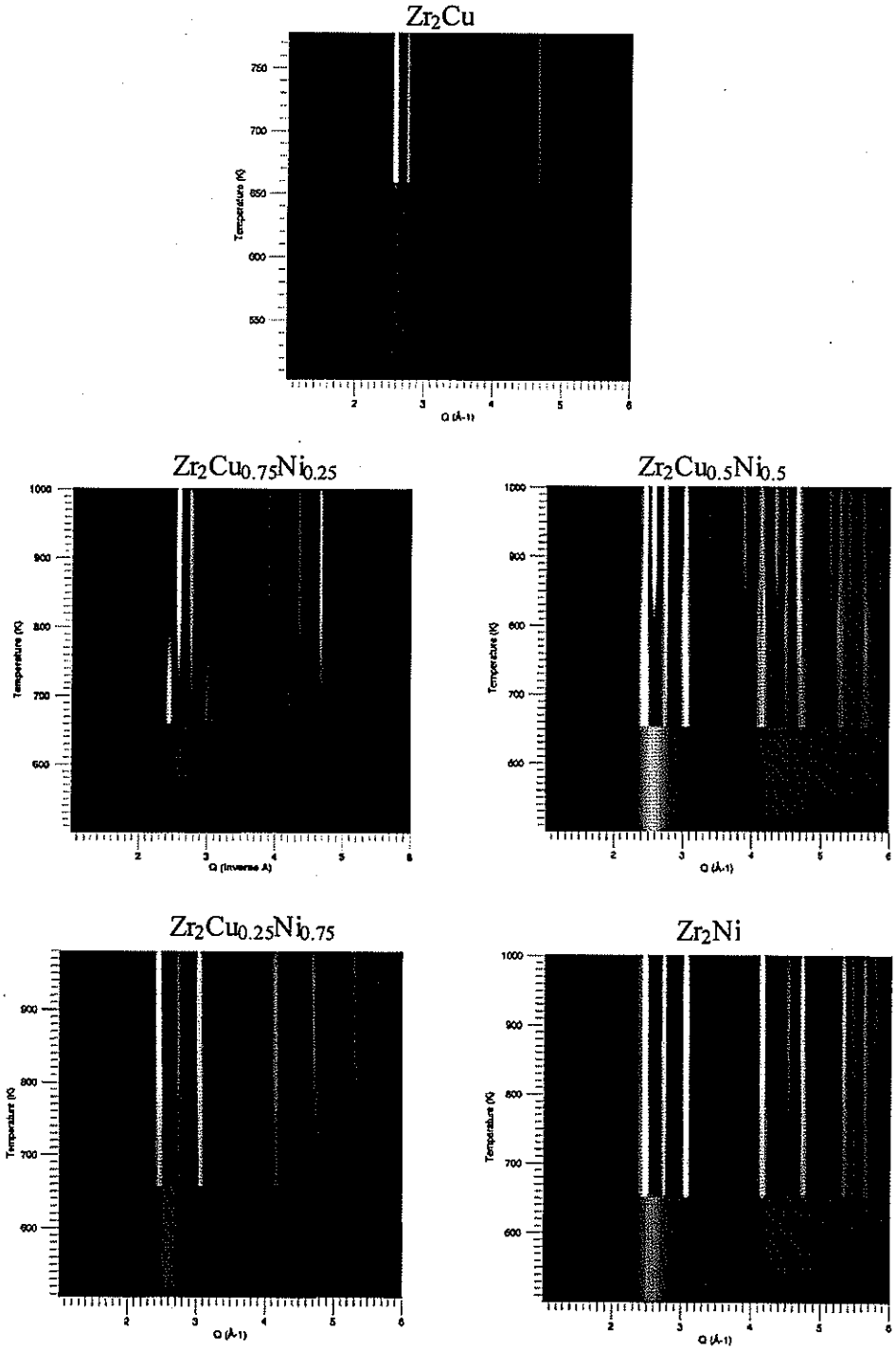

Fig. 2. A 2D representation of the S(Q) as a function of temperatures for x = 0.00, 0.25, 0.50, 0.75 and 1.00.

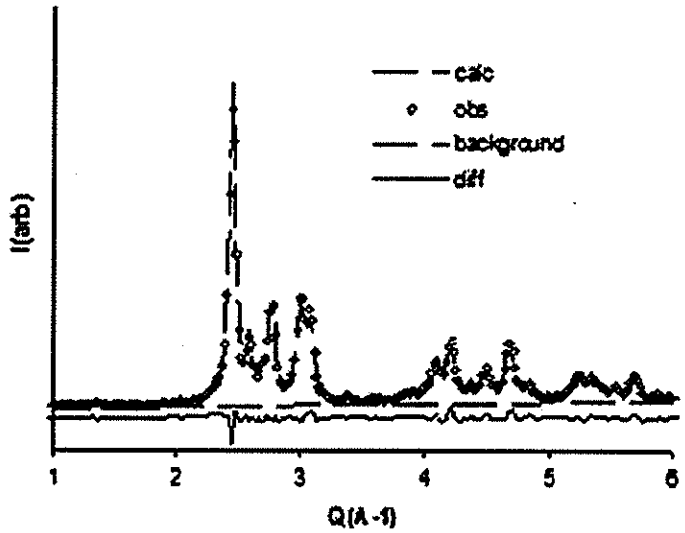

Fig. 3. Rietveld analysis of a 5% devitrified x = 0.25 sample with the glass fraction removed prior to fitting, wRp is 6%.

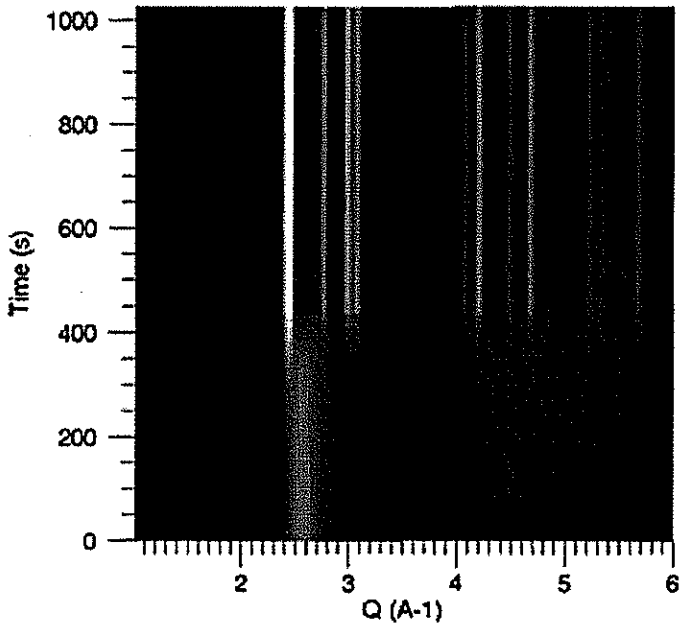

Fig. 4. Isothermal anneal at 628 K for the x = 0.25 sample.

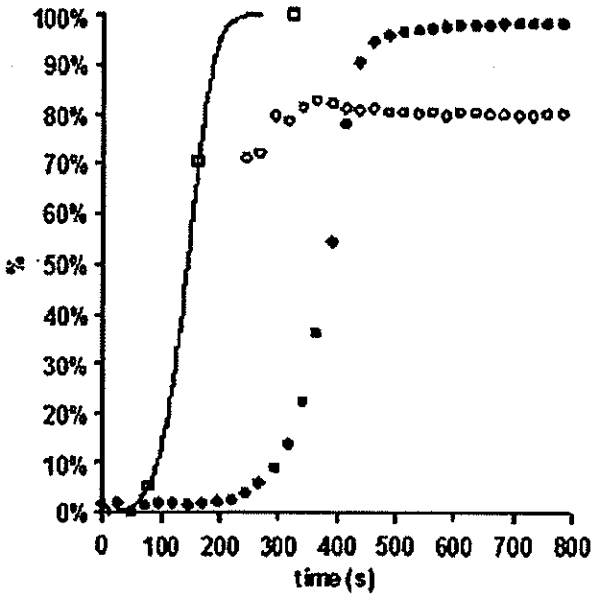

Fig. 5. The fraction crystallized based on the DSC (solid curve) and HEXRD (closed circles) results as a function of time for x = 0.25. The faster rise and sharper transition for the DSC results indicate that ?T was slightly smaller than that of the HEXRD. The open circles indicate the percentage of *C16*:*C11b* phases based on Rietveld refinement of the HEXRD data. The open squares represent the hold times before quenching in the DSC for the TEM samples.

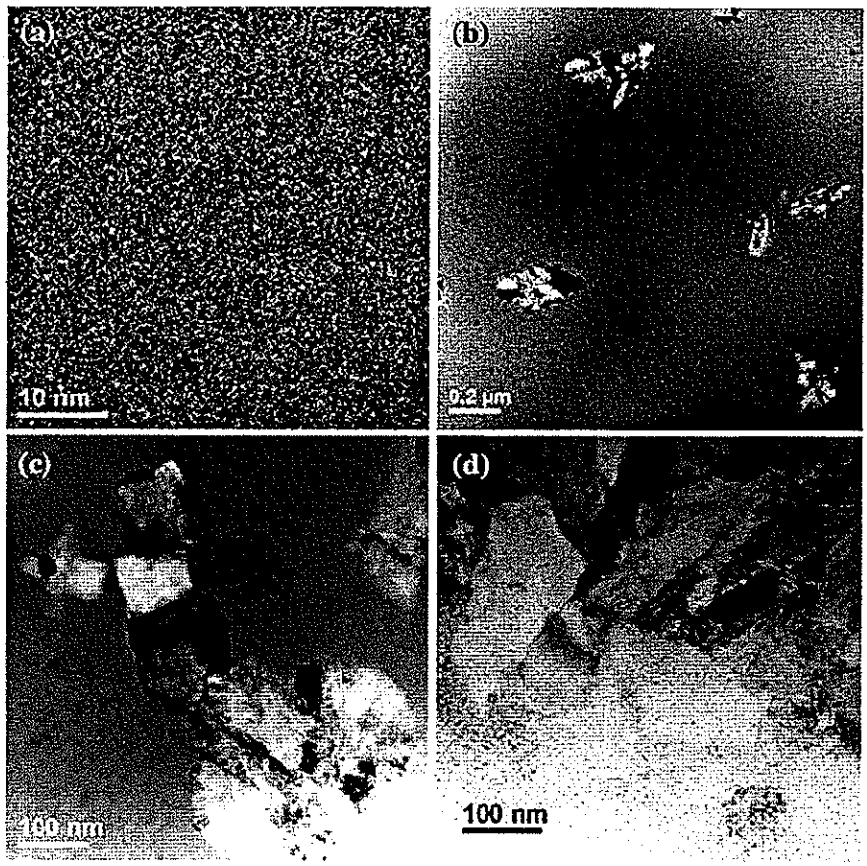

Fig. 6. TEM micrographs representing the 4 different annealing times shown in Fig. 5.

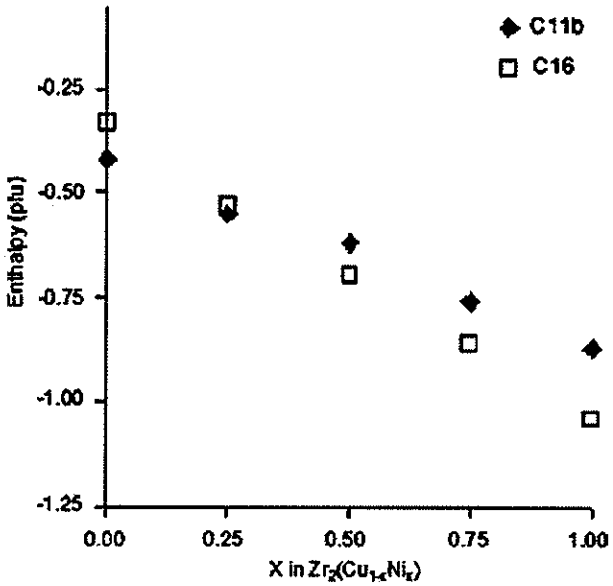

Fig. 7. Formation enthalpies as a function of Ni:Cu for both the *C11b* and *C16* structures.

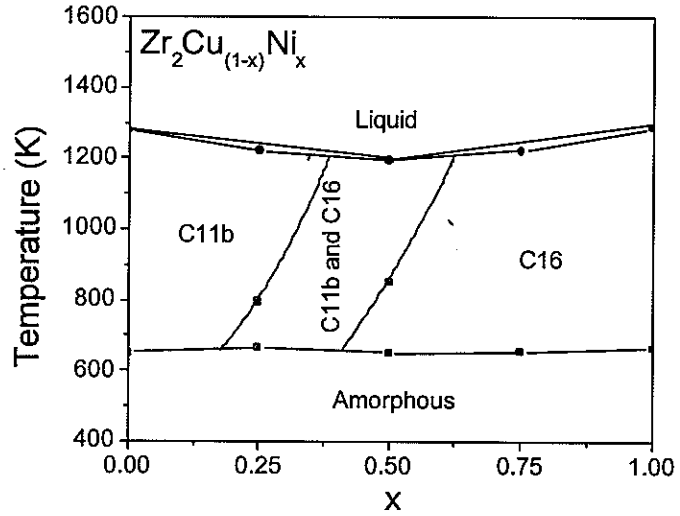

Fig. 8. Schematic phase diagram for the $Zr_2Ni_xCu_{1-x}$system. T_x and T_m data points are from DSC and DTA analysis, respectively.

CHAPTER 6. GENERAL CONCLUSIONS

Summary

The crystallization pathways selections in the pseudo-binary $Zr_2Pd_xCu_{(1-x)}$ and $Zr_2Ni_xCu_{(1-x)}$ (x = 0, 0.25, 0.5, 0.75 and 1) systems were studied in this thesis. The relationship between the disordered to ordered structures and the various factors, such as topology, atomic size and electronic structure, of phase selections were explored. The findings from this study allow the following conclusions to be made:

1. Crystallization pathways of $Zr_2Pd_xCu_{(1-x)}$ and $Zr_2Ni_xCu_{(1-x)}$ metallic glass have been identified by HEXRD, DSC and TEM:

(a) For $Zr_2Pd_xCu_{(1-x)}$ system:

x = 0, Glassy phase → *C11b*

x = 0.25, 0.75 and 1, Glassy phase → *i*-phase + amorphous → *C11b*

x = 0.5, Glassy phase → *i*-phase + amorphous → *C16* + *C11b* → *C11b*

(b) For $Zr_2Ni_xCu_{(1-x)}$ system:

x = 0, Glassy phase → *C11b*

x = 0.25, Glassy phase → *C11b* + *C16* → *C11b*

x = 0.5, Glassy phase → *C16* →*C11b* + *C16*

x = 0.75 and 1, Glassy phase → *C16*

2. *I*-phase formation is mainly caused by topological factor in Noble metal containing Zr-based metallic glass:

2. *I*-phase formation is mainly caused by topological factor in Noble metal containing Zr-based metallic glass:

(a) The total scattering functions S(Q) show that, with increasing Pd content, there is a systematic increasing development of the high Q-side of the second diffuse scattering peak.

(b) The radial distance of Zr-TM (TM = Pd, Cu) increases, while Zr-Zr bond length remains constant with increasing x. It is in good agreement with the Goldschmidt atomic radii.

3. A meta-stable crystallization phase *C16* was observed only at x = 0.5 in $Zr_2Pd_xCu_{(1-x)}$ system. *Ab initio* calculation show that, at x = 0.5, *C16* phase has a minimum in energy; the energy is closest to that of *C11b* phase. The competition is shown to be dominated by electronic structure rather than by size effects, with the favored composition for the *C16* phase forming a pseudo-gap at the Fermi energy.

4. All compositions in $Zr_2Pd_xCu_{(1-x)}$ system share the same tetragonal *C11b* phase as equilibrium phase, which is in good agreement with the *ab initio* calculation:

(a) With increasing homologous temperature T_H, the anisotropic ratio of homologous lattice parameter c_H/a_H increases. It was found that the bonding in the (0 0 1) plane is more rigid than alone c-axis. Moreover, a more anisotropic coefficient of thermal expansion (CTE) for Zr_2Pd than for Zr_2Cu was obtained and was confirmed by the first principles calculation.

(b) With increasing x, lattice parameter *a* and cell volume increase, while lattice parameter *c* reaches a maximum value of 11.312(2)Å at x = 0.5, then shrinks a lot

from x = 0.5 to 1. Those trends are in good agreement with the *ab initio* calculation. Both size and electronic factors contributed to the *C11b* structural changes as x.

5. In the crystallization pathways of $Zr_2Ni_xCu_{(1-x)}$ system, we observed that:

(a) In the amorhous structure of $Zr_2Ni_xCu_{(1-x)}$ system, the changes of TM-Zr, Zr-Zr bond distributions led to the preferential *C11b* or *C16* formation.

(b) For x = 0.25, the coexistence of *C11b* and *C16* was observed in the initial devitrification process. The *C11b* grains show Cu-rich while *C16* grains show Ni-rich during the grain growth process by TEM - EDS.

(c) We observed that the first devitrification product in the Zr_2Ni is the *C16* structure instead of the FCC, 'big-cube' phase [1], if oxygen is kept sufficiently low.

(d) The pseudo binary phase diagram of $Zr_2Ni_xCu_{(1-x)}$ system was proposed. The phase selections are main related topology in the amorphous structure and the calculations of the enthalpy of formation.

Recommendations for future research

The devitrification process of the $Zr_2Pd_xCu_{(1-x)}$ and $Zr_2Ni_xCu_{(1-x)}$ (x = 0, 0.25, 0.5, 0.75 and 1) metallic glass shows different phase behavior in the primary transitions. For example, the binary Zr_2Cu, Zr_2Pd and Zr_2Ni metallic glass lead to amorphous to *C11b*, *i*-phase and *C16* phase transitions; a combination of *C11b* and *C16* phases was observed in the primary devitrification process in $Zr_2Ni_{0.25}Cu_{0.75}$. Thus, it is very interesting to understand the crystallization kinetics in these two systems to clarify the temperature dependence nucleation and growth of crystalline phases in the metallic supercooled liquid. I will investigate the high

stability of the supercooled region against crystallization and clarifying the effect of additive element on the structure dynamics in amorphous alloys.

There most commonly used techniques to study the crystallization kinetics are non-isothermal and isothermal experiments [2, 3].

Kissinger equation is usually used for the non-isothermal kinetic studies [4]:

$$\ln\left(\frac{B}{T^2}\right) = -\frac{E}{RT} + C$$

Where B is the heating rate, E is the activation energy for the phase transition process, R is the gas constant and T is a specific temperature such as crystallization temperature.

Isothermal crystallization transformation of an amorphous alloys is often analyzed using the so-called Johnson–Mehl–Avrami (JMA) equation and Arrhenius equation [5, 6], which are described as:

$$x(t) = 1 - e^{[-k(t-\tau)^n]}$$

$$\tau = \tau_o e^{\left(\frac{E_a}{RT}\right)}$$

Where x(t) is the fraction transformed after time t, τ is the incubation time, k is a rate constant and n is an exponent which need not be an integer, E_a is .the activation energy.

Furthermore, I will combine the calorimetry information with accurate structural information, which will be obtained by *in situ* HEXRD observation and Rietveld refinement. From the crystallization kinetics study, we will reveal the crystallization mechanism during the three dimension nucleation and growth process during the initial crystallization process. Kinetics models for the $Zr_2Pd_xCu_{(1-x)}$ and $Zr_2Ni_xCu_{(1-x)}$ systems will be obtained and

compared. My previous work on the stability of amorphous alloys and phase selection process lends a promising start to these problems.

References

[1] S. Brauer, J. O. Strom-Olsen, M. Sutton, etc., Physical Review B, 45, 7704 (1992).

[2] J. C. Holzer and K. F. Kelton, Acta Metallurgica et Materialia 39, 1833-43 (1991).

[3] J. Saida, M. Matsushita, and A. Inoue, Journal of Applied Physics 88, 6081-6083 (2000).

[4] H.-R. Wang, Y.-L. Gao, G.-H. Min, X.-D. Hui, and Y.-F. Ye, Physics Letters A 314, 81-87 (2003).

[5] J. Z. Jiang, Y. X. Zhuang, H. Rasmussen, J. Saida, and A. Inoue, Physical Review B: Condensed Matter and Materials Physics 64, 094208/1-094208/10 (2001).

[6] J. Saida, M. Matsushita, T. Zhang, A. Inoue, M. W. Chen, and T. Sakurai, Applied Physics Letters 75, 3497-3499 (1999).

ACKNOWLEDGEMENTS

First and foremost, I would like to thank my major professor, Dr. Matthew J Kramer, for his guidance and support throughout this research and the writing of this thesis. Without his direction, this work would not be accomplished.

I would like to thank Professor Yiying Ye and Dr. James Morris for their collaboration in the calculation part. I would like to thank Dr. Daniel J. Sordelet for many helpful discussions. I would thank Kelvin Dennis, Matthew Besser, Fran Laabs, Lester Reed, Yaqiao Wu and Wei Tang for their experimental support.

I would like to thank Dr. Steve W Martin, the director of graduate education in the department of Materials Science and Engineering, for his encouragement. I would also like to thank my committee members for their time and efforts to this work.

This work was performed at Ames Laboratory under Contract No. DE-AC02-07CH11358 with the U.S. Department of Energy. The United States government has assigned the DOE Report number IS-T 2586 to this thesis.